

UNCLASSIFIED

AD NUMBER

AD801951

LIMITATION CHANGES

TO:

Approved for public release; distribution is unlimited.

FROM:

Distribution authorized to U.S. Gov't. agencies and their contractors; Critical Technology; OCT 1966. Other requests shall be referred to Air Force Materials Laboratory, Research and Technology Division, Attn: Metals and Ceramics Division, Wright-Patterson AFB, OH 45433. This document contains export-controlled technical data.

AUTHORITY

AFML ltr dtd 29 Mar 1972

THIS PAGE IS UNCLASSIFIED

①

801951

AFML-TR-66-290 *1/12*

IRIDIUM-BASE ALLOYS AND THEIR BEHAVIOR IN THE  
PRESENCE OF CARBON

D. P. Harmon

Aerojet-General Corporation

TECHNICAL REPORT NO. AFML-TR-66-290-FINAL REPORT

October 1966

This document is subject to special export controls, and each transmittal to foreign governments or foreign nationals may be made only with prior approval of Metals and Ceramics Division, Air Force Materials Laboratory, Wright-Patterson Air Force Base, Ohio.

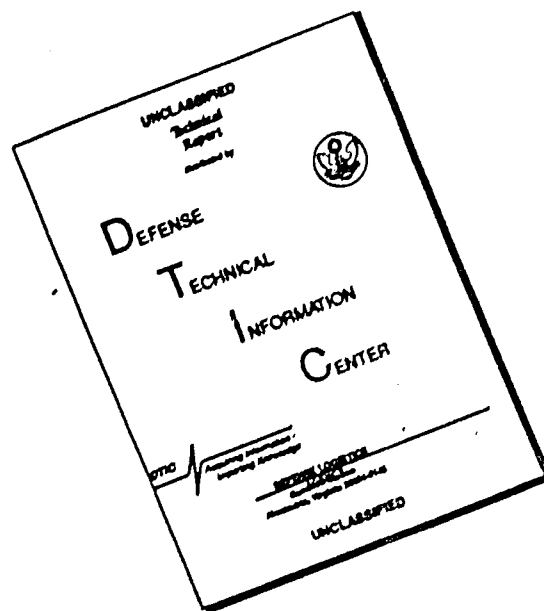
DDC  
NOV 17 1966

Air Force Materials Laboratory  
Research and Technology Division  
Air Force Systems Command  
Wright-Patterson Air Force Base, Ohio

*B*

AD No. \_\_\_\_\_  
DDG FILE COPY

# DISCLAIMER NOTICE



THIS DOCUMENT IS BEST QUALITY AVAILABLE. THE COPY FURNISHED TO DTIC CONTAINED A SIGNIFICANT NUMBER OF PAGES WHICH DO NOT REPRODUCE LEGIBLY.

⑥ IRIDIUM-BASE ALLOYS AND THEIR BEHAVIOR IN THE  
PRESENCE OF CARBON.

⑨ Final rept.

⑩ D. P. Harmon

⑪ Oct 66

⑫ 115 p.

⑬ AF 33(615)-2668

⑱ AFML ⑲ TR-66-290

This document is subject to special export controls and each transmittal to foreign governments or foreign nationals may be made only with prior approval of Metals and Ceramics Division, Air Force Materials Laboratory, Wright-Patterson Air Force Base, Ohio.

(40004)

14413  
ack

## FOREWORD

This is the final report describing the work performed at the Materials Research Laboratory of the Aerojet-General Corporation, Sacramento, California under USAF Contract No. AF 33(615)-2368. The contract was initiated 1 June 1965, and was administered under the direction of the Air Force Materials Laboratory, Research and Technology Division, with Lt. P. J. Marchiando acting as Project Engineer and Dr. E. Rudy, Aerojet-General Corporation as Principal Investigator.

The author wishes to acknowledge the guidance given by Dr. E. Rudy during the course of the investigation, and to thank Dr. Y. A. Chang for his consultation on the thermochemical evaluation of the system. Special thanks go to D. Spencer for the invaluable help given by him in gathering the experimental data. The support given by J. Hoffman and R. Cobb is also gratefully appreciated. The report was technically edited and corrected by Dr. C. E. Brukl.

The chemical analytical work was carried out under the supervision of Mr. W. E. Trahan, Quality Control Division. The drawings were prepared by R. Cristoni and the report was typed by Mrs. J. Weidner.

The manuscript of this report was released by the author in July 1966 for publication as an RTD Technical Report.

This technical report has been reviewed and is approved.

  
W. G. RAMKE  
Chief, Ceramics and Graphite Branch  
Metals and Ceramics Division  
Air Force Materials Laboratory

## ABSTRACT

Experimental results pertaining to the melting temperatures of selected iridium-osmium-rhodium, iridium-osmium-platinum, and iridium-rhenium-rhodium alloys are described. The eutectic temperatures of these alloy-carbon mixtures were measured, and in addition, the compositions of the respective eutectics were determined by metallographic examination of chemically analyzed alloys. A brief theoretical analysis of the data was performed with the specific objective of establishing numerical relations between the melting point depression and properties of the melt as well as the component metals.

The thermal expansion characteristics of several of the iridium-base alloys were measured up to 1800°C by high temperature, X-ray diffraction as well as by dilatometric techniques.

## TABLE OF CONTENTS

	PAGE
I. INTRODUCTION AND SUMMARY . . . . .	1
A. Introduction . . . . .	1
B. Summary . . . . .	2
1. Melting Temperatures of the Metal Components. . . . .	2
2. Metal Components and Carbon . . . . .	5
3. Theoretical Analysis of the Data . . . . .	9
4. Thermal Expansion Characteristics of the Metal Alloy Systems . . . . .	9
II. LITERATURE REVIEW . . . . .	10
A. Metal Systems . . . . .	10
B. Metal-Carbon Systems . . . . .	15
C. Thermal Expansion Values . . . . .	18
III. EXPERIMENTAL PROGRAM . . . . .	18
A. Starting Materials . . . . .	18
B. Experimental Techniques . . . . .	20
1. Alloy Preparation . . . . .	20
2. Melting Point Studies (Pirani-Technique) . . . . .	26
3. Differential Thermal Analytical Investigations . . . . .	28
4. Special Experimental Studies . . . . .	33
5. Thermal Expansion Measurements . . . . .	35
6. X-Ray, Metallographic, and Chemical Analysis . . . . .	44
C. Results . . . . .	45
1. Melting Temperatures and Phase Equilibria of Iridium Base Metal Alloys . . . . .	45

TABLE OF CONTENTS (Cont'd)

	PAGE
2. Solidus Temperatures of the Metal Alloys in the Presence of Carbon . . . . .	60
3. Theoretical Analysis of the Data . . . . .	97
4. Thermal Expansion Measurements . . . . .	107
IV. DISCUSSION . . . . .	111
References . . . . .	113

## LIST OF ILLUSTRATIONS

FIGURE		PAGE
1	Solidus Temperatures of Iridium-Osmium-Rhodium Alloys	4
2	Solidus Temperatures of Iridium-Osmium-Platinum Alloys	4
3	Solidus Temperatures of Iridium-Rhenium-Rhodium Alloys	5
4	Eutectic Trough Melting Temperatures in the Ir-Re(Os, Rh, Pt)-C Ternary Systems.	6
5	Solidus Temperatures of Iridium-Osmium-Rhodium Alloys in the Presence of Carbon	7
6	Solidus Temperatures of Iridium-Osmium-Platinum Alloys in the Presence of Carbon	8
7	Solidus Temperatures of Iridium-Rhenium-Rhodium Alloys in the Presence of Carbon	8
8	Thermal Expansion Characteristics of the Iridium-Base Alloys Compared to Commercial Grades of Graphite	9
9	The Iridium-Osmium Phase Diagram	12
10	The Iridium-Rhenium Phase Diagram	13
11	The Iridium-Platinum Phase Diagram	14
12	Lattice Parameters of the FCC-Solid Solutions of Iridium with Rhenium, Rhodium, and Platinum	15
13	The Rhenium-Carbon Phase Diagram	16
14	Cold-Pressing Die for Preparation of Pirani Melting Point Specimens	21
15	Cold-Pressed Pirani Melting Point Specimen	21
16	Compositions of Iridium-Osmium-Rhodium Alloys Prepared for Melting Temperature Investigation	22
17	Compositions of Iridium-Rhenium-Rhodium Alloys Prepared for Melting Temperature Investigations	22
18	Electron Beam Melted Iridium-Base Alloy Ingot	25
19	Machined Sample for Dilatometer Studies	25

LIST OF ILLUSTRATIONS (Cont'd)

FIGURE		PAGE
20	View of the Interior Portion of the Melting Point Furnace	26
21	Chart for Temperature Corrections to be Applied to the Temperature Measurements Performed in the Melting Point Furnace.	28
22	Schematic Drawing of the Experimental Set-up of the Differential Thermal Analytical Apparatus	30
23	Over-all View of the DTA-Apparatus	31
24	Sectioned Graphite Crucible Subsequent to a DTA-Run, Showing the Sample and Cap which Serves as the Black Body Temperature Reference Hole	32
25	Experimental Set-up for Performing the Thermal Expansion Measurements Using the High Temperature X-Ray Diffraction Apparatus	36
26	Temperature Correction Curve for Pyrometric Readings on the Surface of the Tantalum Heating Elements Used in the High Temperature X-Ray Studies	39
27	Literature Values and Calculated Expansion Curve for Platinum	40
28	Brinkmann High Temperature Dilatometer Model T 1X (Shown with Alumina Measuring System)	41
29	Schematic Drawing of Dilatometric Set-up.	43
30	Thermal Distribution Curve for the Silicon Carbide Furnace of the Dilatometer (Data Supplied by Brinkmann)	43
31	Iridium-Rhenium Phase Diagram Showing Melting Data Points Obtained in this Investigation	47
32	Iridium-Osmium Phase Diagram Showing Melting Data Points Obtained in this Investigation	48
33	Iridium-Platinum Solidus-Liquidus Curves Showing Melting Data Points Obtained in this Investigation	49
34	Iridium-Rich Portion of Iridium-Rhodium Phase Diagram	50
35	Lattice Parameters of the Face-Centered-Cubic Solid Solutions of the Iridium-Base Binary Alloys	51
36	Incipient Melting Temperatures of Iridium-Osmium-Rhodium Alloys as a Function of Composition	53

LIST OF ILLUSTRATIONS (Cont'd)

FIGURE		PAGE
37	Incipient Melting Temperatures of Iridium-Osmium-Platinum Alloys as a Function of Composition	56
38	Incipient Melting Temperatures of Iridium-Rhenium-Rhodium Alloys as a Function of Composition	59
39	Differential Heating and Cooling Curves of a Rhenium-Carbon Alloy.	61
40	Re-C (90/10), Arc-Melted Alloy	62
41	Re-C (82/18), Arc-Melted Alloy	63
42	Re-C (76/24), Arc-Melted Alloy	63
43	Rhenium-Carbon Diffusion Couple	64
44	Rhenium-Carbon Diffusion Couple	65
45	Modified Rhenium-Carbon Phase Diagram	66
46	Differential Heating and Cooling Curves of an Osmium-Carbon Alloy	67
47	Os-C (73.5/26.5), DTA Alloy Cooled at 13°C per Second from 2900°C.	68
48	Os-C (96.5/3.5), Arc-Melted Alloy	69
49	Os-C (91.4/8.6), Arc-Melted Alloy	69
50	Os-C (81.6/18.4), Arc-Melted Alloy	70
51	Osmium-Carbon Diffusion Couple	70
52	Tentative Osmium-Carbon Phase Diagram	71
53	DTA Curve Showing Eutectic Solidification of Rh-C, Pt-C, and Ir-C Alloys	73
54	Rh-C (92/8), Arc-Melted Alloy	73
55	Rh-C (83/17), Arc-Melted Alloy	74
56	Rh-C (77/23), Arc-Melted Alloy	74
57	Tentative Rhodium-Carbon Phase Diagram	75
58	Ir-C (95.5/4.5), Arc-Melted Alloy	75

LIST OF ILLUSTRATIONS (Cont'd)

FIGURE		PAGE
59	Ir-C (93.5/6.5), Arc-Melted Alloy	76
60	Ir-C (90.8/9.2), Arc-Melted Alloy	76
61	Tentative Iridium-Carbon Phase Diagram	77
62	Iridium Foils Heated to 2150°C for 3 Hours in a Helium Atmosphere	78
63	Pt-C (97.3) DTA Alloy Rapidly Cooled from 1800°C	79
64	Pt-C (92.5/7.5), Arc-Melted Alloy	80
65	Tentative Platinum-Carbon Phase Diagram	80
66	Differential Heating Curves of Ir-Rh-C Alloys Showing Eutectic Trough Melting	81
67	Differential Heating Curves of Ir-Os-C Alloys Showing Eutectic Trough Melting	82
68	Ir-Os-C (81/10/9): Alloy Cooled in the DTA at 13°C per Second from the Melt	83
69	Ir-Pt-C (71/18/11): Alloy Cooled in the DTA at 13°C per Second from the Melt	83
70	Compositions of the Eutectic Troughs in the Iridium-Base Ternary Systems	84
71	Solidus Temperatures of Iridium-Osmium-Rhodium Alloys in the Presence of Carbon	87
72	Representative DTA Curves Showing Eutectic Melting in the Iridium-Osmium-Rhodium-Carbon Quaternary System	88
73	Approximate Eutectic Surface Carbon Concentrations for the Quaternary Systems Ir-Os-Rh-C, Ir-Os-Pt-C, and Ir-Re-Rh-C.	89
74	Solidus Temperatures of Iridium-Osmium-Platinum Alloys in the Presence of Carbon	92
75	Ir-Os-Pt-C(65.23/5/7): Arc-Melted Alloy	93
76	Ir-Os-Pt-C (76.5/9/4.5/10): Arc-Melted Alloy	93

## LIST OF ILLUSTRATIONS (Cont'd)

FIGURE		PAGE
77	Ir-Os-Pt-C (55/25/5/15): Arc-Melted Alloy Showing Primary Graphite in a Metal Carbon Eutectic.	94
78	Solidus Temperatures of Iridium-Rhenium-Rhodium Alloys in the Presence of Carbon	96
79	Correlation Between the Difference in Melting Points of the Platinum-Group Metals and the Critical Closing Temperature of the Miscibility Gap.	102
80	Calculated Iridium-Osmium Phase Diagram	104
81	Calculated Metal-Carbon Binary Systems	105
82	Calculated Solidus Temperatures for the Ternary Systems Iridium-Osmium-Carbon and Iridium-Platinum-Carbon	107
83	Compositional Field for Iridium-Osmium-Rhodium Alloys for which the Thermal Expansion Characteristics were Estimated	108
84	Compositional Field for Iridium-Osmium-Platinum Alloys for which the Thermal Expansion Characteristics were Estimated	108
85	Compositional Field for Iridium-Rhenium-Rhodium Alloys for which the Thermal Expansion Characteristics were Estimated	109
86	Representative X-ray Diffraction Peaks Obtained During the High Temperature X-ray Diffraction Measurements	110

## LIST OF TABLES

TABLE		PAGE
1	Melting Points of the Metallic Elements Used in the Present Investigation	3
2	Compositions and Temperatures of the Binary Metal-Carbon Eutectics	6
3	Equations for the Mean Coefficients of Thermal Expansion for Some Iridium-Base Alloys	10
4	Literature Values for the Melting Points of Platinum, Rhodium, Iridium, Osmium, and Rhenium	11
5	Eutectic Temperatures in the Platinum Group Metal-Carbon Systems	18
6	Melting Temperatures of Iridium-Osmium-Rhodium Alloys	52
7	Melting Temperatures of Iridium-Osmium-Platinum Alloys	55
8	Melting Temperatures of Iridium-Rhodium-Rhenium Alloys	58
9	Solidus Temperatures of Iridium-Osmium-Rhodium Alloys in the Presence of Carbon	86
10	Solidus Temperatures of Iridium-Osmium-Platinum Alloys in the Presence of Carbon	91
11	Solidus Temperatures of Iridium-Rhenium-Rhodium Alloys in the Presence of Carbon	95
12	Liquid Interaction Parameter Values Calculated from the Established Metal-Carbon Binaries (Regular Liquid Solution Behavior)	101
13	Relative Free Energy of Transition (fcc $\rightleftharpoons$ hcp) for the Platinum-Group Metals and Rhenium, Along with the Approximate Solid Phase Interaction Parameters for Metal Binary Systems (Regular Solution)	104
14	Thermal Expansion Data from the Dilatometric and High Temperature X-Ray Diffraction Studies.	112

## I. INTRODUCTION AND SUMMARY

### A. INTRODUCTION

It is well-known that graphite has many desirable characteristics, particularly in respect to its high temperature properties. However, because of its low resistance to oxidation, the complete benefit of its high-temperature potential cannot be fully realized for many applications. Extensive efforts have been made over the past few years to develop surface coatings and impregnates which would satisfactorily protect graphite in oxidizing atmospheres at high temperatures. The majority of these efforts have been hindered by the complex nature of the chemical equilibria between graphite and the protective material, and as yet, a suitable graphite composite system has not been developed which is operative above 2000°C.

Oxidation resistant coatings have shown the most promise; although, to date refractory coatings are only able to protect graphite at temperatures below 1700°C over a substantial period of time. Recently, however, investigations of graphite coatings consisting of platinum-group metals have shown that, in selected cases, exceptional oxidation protection is provided above 2000°C<sup>(1)</sup>. Unalloyed iridium coatings have shown the most promise, but, for this combination, the limiting operational temperature is 2110°C, the reported iridium-carbon eutectic temperature<sup>(1)</sup>.

In order to more thoroughly pursue the possibility of applying the platinum-metals as refractory, oxidation resistant coatings for graphite, a program was initiated in this laboratory under the authority of the Air Force Systems Engineering Group, Wright-Patterson Air Force Base, Dayton, Ohio. Platinum-metal alloy systems, specifically iridium-base alloys, were investigated to determine which combinations might exhibit greater thermal stability with respect to graphite than unalloyed coatings. The iridium-rich portion of the iridium-osmium-rhodium and iridium-osmium-platinum ternary systems were investigated since they appeared to be the most promising for coating applications.

The selection of these systems was based on two requirements: (1) that the major alloying element should be iridium, (2) that the alloys should be primarily single phase and exhibit eutectic temperatures with carbon in excess of 2000°C. Considerations employed for choosing the particular alloying components with iridium were: (1) of the platinum-metals only osmium has a higher eutectic temperature with carbon than does iridium, thus, in order to increase the refractoriness of the coating, osmium additions are necessary, and (2) because of the possible detrimental effect osmium additions might have on the alloys' oxidation characteristics, it should be advantageous to add a certain amount of a more noble element, rhodium or platinum, to these iridium-osmium alloys.

In addition to the above two systems, the rhenium-iridium-rhodium alloy system was investigated. These more refractory alloys are believed to have possible applications as an interfacial layers between graphite and the above mentioned alloy combinations.

The results presented in the following pages of this report pertain to the investigations of the physical compatibility of these metals with graphite, in particular, to the determination of the eutectics between the alloys and graphite as well as the measurement of the thermal expansion characteristics of the metallic coating systems.

## B. SUMMARY

The program was conducted in four separate parts; the results of each of these phases are summarized below:

### 1. Melting Temperatures of the Metal Components

The melting temperatures were determined for the unary, binary, and ternary metal compositions of interest in these investigations. The melting points of the elements rhenium, osmium, rhodium, iridium, and platinum were checked against the currently accepted literature values, and, with the exception of rhenium, they were found to be in good agreement (Table 1). The value of the melting point of rhenium was observed

to be unexplainably lower than previous literature values ( $3067 \pm 13$  as compared to approximately  $3180^\circ\text{C}$ ); moreover, this value was reproduced with a number of samples, prepared by different procedures, including electron beam melting as well as with four separate batches of rhenium.

The melting temperatures of the iridium-rich binary metal alloys were found to confirm previously reported data — no gross differences were observed between the present values and the previous literature citations.

The melting temperatures of the ternary iridium-rich metal alloys are summarized in Figures 1, 2, and 3. The melting temperatures of platinum containing alloys were somewhat lower than the similar alloys with rhodium, and as would be expected, the iridium-rhenium-rhodium system was observed to be the most refractory. The majority of the alloys was observed to be single phase; the exception was most of the rhenium- and osmium-rich compositions.

Table 1. Melting Points of the Metallic Elements Used in the Present Investigation

Metal	Observed Melting Point, $^\circ\text{C}$
Rhenium	$3067 \pm 13^\circ$
Osmium	$3055 \pm 1^\circ$
Rhodium	$1956 \pm 3^\circ$
Iridium	$2440 \pm 13^\circ$
Platinum	$1770 \pm 7^\circ$

(The error limits attached to the melting points refer to the reproducibility of the measurements, and do not take into account the calibration uncertainties of the pyrometer.)

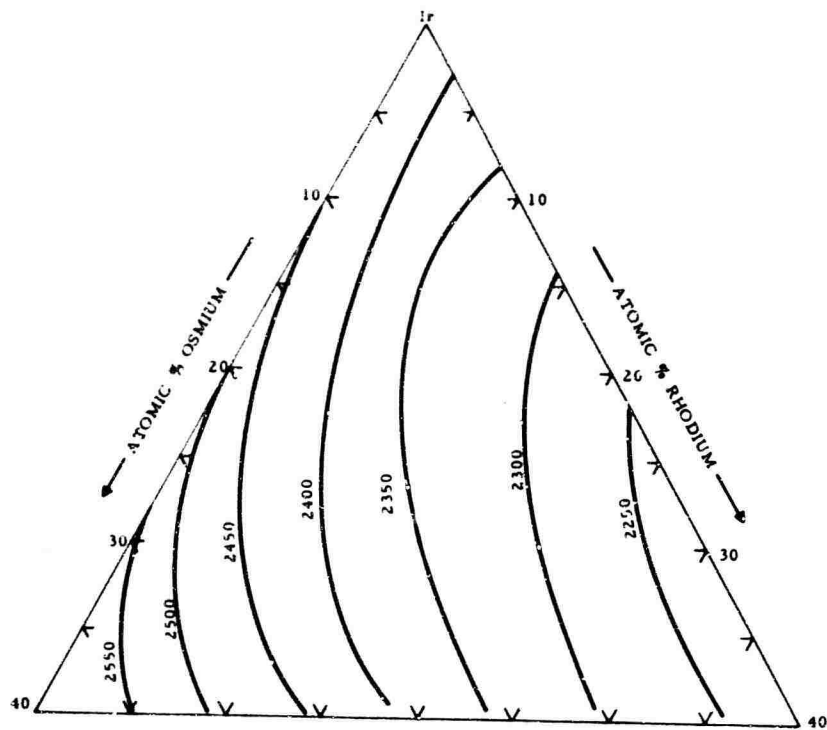


Figure 1. Solidus Temperatures of Iridium-Osmium-Rhodium Alloys.

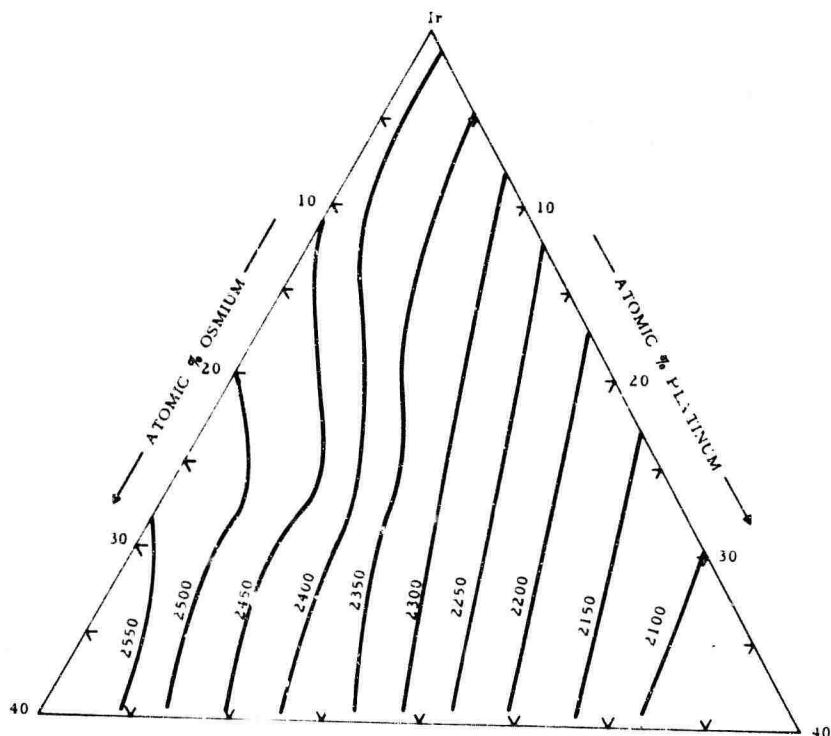


Figure 2. Solidus Temperatures of Iridium-Osmium-Platinum Alloys.

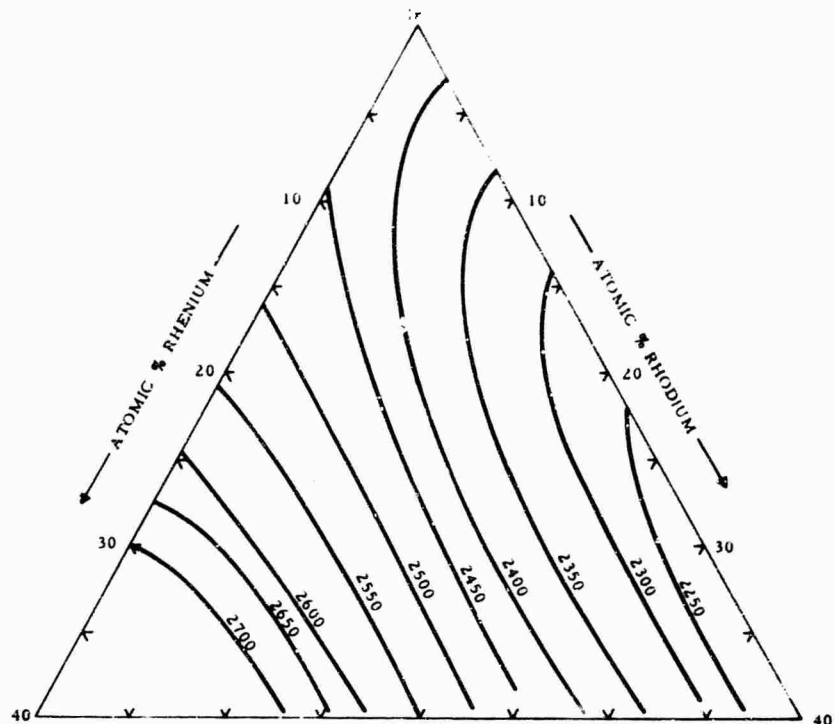


Figure 3. Solidus Temperatures of Iridium-Rhenium-Rhodium Alloys.

2. Solidus Temperatures Between the Metal Components and Carbon

The eutectic temperatures between carbon and the above metal elements, the iridium-rich binary, as well as the ternary alloys were measured; the compositions of these eutectics were determined. The metal-carbon binary eutectic temperatures, as well as the eutectic compositions, are given in Table 2. In particular, it should be noted that the iridium-carbon eutectic temperature occurs at  $2303 \pm 15^\circ\text{C}$ , and not at  $2110^\circ\text{C}$  as reported by Criscione, et al. <sup>(1)</sup>. This higher value is in agreement with the earlier reported temperature of  $2296^\circ\text{C}$  <sup>(2)</sup>. The investigation showed that contaminate elements, such as silicon, would significantly lower the iridium-carbon eutectic temperature.

In every case, the binary carbide systems were found to be of the simple eutectic-type; the earlier reported "carbide" phases were not observed in any of the alloys with X-ray and metallographic analyses.

Table 2. Compositions and Temperatures of the Binary Metal-Carbon Eutectics.

System	Eutectic Composition (At % C)	Eutectic Temperature (°C)
Rhenium-Carbon	20 $\pm$ 2	2466 $\pm$ 15
Osmium-Carbon	17.5 $\pm$ 2	2732 $\pm$ 15
Rhodium-Carbon	16 $\pm$ 2	1662 $\pm$ 15
Iridium-Carbon	6.5 $\pm$ 2	2303 $\pm$ 15
Platinum-Carbon	3 $\pm$ 2	1732 $\pm$ 15

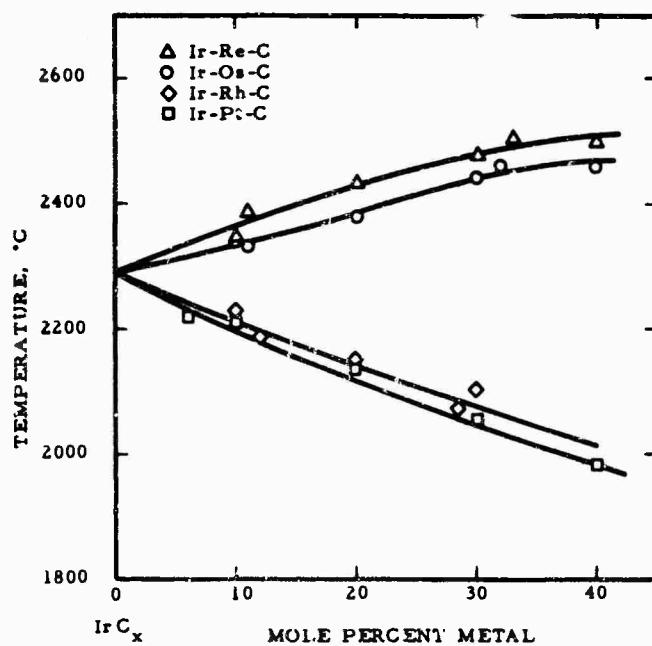


Figure 4. Eutectic Trough Melting Temperatures in the Ir-Re(Os, Rh, Pt)-C Ternary Systems.

The eutectic trough temperatures of the iridium-rich ternary alloys were determined as depicted in Figure 4. The iridium-rhenium-carbon alloys exhibited the highest eutectic trough temperatures; whereas, the platinum containing alloys were observed to be the lowest melting. The eutectic trough compositions were found to vary curvilinearly in the ternary systems as a function of the second metal addition.

The solidus temperatures of the ternary metal alloys in the presence of carbon are summarized in Figures 5, 6, and 7. As can be seen, all of the eutectic-surface(s)—temperatures were above 2000°C, and the majority of these are above 2200°C. The alloys' melting temperatures were observed to be lowered, on the average, by approximately 100°C in the presence of graphite. However, more pronounced temperature depressions were measured with the rhenium-rich metal specimens. X-ray and metallographic evaluation revealed the majority of the samples to be composed of two phases, i. e., the face-centered cubic metal solid solution and graphite. From metallographic examinations of chemically analyzed alloys, the carbon concentrations of the eutectic surface(s) were estimated to vary between 6 and 14 atomic percent.

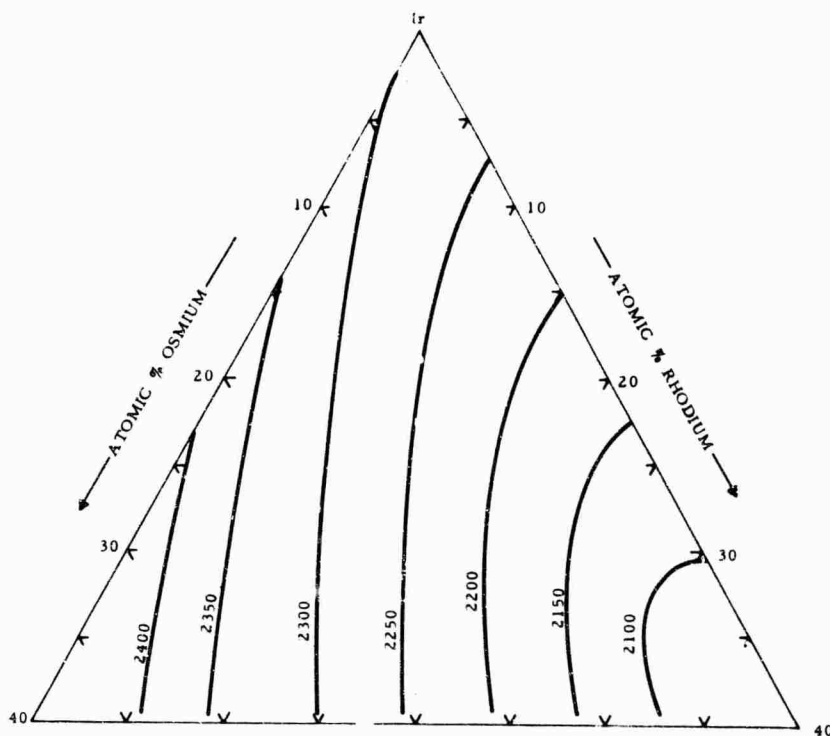


Figure 5. Solidus Temperatures of Iridium-Osmium-Rhodium Alloys in the Presence of Carbon.

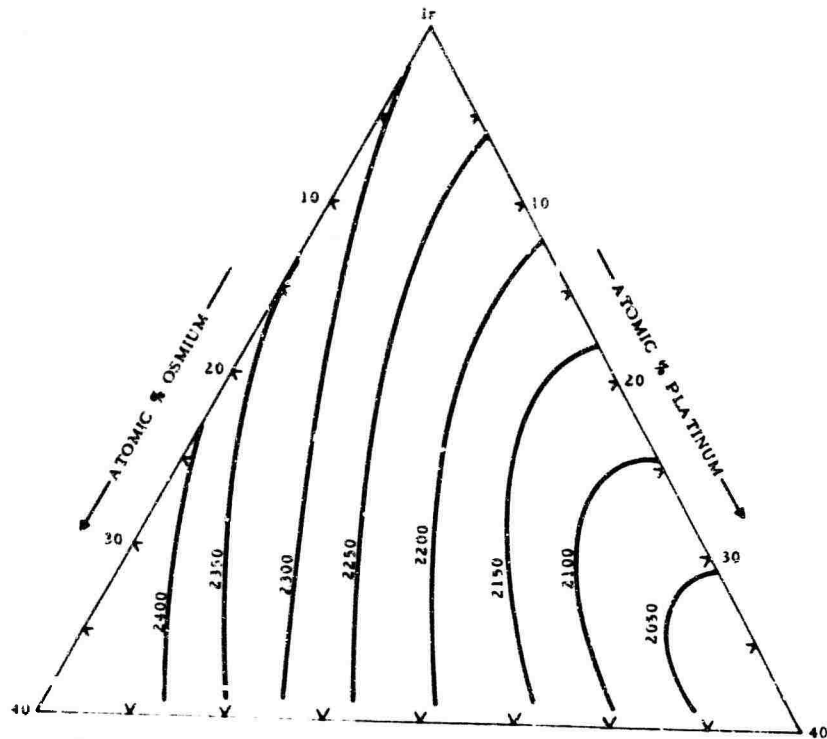


Figure 6. Solidus Temperatures of Iridium-Osmium-Platinum Alloys in the Presence of Carbon.

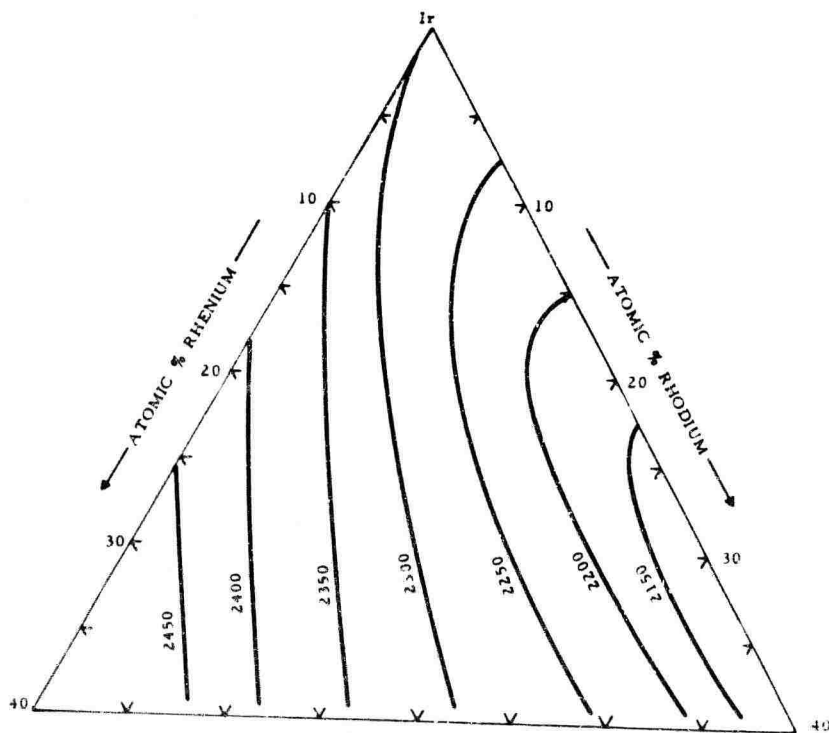


Figure 7. Solidus Temperatures of Iridium-Rhenium-Rhodium Alloys in the Presence of Carbon.

### 3. Theoretical Analysis of the Data

A thermochemical evaluation of the metal and metal-carbon systems was performed in an effort to derive parameters which would allow the 'a priori' prediction of the solidus temperatures between the metal components and graphite. The simplified approach which was used here was found to adequately describe the melting temperature depression of the metal components brought about by carbon additions.

### 4. Thermal Expansion Characteristics of the Metal Alloy Systems

The thermal expansion properties of seven alloys were measured up to 1800°C using X-ray diffraction and dilatometric techniques. The expansion characteristics of these alloy systems are depicted in Figure 8 along with the thermal expansion range for presently available commercial graphites. The equations describing the mean coefficients of thermal expansion for these alloys were computed by an IBM-7094 computer and are given in Table 3.

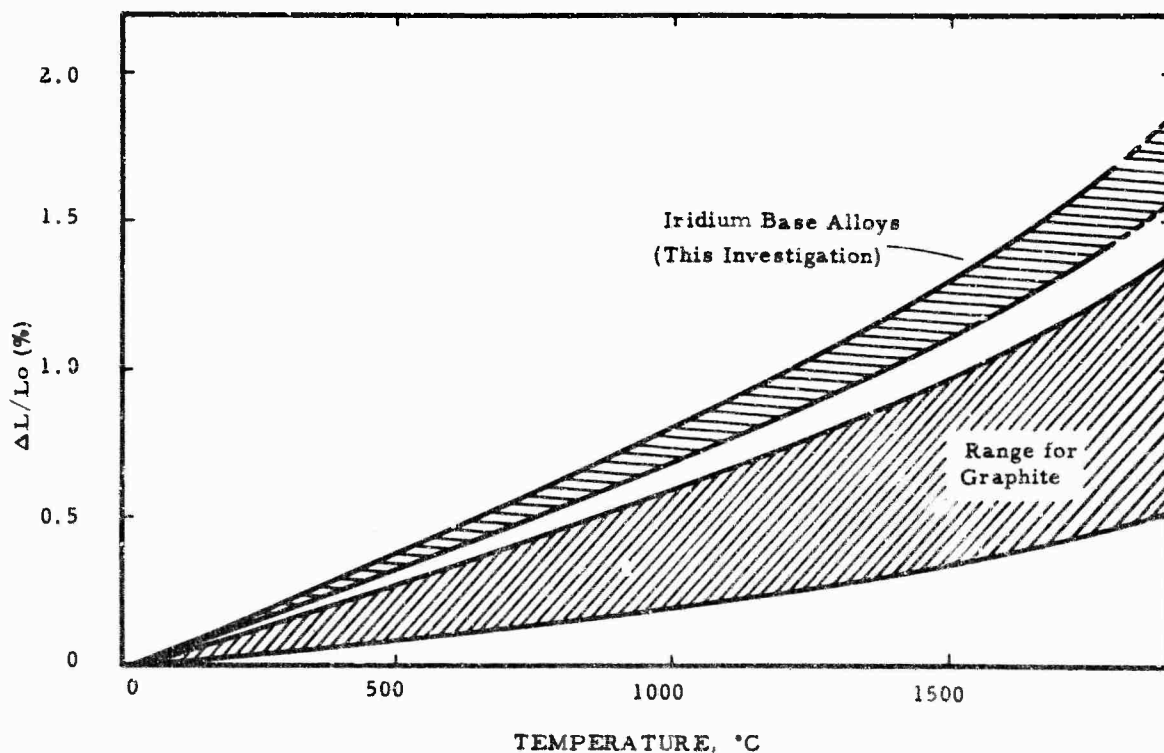


Figure 8. Thermal Expansion Characteristics of the Iridium-Base Alloys Compared to Commercial Grades of Graphite.

Table 3. Equations for the Mean Coefficients of Thermal Expansion for Some Iridium-Base Alloys

Alloy System	Composition (Atomic Percent)	$\alpha$
Ir-Re	90/10	$6.18 + 0.11 + 0.78 \times 10^{-3} T + 0.19 \times 10^{-6} T^2$
Ir-Os	75/25	$6.08 + 0.13 + 0.69 \times 10^{-3} T + 0.24 \times 10^{-6} T^2$
Ir-Rh	75/25	$7.46 + 0.13 + 0.20 \times 10^{-3} T + 0.48 \times 10^{-6} T^2$
Ir-Pt	75/25	$7.44 + 0.07 - 0.16 \times 10^{-3} T + 0.76 \times 10^{-6} T^2$
Ir-Os-Rh	75/12.5/12.5	$6.20 + 0.09 + 1.36 \times 10^{-3} T + 0.01 \times 10^{-6} T^2$
Ir-Os-Pt	75/12.5/12.5	$6.67 + 0.14 + 0.79 \times 10^{-3} T + 0.24 \times 10^{-6} T^2$
Ir-Re-Rh	75/12.5/12.5	$6.27 + 0.11 + 0.68 \times 10^{-3} T + 0.25 \times 10^{-6} T^2$

## II. LITERATURE REVIEW

### A. METAL SYSTEMS

The melting points of the metallic elements of interest for this investigation are given in Table 4; probably the best known value for this group is the melting point of platinum. Giessen<sup>(7)</sup>, in his investigation of the tantalum-iridium system, indicated that the iridium-rich alloys were sensitive to oxygen pick-up, and therefore the value of 2357°C for the melting point of iridium might be lower than the true melting temperature. The reported melting temperatures of rhenium (~3180°C) and osmium (3050°C) make these metals the second and third highest melting elements respectively; only tungsten, (3423°C)<sup>(18)</sup> melts higher.

Since the alloy systems to be investigated should be primarily single phase, it is necessary to have a knowledge of the alloying behavior of iridium with the secondary-metal constituent, i.e., rhenium, osmium, rhodium, and platinum. A survey of the literature shows that the iridium-rhenium, iridium-osmium, and iridium-platinum binary metal systems have been investigated. Because of the fact that the metal components of these binary

Table 4. Literature Values for the Melting Points of Platinum, Rhodium, Iridium, Osmium, and Rhenium.

Metal	Melting Point °C	Reference
Platinum	1760 $\pm$ 2	Oriani & Jones, 1954 (3)
Platinum	1769 $\pm$ 11	Roeser, et al., 1931 (4)
Rhodium	1966 $\pm$ 3	Stimson, 1961 (3)
Rhodium	1960*	Oriani & Jones, 1954 (5)
		Roeser and Wensel, 1934 (6)
		Stimson, 1961 (5)
Iridium	2357 $\pm$ 25	Giessen, 1962 (7)
Iridium	2378 $\pm$ 10	Rapperport & Smith (8)
Iridium	2443*	Stimson, 1961 (5)
		Raub, 1959 (9)
Iridium	2454	Tylkina, et al., 1962 (10)
Osmium	2970	Taylor, et al. (11, 12)
Osmium	3045 $\pm$ 30	Knapton, et al., 1960 (13)
Osmium	3050*	
Rhenium	3140 $\pm$ 20	Knapton, et al., 1960 (13)
Rhenium	3160	Jaeger and Rosenbohm, 1933 (14)
Rhenium	3170 $\pm$ 60	Agte, et al., 1931 (15)
Rhenium	3180 $\pm$ 20	Sims, et al., 1955 (16)

\*Current accepted literature value (17)

systems have different crystal structures (hexagonal closest-packed and face-centered cubic), two basic types of phase equilibrium diagrams are encountered.

Osmium, as well as rhenium, crystallizes with a hexagonal (hcp) lattice, and both form characteristic, peritectic-type equilibrium diagrams with the face-centered cubic iridium<sup>(10, 19)</sup>, (Figures 9 and 10). An extensive  $\alpha$ -fcc solid solution is formed in both systems, and the addition of both osmium and rhenium raise the melting temperature of iridium by

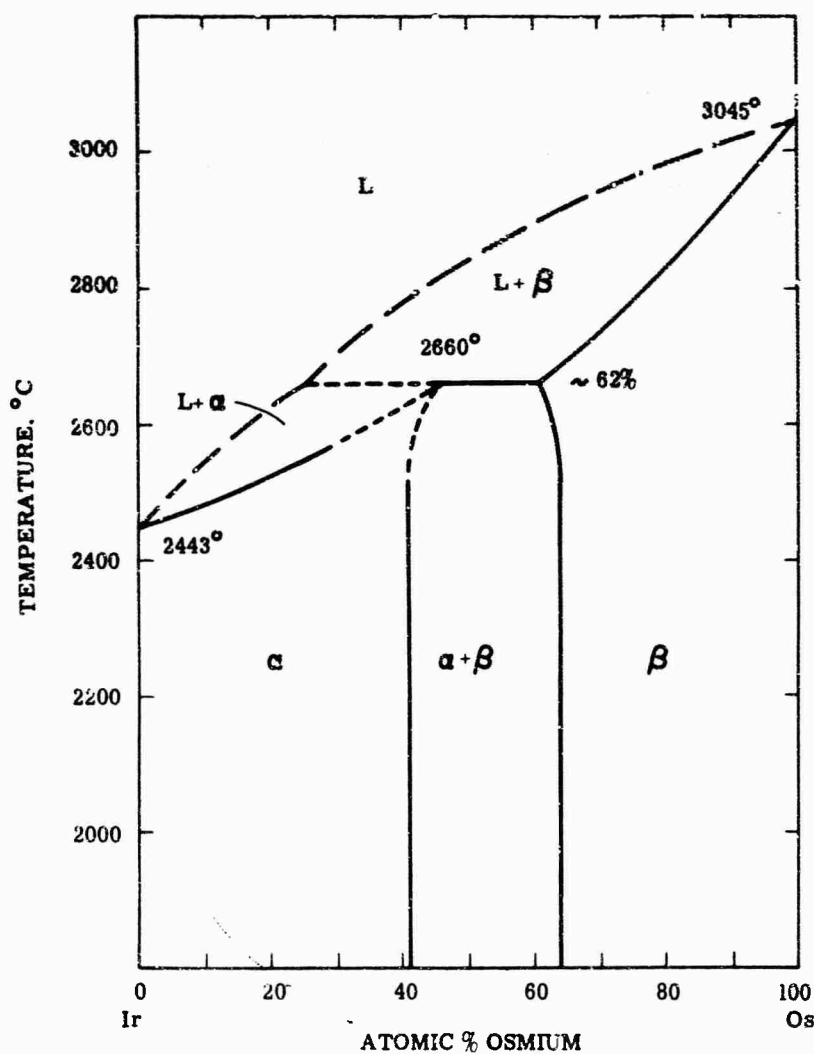


Figure 9. The Iridium-Osmium Phase Diagram.  
(R.D. Reiswig and J.M. Dickinson, 1964)

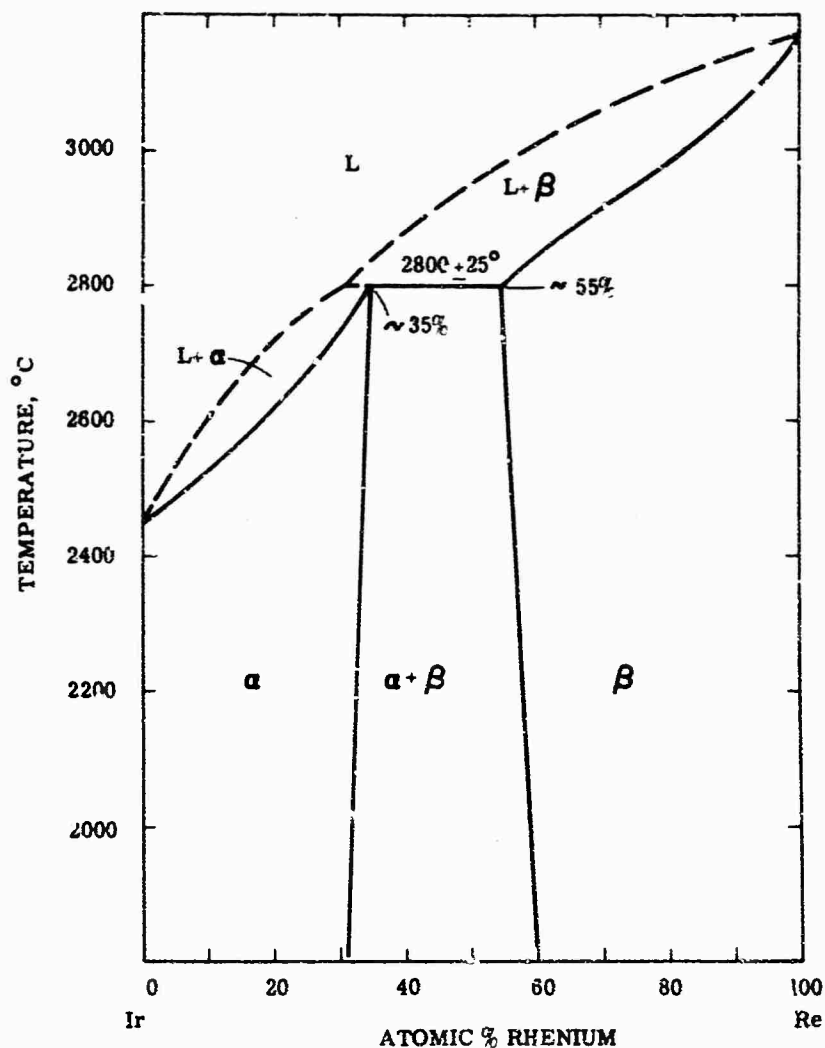


Figure 10. The Iridium-Rhenium Phase Diagram.  
(M.A. Tylkina, et al., 1964)

several hundred degrees, i.e. with  $\sim 46$  atomic percent osmium the solidus temperature is increased to  $2660^\circ\text{C}$ <sup>(19)</sup>; whereas an addition of approximately 35 atomic percent rhenium raises the melting temperature to  $2800^\circ\text{C}$ <sup>(10)</sup>. Earlier work by Haase and Schneider,<sup>(20)</sup> in investigating the iridium-rhenium system for possible thermocouple application, indicated the  $\alpha$ -fcc solid solution to extend to only 5 atomic percent rhenium; however, Tylkina, et al.<sup>(10)</sup>, suggested that these alloys did not reach complete equilibrium.

The alloy system of platinum with iridium shows the two face-centered cubic cells form a continuous series of solid solutions at high temperatures; at lower temperatures the solid solution becomes immiscible<sup>(21, 22)</sup> (Figure 11). The melting temperatures were indicated to vary nearly linearly from the melting point of platinum to that of iridium.

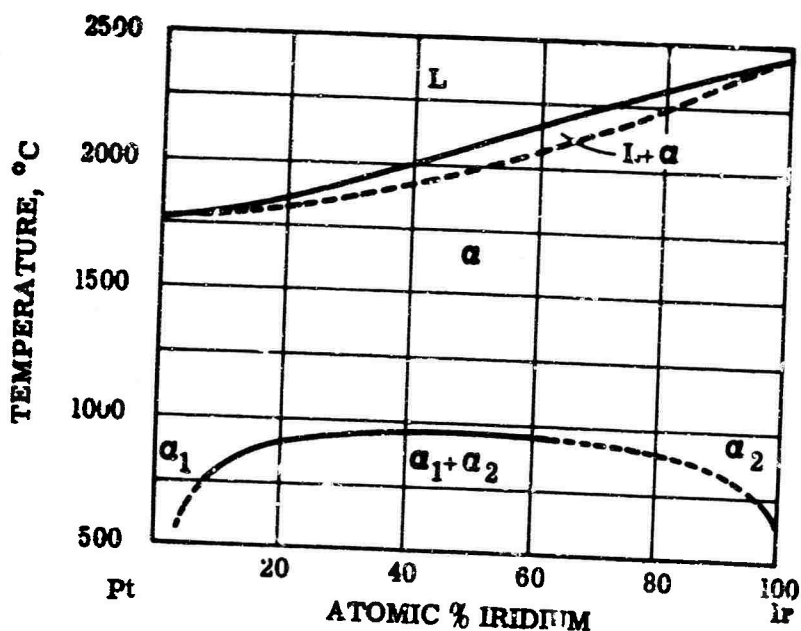


Figure 11. The Iridium-Platinum Phase Diagram.  
(Compiled by A.S. Darling, 1960).

Although the iridium-rhodium system has not been investigated, it is believed that it will resemble the iridium-platinum diagram; a miscibility gap will probably exist at lower temperatures and a complete series of solid solutions will be formed at elevated temperatures<sup>(9)</sup>. Figure 12 gives the lattice parameters reported for the iridium-rhodium alloys<sup>(9)</sup> as well as those reported for iridium-rhenium<sup>(10)</sup> and iridium-platinum<sup>(21)</sup> combinations. It should be noted that the value given for the lattice parameter of pure iridium by Tytkina, et al.<sup>(10)</sup>, was  $3.8312 \text{ \AA}$ ; it is believed that this value is actually in kX units and should be listed as  $3.8389 \text{ \AA}$ , since this value compares much more favorably with the currently accepted literature value of  $3.8394 \text{ \AA}$ <sup>(23)</sup>. Figure 12 has been corrected accordingly.

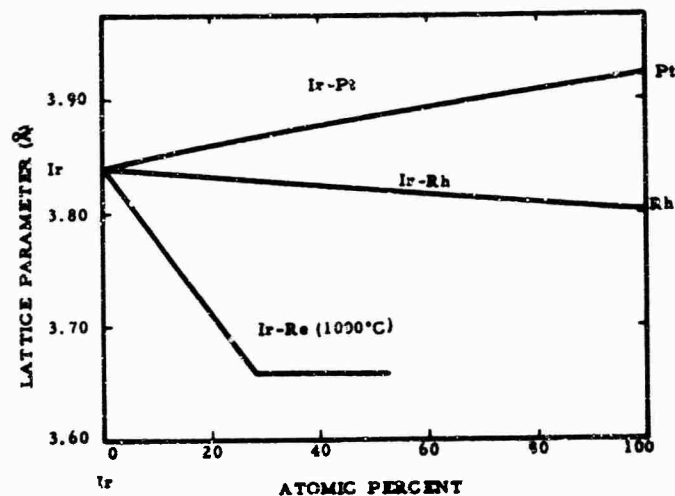


Figure 12. Lattice Parameters of the FCC-Solid Solutions of Iridium with Rhenium, Rhodium, and Platinum.

No information pertaining to ternary or higher order systems involving these particular metals was found in the literature.

#### B. METAL-CARBON SYSTEMS

The interaction of the platinum group metals as well as rhenium with carbon has not been extensively reported in the literature, although recently partial investigations have been reported by M.R. Nadler and C.P. Kempter<sup>(2)</sup>, E. Raub and G. Falkenburg<sup>(24)</sup>, and J.M. Criscione et al.<sup>(1)</sup>.

In earlier experiments by T.J. Collier, et al.<sup>(25)</sup>, the platinum-carbon eutectic temperature was rigorously determined to be  $1734 \pm 3^\circ\text{C}$  ( $1730 \pm 3^\circ\text{C}$  corrected to conform with the 1949 International Temperature Scale<sup>(26)</sup>) at a carbon concentration of less than 1.2 weight percent (16.5 atomic percent). The latter value was the analyzed carbon content of an originally pure platinum ingot which was held in contact with a graphite crucible above the eutectic temperature for one-half hour. Metallographic examination showed the presence of rather large graphite flakes in a eutectic

matrix, thus indicating the eutectic composition to be less than 16.5 atomic percent carbon. These investigators<sup>(25)</sup> also observed a slight expansion of the platinum lattice in the presence of graphite subsequent to melting.

The most complete investigation that has been reported on these particular metal-carbon diagrams is that by J. E. Hughes<sup>(27)</sup> in the rhenium-carbon system (Figure 13). The results of this research showed the

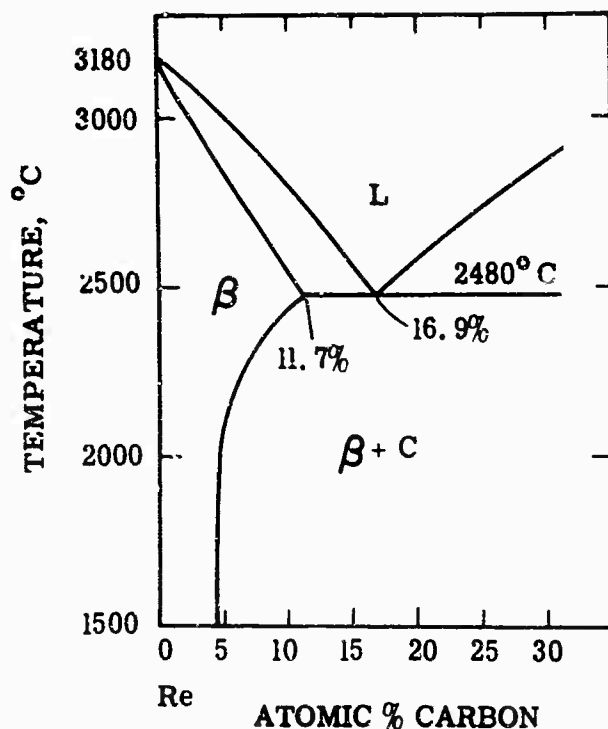


Figure 13. The Rhenium-Carbon Phase Diagram. (J. E. Hughes, 1959)

hexagonal rhenium lattice takes approximately 11.7 atomic percent carbon into solution. The carbon additions were observed to increase the lattice parameters to:  $a=2.792 \text{ \AA}$  and  $c = 4.471 \text{ \AA}$  as compared to starting parameters of:  $a = 2.760 \text{ \AA}$ , and  $c = 4.458 \text{ \AA}$ . The system was reported to be of the eutectic-type in which no intermediate phases occur; the eutectic was located at 16.9 atomic percent carbon and 2480°C. However, in a recent investigation of metal diffusion in pyrolytic graphite by Hammond<sup>(28)</sup>, it was

indicated that a previously unreported carbide phase was formed. It was reported that metallic rhenium would react with graphite near 2100°C to produce the new phase. Only small quantities of this phase could be obtained, but a diffraction pattern was produced which could be indexed with a simple cubic lattice with a parameter of 2.8 Å. The composition of the phase was not determined, and strong indications were given that the phase is metastable.

The phase diagrams of Ir (Os, Rh)-C have not been completely investigated, although partial investigations have been performed. M. R. Nadler and C. P. Kempter<sup>(2)</sup> measured the eutectic temperatures of the platinum group metals with carbon (Table 5), but they did not indicate the compositions of the eutectics. J. M. Criscione et al.<sup>(1)</sup> have reported the eutectic temperature in the iridium-carbon system to be  $2110 \pm 25^\circ\text{C}$ ; this temperature is considerably lower than that shown in Table 5. In this respect, F. Raub and G. Falkenburg<sup>(24)</sup> report that small impurities, especially silicon, form low melting phases with the platinum group metals which in turn would cause drastic melting point depressions in the metal-carbon systems. These authors<sup>(24)</sup> also have indicated that the platinum group metals form simple eutectic systems with carbon; the carbon solubility is low and does not lead to measurable changes in the lattice parameters in the metal phase. On the other hand, Kempter and Nadler<sup>(29)</sup> have reported the existence of intermediate carbide phases, namely OsC and RuC, in the respective binary systems. Subsequent research by Jeantet and Knapton<sup>(30)</sup> failed to find these carbides, and they indicated that the reported phases were actually impurity metal carbides. Further investigations by Kempter<sup>(31)</sup> showed that these phases do exist and exhibit a hexagonal WC-type structure. It was noted, however, that "little is known of the optimum conditions of preparation" and "that the yield of RuC and OsC was strongly dependent on the metal:graphite ratio of the starting material, the synthesis temperature, and heating time, thus suggesting that the two carbides are metastable or have a narrow range of temperature stability"<sup>(31)</sup>.

The only result pertaining to ternary or higher order metal-carbon systems that was reported in the literature was a single melting temperature of  $1932 \pm 17^\circ\text{C}$  for an iridium-rhodium-carbon alloy (Ir-50 Rh, wt %)<sup>(2)</sup>.

Table 5. Eutectic Temperatures in the Platinum Group Metal-Carbon Systems (M.R. Nadler and C.P. Kempter, 1960).

Metal	Melting Point °C	Metal-Carbon Solidus Temperature °C
Ruthenium	2250	1942 ± 16
Rhodium	1960	1694 ± 17
Palladium	1552	1504 ± 16
Osmium	3045	2732 ± 22
Iridium	2443	2296 ± 16
Platinum	1769	1736 ± 13

### C. THERMAL EXPANSION VALUES

Little information was available in the literature concerning the thermal expansion characteristics of alloys of the metals of interest; only values on iridium-platinum alloy combinations were given<sup>(21, 22)</sup>. The coefficient of thermal expansion were observed to follow a nearly linear compositional dependence from the end elemental values at 300°C.

Values for the linear thermal expansion of these particular metals investigated can be found in most metallurgical reference book<sup>(32, 33)</sup>.

## III. EXPERIMENTAL PROGRAM

### A. STARTING MATERIALS

High purity metal powders of elemental rhenium, osmium, rhodium, iridium, and platinum were the major constituents in the alloys investigated in this program. Carbon containing alloys were made by either adding high purity spectrographic graphite powder to the alloy or by reacting the molten alloy with the graphite crucible in the furnace of the differential analytical apparatus. Chemical analysis of these starting metals were supplied by the vendor, and purity levels of these materials are given below.

The iridium, rhodium, and platinum powders were purchased from J. Bishop and Co., Malvern, Pennsylvania. Impurities in the iridium powder (-325 mesh) were given as (in ppm): Rh-200; Fe-10; Pb-20; K-100; Si-30; Na-50, and the total of all other impurities <25. The rhodium powder (-200 mesh) had analyzed impurity levels of (in ppm): Fe-30; Si-100; Na-20; and the sum of the rest of the impurities <20. The platinum powder had a particle size of <200 mesh and impurity levels of (in ppm): Pd-10; Ir-30; Rh-10; Au-20 with the total of all other impurities being <12.

The osmium powder was purchased from Englehard Industries, Inc., Newark, N.J., and had a purity level of 99.84%. The supplier analysis listed the impurities as  $\text{SiO}_2$ -0.08% and Fe-0.08%.

The rhenium powder was supplied by Chase Brass and Copper Co., Inc., Waterbury, Conn.; the particle size was <200 mesh and the analyzed impurity levels were (in ppm): Fe-23; Al-<1; Ni-<1; Si-<1; and the sum of the other impurities <10.

For carbon containing alloys in which the graphite was introduced into the alloy as powder during its preparation, a spectrographic grade of graphite powder was used. The graphite powder (<74  $\mu$ ) was obtained from Union Carbide; typical analyses specify <6 ppm total impurities and <1 ppm of any one elemental constituent. However, the majority of the carbon containing alloys were prepared by reacting a metal alloy above its solidus temperature 'in situ' with a graphite crucible; in this way graphite was introduced to the alloy. The graphite crucibles used in these experiments were degassed at high temperatures (>2500°C) 'in vacuo' for a period of approximately 10 minutes prior to use. The semiquantitative spectrographic analysis revealed the impurities in the graphite crucibles as follows: Fe, Si and Ca present in residual amounts (.10-.01%); B, Al, Mg, Cu present in trace amounts (.01-.001%); S-.04%, ash-0.30%.

## B. EXPERIMENTAL TECHNIQUES

### 1. Alloy Preparation

The alloys for these investigations were prepared by standard powder metallurgical techniques, and the description of these processes are given in the following paragraphs under the proper heading.

#### a. Melting Point Alloys (Pirani Technique)

Alloys which were to be used for melting temperature determination were prepared almost exclusively by cold-pressing the powder materials. For this operation, two specially fabricated split-dies were available; one produces a 24 mm long sample and, the other 34 mm long samples (Figure 14). The pressed specimen requires no further grinding, drilling, etc.; this saves on the costly material which would be lost in these operations. Figure 15 shows a cold-pressed, 24 mm long Pirani melting point alloy; note the black-body hole for temperature measurements which is formed during the pressing by a retractable 0.6 mm diameter pin.

The majority of the alloys did not have sufficient strength to be used in the melting point furnace after cold pressing, and, therefore, were sintered prior to melting. The sintering was performed at temperatures between 1400°C and 1800°C depending on the composition of the sample. The alloys were placed on a tantalum plate which was in turn loaded in a tantalum can and then heat treated in high vacuum ( $<10^{-5}$  torr) in a Degussa bell furnace fitted with a direct resistance heated tantalum tube element.

Figures 16 and 17 give the compositions of the iridium-osmium-rhodium and iridium-rhenium-rhodium alloys which were prepared for melting point determinations. The compositions of the iridium-osmium-platinum alloys were identical to those prepared in the iridium-osmium-rhodium system (Figure 16).

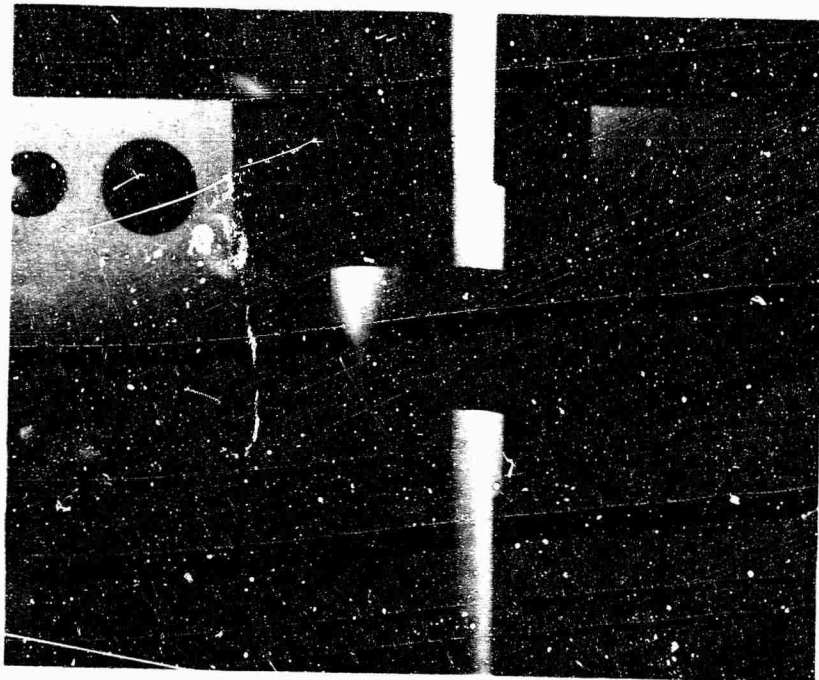


Figure 14. Cold-Pressing Die for Preparation of Pirani Melting Point Specimens.

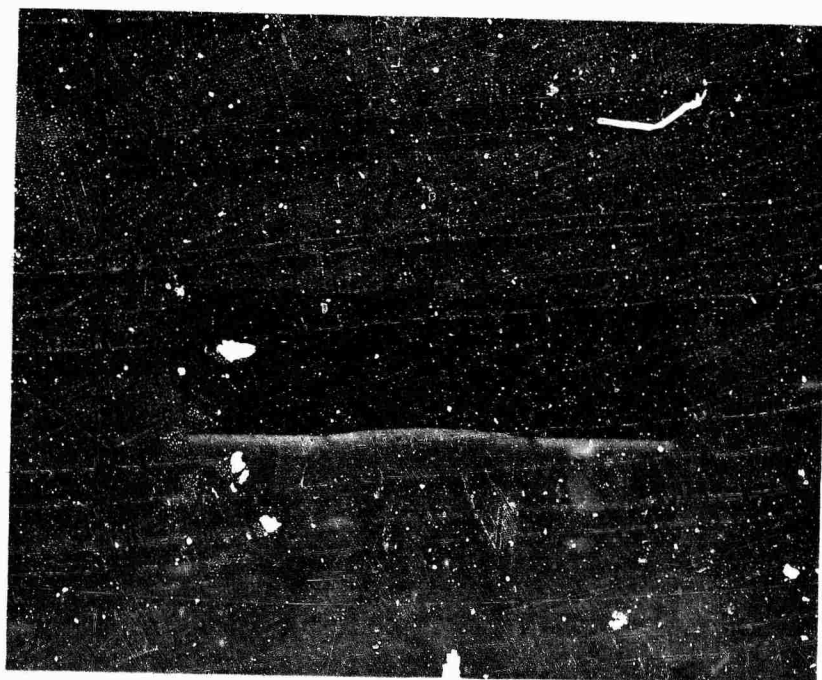


Figure 15. Cold-Pressed Pirani Melting Point Specimen (3 x 4 x 24 mm).

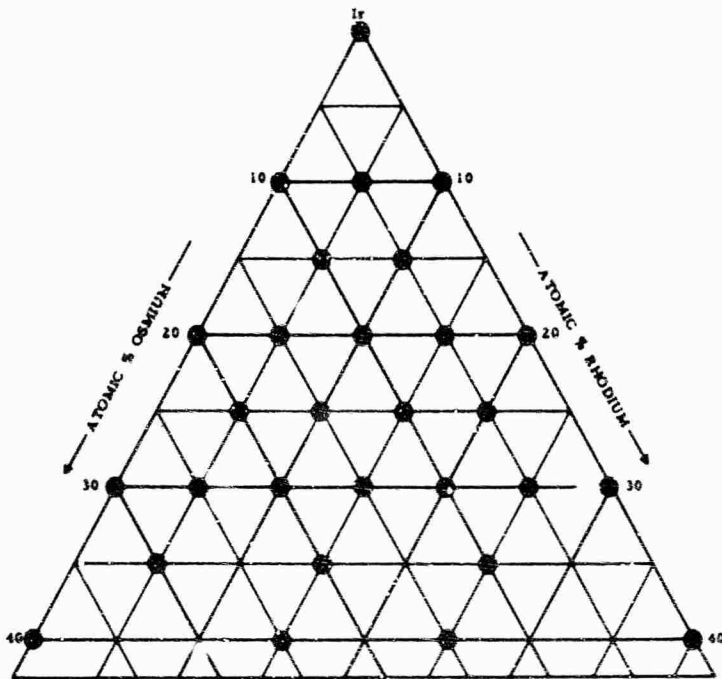


Figure 16. Compositions of Iridium-Osmium-Rhodium Alloys Prepared for Melting Temperature Investigation.

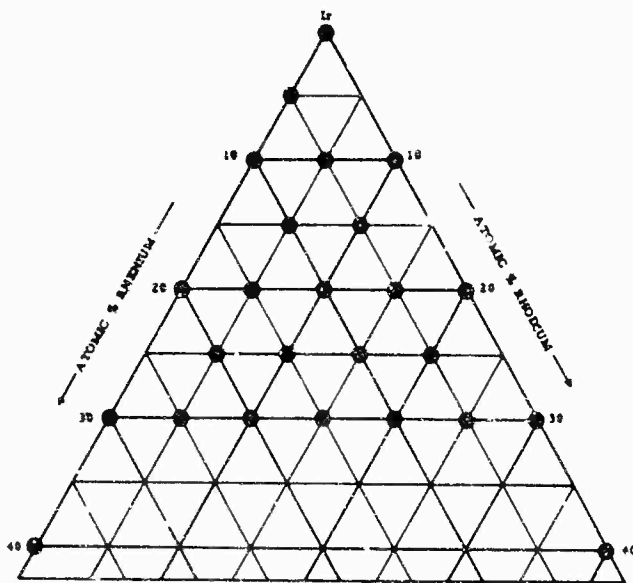


Figure 17. Compositions of Iridium-Rhenium-Rhodium Alloys Prepared for Melting Temperature Investigations.

## b. Arc-Melted Alloys

Arc-melted alloys for metallographic studies were prepared by initially hot-pressing a well-blended mixture of elemental powders in cylindrical graphite dies; these pellets were then arc-melted.

The design of the hot press employed in operation allows very-fast heating and cooling rates, thus minimizing the reaction of the alloy material with the graphite container; a complete hot pressing cycle required only two to five minutes. The pressure applied to the powder during this operation is of the order of several hundred atmospheres, and the temperature capability of this apparatus is greater than 3400°C. Previous studies in the laboratory have shown the reaction zones of the pressed material with graphite to be nominal<sup>(34)</sup>; however, the samples were always surface ground prior to arc-melting to remove any graphite which might be present.

Arc-melting of the alloy material was accomplished with a Zak button arc furnace. The hot-pressed buttons were placed in formed crucibles in the copper hearth; the system was purged three times with high purity helium before melting. A non-consumable tungsten electrode was employed during the melting operation. The buttons were turned over at least once to insure that entire alloy had been molten, as well as to obtain a homogeneous alloy. Chemical analysis of the carbon containing arc-melted samples showed the carbon losses to be 0.5 to 2.0 atomic percent; the later value was observed only in the higher melting specimens.

Samples were prepared for metallographic studies in the binary, ternary, and quaternary systems. The primary purpose of these investigations was to define the compositional region of the eutectics. Generally, three to five, two-gram alloys were prepared for the metal-carbon binary systems. The specimens were placed at five atomic percent intervals and therefore, the eutectic location could be estimated within at least  $\pm 2$  atomic percent carbon. A smaller number of ternary alloys were arc-melted since a

number of DTA specimens were available for metallographic studies. For the eutectic surface determinations, twenty-three alloy combinations were prepared by arc-melting in addition to the DTA alloys. It was found that these alloys, in conjunction with the previously determined binary and ternary eutectic compositions, were sufficient to closely approximate the composition of the eutectic surfaces in the three quaternary systems.

c. Dilatometric Specimen and AFML Test Body  
Fabrication

Seven alloys were prepared to obtain representative thermal expansion data for the systems investigated. These alloys are also to be delivered to the Air Force Materials Laboratory for further studies.

The alloys were prepared by electron-beam melting the cold-pressed alloy bars in a 75 KW Heraeus furnace. The vacuum during melting was maintained at pressures of less than  $5 \times 10^{-5}$  Torr. The alloys were melted, turned over, and remelted until a dense, gas-free, homogeneous ingot was obtained (Figure 18). Each ingot weighed approximately sixty grams. These ingots were subsequently given a homogenizing treatment at 1600°C for six hours prior to machining them to the desired shape.

The machining of the alloys presented some difficulty. Because of the shape and also because of the hardness and toughness of the alloys, they could not be turned down on a lathe equipped with a cutting tool. However, they could be relatively easily shaped on a lathe which was equipped with a grinding wheel. The finished product was a cylinder between 1 and 1-3/4" in length and approximately 0.20" to 0.30" in diameter. The osmium containing alloys were more difficult to handle than the other alloys, and they could be fractured during preparation if excessive care was not exercised. Figure 19 shows a finished thermal expansion specimen.

An X-ray diffraction pattern was made of the material from each of the ten specimens to determine the final composition. From these results it was concluded that the final compositions were within  $\pm 3$  atomic percent of the starting compositions.

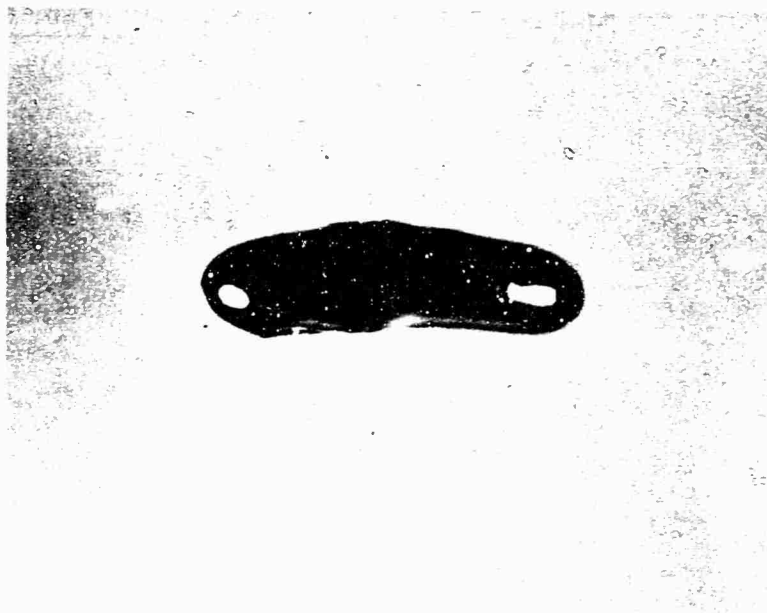


Figure 18. Electron-Beam-Melted Iridium-Base Alloy Ingot .

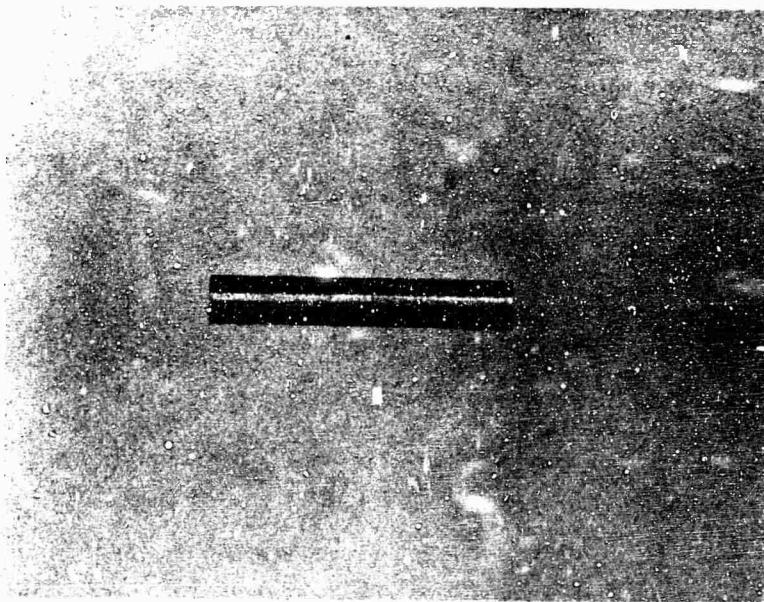


Figure 19. Machined Sample for Dilatometric Studies.

## 2. Melting Point Studies (Pirani-Technique)

The apparatus used in these studies employs direct resistance heating to melt the sample material. In the furnace a small alloy bar is placed against two tungsten plates and is then clamped between two water cooled copper electrodes. One of the electrodes is movable to allow for the thermal expansion and/or sintering which occurs while the sample is being heated. This electrode is provided with a lever arm which can be adjusted externally to apply a desired constant load which ensures good electrical contact between the specimen and the electrodes. Figure 20 shows an interior view of the furnace. For a more detailed description of the apparatus, refer to a report which will appear under another contract carried out in this laboratory<sup>(35)</sup>.

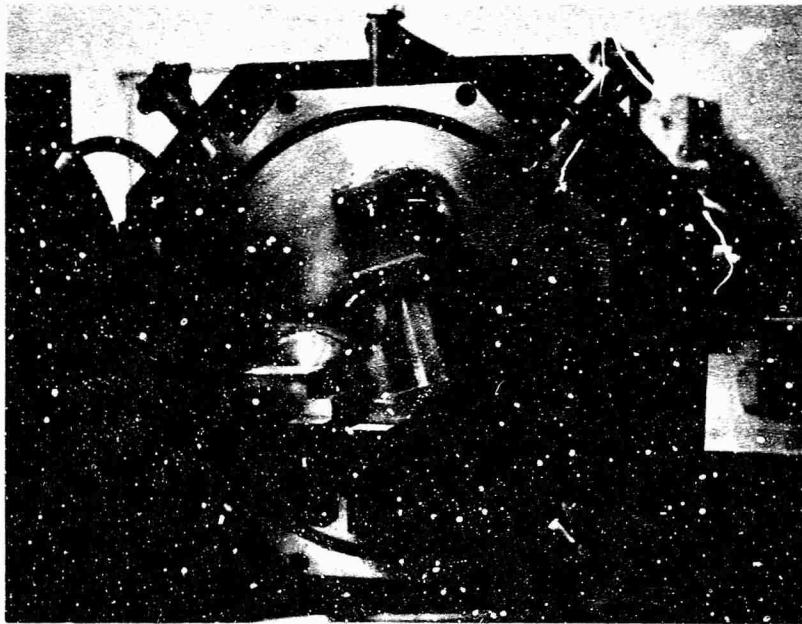


Figure 20. View of the Interior Portion of the Melting-Point Furnace.

The furnace can be operated in vacuum or in an inert gas at pressures up to 2.5 atmospheres. The general operational procedures in these studies was to purge the chamber three times with high purity helium, then degass the alloy in vacuum between 1400° to 1600°C and finally fill the chamber to 1-1/2 atmospheres of helium before melting the alloy.

The temperature of the sample was measured with 'Pyro' optical micropyrometer using the black body hole as the temperature reference sight. The micropyrometers are regularly checked against a standard temperature source which has been calibrated and certified by the National Bureau of Standards. In addition, the pyrometers are also periodically checked directly against a standard pyrometer which also has been calibrated and certified by the National Bureau of Standards.

The temperature corrections which are to be applied to these measurements have been described and validated in an earlier report<sup>(34)</sup>. The corrections that are applied for the quartz viewing port in the furnace as well as for deviation of the black body configuration are given in Figure 21. The latter correction factor is applied because the emissivity is dependent upon the depth to diameter ratio of the black-body hole; in the case of these samples the ratio was approximately 4:1 (2.5 mm depth x 0.6 mm dia), and curve number 4 in Figure 21 gives the applicable correction.

The reproducibility of the measurements are  $\pm 5^\circ\text{C}$  at  $2000^\circ\text{C}$ ,  $\pm 10^\circ\text{C}$  at  $2700^\circ\text{C}$ , and  $\pm 15^\circ\text{C}$  at  $3300^\circ\text{C}$ . These values are in terms of the mean deviation of individual measurements of samples which melt congruently. These uncertainties do not take into account the errors in the calibration pyrometers; but since these errors are of comparable magnitude of those resulting from experimental error, the reported uncertainty in the measurements is  $\sqrt{2}$  times above given values.

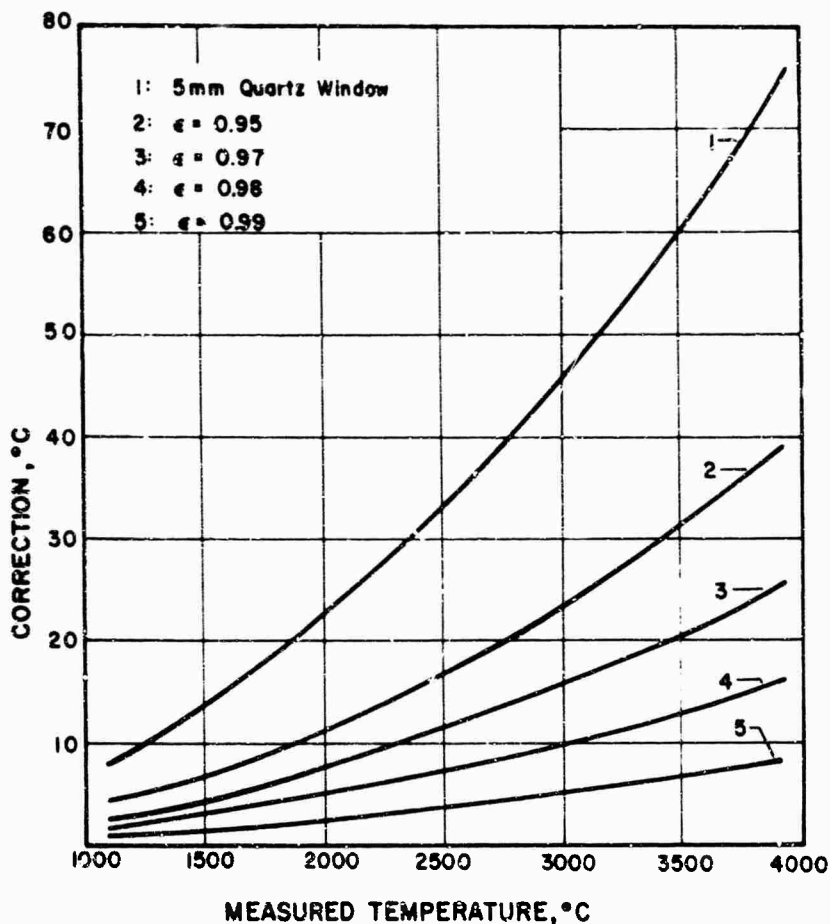


Figure 21. Chart for Temperature Corrections to be Applied to the Temperature Measurements Performed in the Melting Point Furnace.

### 3. Differential Thermal Analytical Investigations

#### a. Equipment Description

This apparatus was used for the determination of the solidus temperatures of the metal alloy graphite combinations for a number of reasons. The first is the conservation of the expensive platinum-group metals; this was accomplished by melting a portion of a previously melted metal alloy in the apparatus in a graphite crucible. By using this technique, both the melting temperature of the metal and the

solidus temperature of the alloy combined with graphite can be accomplished with the same sample. Another advantage of the D.T.A. method is that it is, by design an extremely sensitive device; it allows a greater precision than does the Pirani technique in determining the incipient melting temperature of very heterogeneously melting alloys.

A very complete description of this equipment is given elsewhere<sup>(36)</sup>; therefore, only a brief description of its mode of operation will be given here. This apparatus records the temperature differences, if any, between a reference sample which is known to undergo no phase changes (in our experiments, graphite) and that of the test sample, as the temperature of both is increased (heating cycle) or decreased (cooling cycle). This is accomplished by focussing the emitted radiation from the black body hole of both samples onto a photo cell and alternately interrupting the focussed beam by a chopping mechanism. If a temperature difference does exist between the two samples, it is detected by the photo cell and ultimately results as a  $\Delta T$ -signal on a plotter which records  $\Delta T$  versus temperature. Figure 22 gives a schematic diagram of the set-up of the DTA-apparatus.

The sensitivity of the apparatus, in terms of signal to noise ratio, has been demonstrated to be approximately 20:1 for an enthalpy change of 20 calories at a temperature of 2000°C; enthalpy changes of about 1.5 calories (corresponded to a 1°C temperature difference between the particular test sample and reference material) was clearly distinguishable above the background noise.

The apparatus is equipped with a heating and cooling rate controller with which rates of between 0.5 to 20°C per second are obtainable. This feature allows the augmentation of the  $\Delta T$  signal, i.e. generally, a signal corresponding to a rapid transition can be enlarged by increasing the heating or cooling speeds; the signal resulting from slow transitions may be augmented by decreasing the heating or cooling speeds.

The equipment is capable of operating in either vacuum or at pressures of up to approximately 4 atmospheres. The temperature capability of the furnace is limited (excepting sample-container interactions) only by the sublimation of the

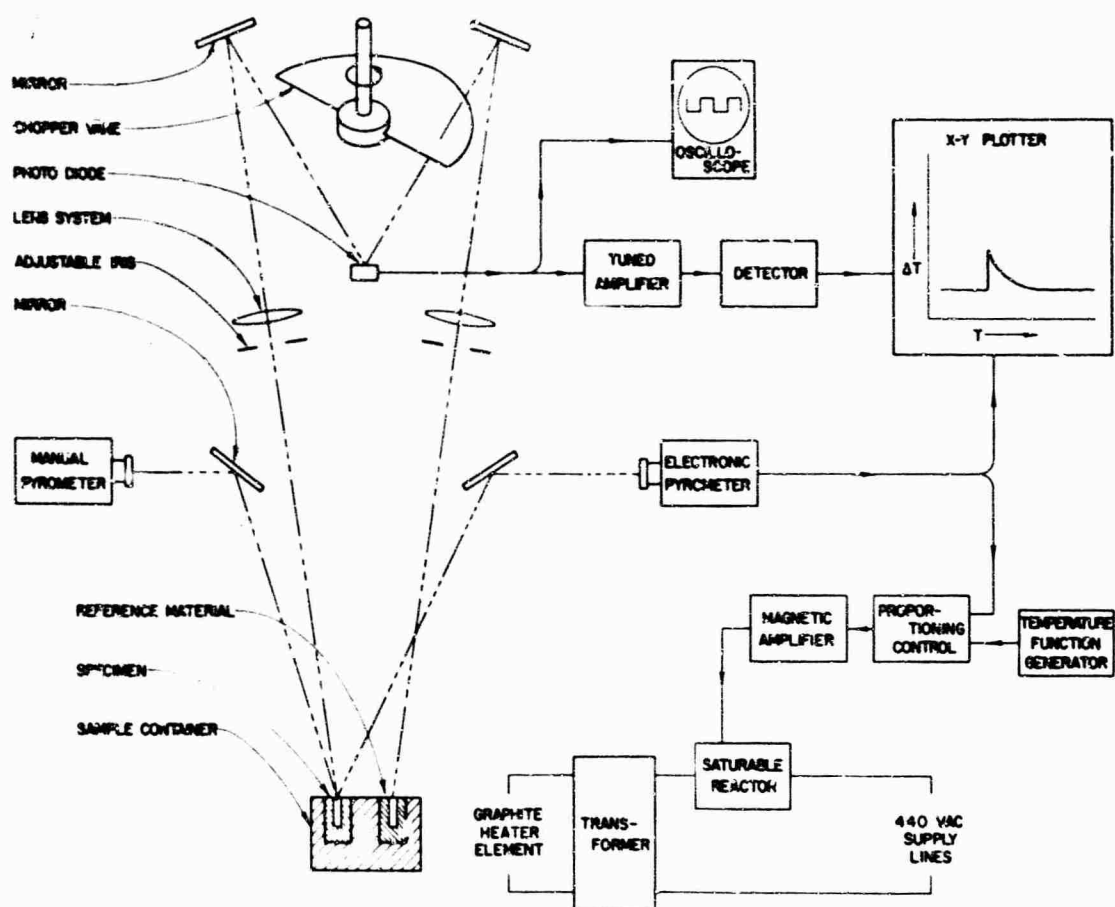


Figure 22. Schematic Diagram Showing the Set-Up of the Differential Thermal Analytical Apparatus.

graphite heater, and therefore, the maximum safe operating temperature is about 3600°C. The temperature is monitored continuously by an electronic radiation pyrometer (thermodot Model TD-6BT-70); this temperature scale is double checked manually by a micropyrometer which is focussed on the black body hole of the test alloy (see Figure 23).

The reproducibility of the temperature measurements are comparable to those obtained from the melting point furnace; however, because of the inherent temperature uncertainties of the apparatus, an accuracy of no greater than  $\pm 20^\circ\text{C}$  is assigned to the temperature measurements reported in these investigations.

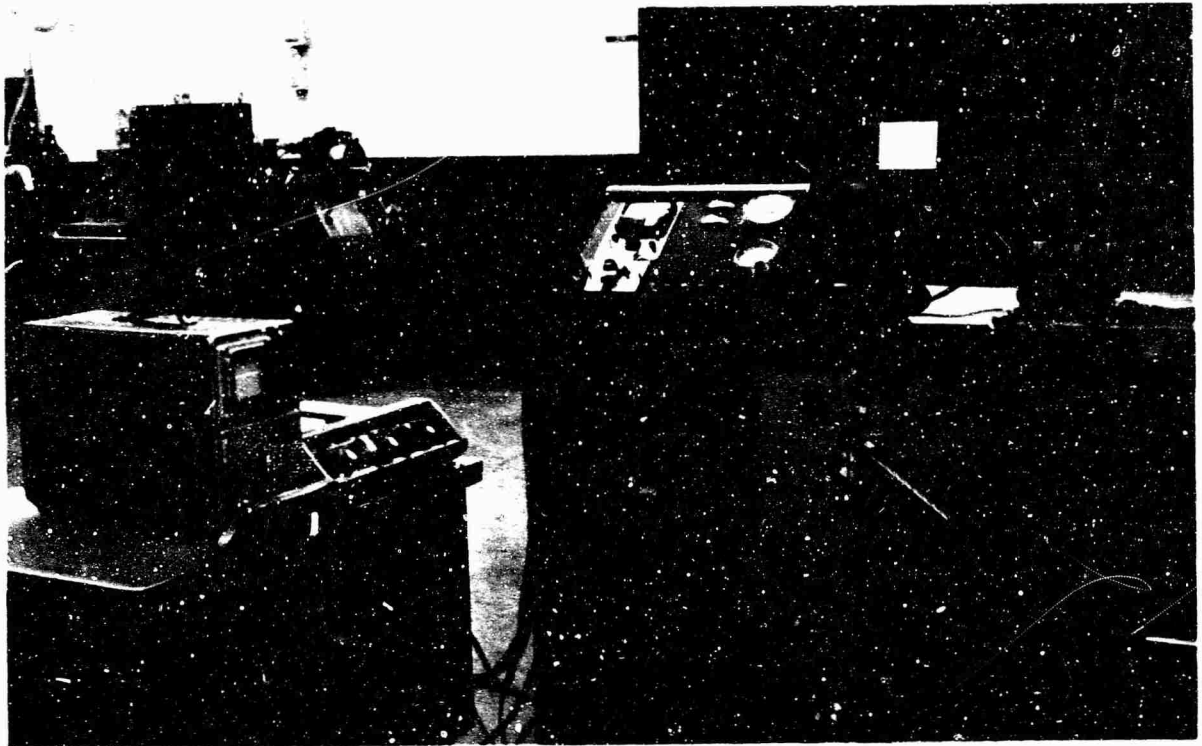


Figure 23. Over-All View of the DTA-Apparatus

- A. Automatic-Recording Electronic Pyrometer
- B. Manually Controlled Micropyrometer

b. Experimental Measurements

A portion of the alloys that had been previously melted in the Pirani-furnace was used for the solidus temperature determination of these alloys in the presence of graphite. Approximately 2 grams of material was placed in a small graphite crucible which had been degassed in vacuum at 2500°C; a cylinder with a hole in it was then inserted in the crucible to serve as a black-body hole (Figure 24).



**Figure 24.** Sectioned Graphite Crucible Subsequent to a DTA - Run, Showing the Sample and Graphite Cap Which Serves as the Black Body Temperature Reference Hole.

The runs were made under 1.5 atmospheres of high purity helium; prior to the runs the system was degassed between 1600 and 2400°C in vacuum. The best results for the heating curves were obtained when the heating rate was  $<3^{\circ}\text{C}$  per second. The majority of alloys were found to readily supercool (even with very slow manually controlled cooling rates,  $<1/4^{\circ}\text{C}$  per second), and therefore, the majority of the cooling curves had to be disregarded for data interpretation.

Normally, sufficient carbon is dissolved after one run above the alloys' melting temperature to observe the eutectic temperature on the next run. Four runs were usually made in order to obtain consistent data for the eutectic temperature. In the binary metal-carbon system, for example, the measurements did not, in any case, vary by more than  $\pm 8^{\circ}\text{C}$  from the mean value obtained for the eutectic temperature; although

as mentioned above, an accuracy of no greater than  $\pm 20^{\circ}\text{C}$  will be assigned to these temperature measurements.

#### 4. Special Experimental Studies

##### a. Effect of Impurities on the Iridium-Carbon Eutectic Temperature

In view of the fact that it has been reported that silicon and sulfur, impurities that are normally present in commercial grades of graphite, form low melting phases with iridium<sup>(24)</sup>, an experiment was performed which would give some indication of the effects of these impurities on iridium-carbon system.

In these investigations, a piece of iridium foil was heat treated in an environment of lampblack which contained a known amount of a selected impurity element. These experiments were performed in the DTA apparatus described above.

The "foil" was produced by hot-rolling a cold-pressed and sintered iridium bar (3 x 4 x 24 mm) to a final thickness of approximately 0.016". The iridium was obtained from the metal powder described in the section on starting materials. The rolled foil was then surface ground, and leached in aqua-regia for a period of two hours.

The carbon (lampblack) which was used in these experiments had been previously out-gassed in vacuum at  $2400^{\circ}\text{C}$  for ten minutes. Part of this material was doped with a silicon contaminant of approximately 1 percent by weight; to another portion, a sulfur impurity was added. In order to help prevent the vaporization of the sulfur before it had a chance to react with the iridium, the sulfur was first reacted with some iridium powder and added to the lampblack as an impurity iridium-sulfur compound.

Three separate runs were performed: (a) iridium foil with pure lampblack, (b) iridium foil with silicon contaminated lampblack,

and (c) iridium foil with sulfur contaminated lampblack. The runs were performed under a protective helium atmosphere and were made at a temperature of 2150°C. The material was held in this environment for a period of three hours.

b. Investigations of the "Carbide" Phases of Osmium and Rhenium

Since conflicting reports exist in the literature concerning the existence of carbides of osmium and rhenium, some special investigations were performed in order to prepare these phases.

It has been reported by Kempter<sup>(31)</sup> that the preparation of OsC was dependent upon a number of variables, i.e. equilibration time and temperature, osmium-carbon ratio, etc. The optimum conditions for the formation of this phase were reported to be with Os:C ratios of 1:10 at elevated temperatures (2600°C). Heat treating for a period of approximately four hours was necessary. In one experiment these conditions were repeated identically; a hot-pressed mixture of osmium and graphite (1:10) was placed inside a small cylindrical graphite tube and heat treated in the melting point furnace under a protective helium atmosphere (1.5 atms) for a period of four hours. In addition to this experiment, two diffusion couples were prepared. The couples were prepared by cold pressing and sintering osmium rods (approximately 2.5 dia. x 25 mm length) and pyrolytically depositing a layer of graphite on them by heating the specimens in a helium-methane atmosphere. A small hole was drilled through the graphite for a temperature measuring sight. The first couple was heat-treated near, but below, the eutectic temperature for four hours in an inert atmosphere. The second couple was heat-treated so that the temperature of the osmium-carbon interface was at the eutectic temperature; the sample was held at this temperature for approximately 15 minutes before sufficient melt was formed to cause the sample to sag.

A Re-C diffusion couple was also prepared by the above techniques; this material was equilibrated at approximately 2400°C

for 1-1/2 hours . The temperature was then slowly raised so that the inter-  
face temperature was at the rhenium-carbon eutectic temperature. The  
material was held at this temperature for a period of approximately  
10-15 minutes before the sample started to sag.

The above diffusion couples were examined  
metallographically as well as by X-ray diffraction techniques. The osmium-  
carbon (1:10) alloy was examined only by X-ray diffraction.

## 5. Thermal Expansion Measurements

### a. High Temperature X-ray Diffraction Camera Method

#### (1) Equipment Description and Experimental Techniques

The high temperature X-ray diffraction  
apparatus used in these investigations was a commercially available MRC  
(Model X-86-N-2) Norelco diffractometer attachment. The camera is reported  
to be operable above 2000°C, and is designed to be used in vacuum. The  
camera is designed to scan angles of between 0 and 160° (2θ); however, with the  
protective X-ray radiation shields installed on the diffractometer, the upper  
angle was limited to angles below 140° (2θ). A tantalum ribbon (0.0025" thick)  
was used as both the heating element and sample holder. The temperature  
measurements were made pyrometrically by viewing the heating element through  
a quartz window in the front cover of the camera. Alignment of the equipment  
was accomplished following manufacturer's directions. Figure 25 shows the  
experimental set-up of the apparatus.

Two approaches were used for making  
the temperature measurement during these experiments. The first method was a  
novel approach in which a small tantalum sight tube was positioned on the  
heater to act as a black body hole. The tube was surrounded by the powdered  
material to insure that its interior temperature was representative of that

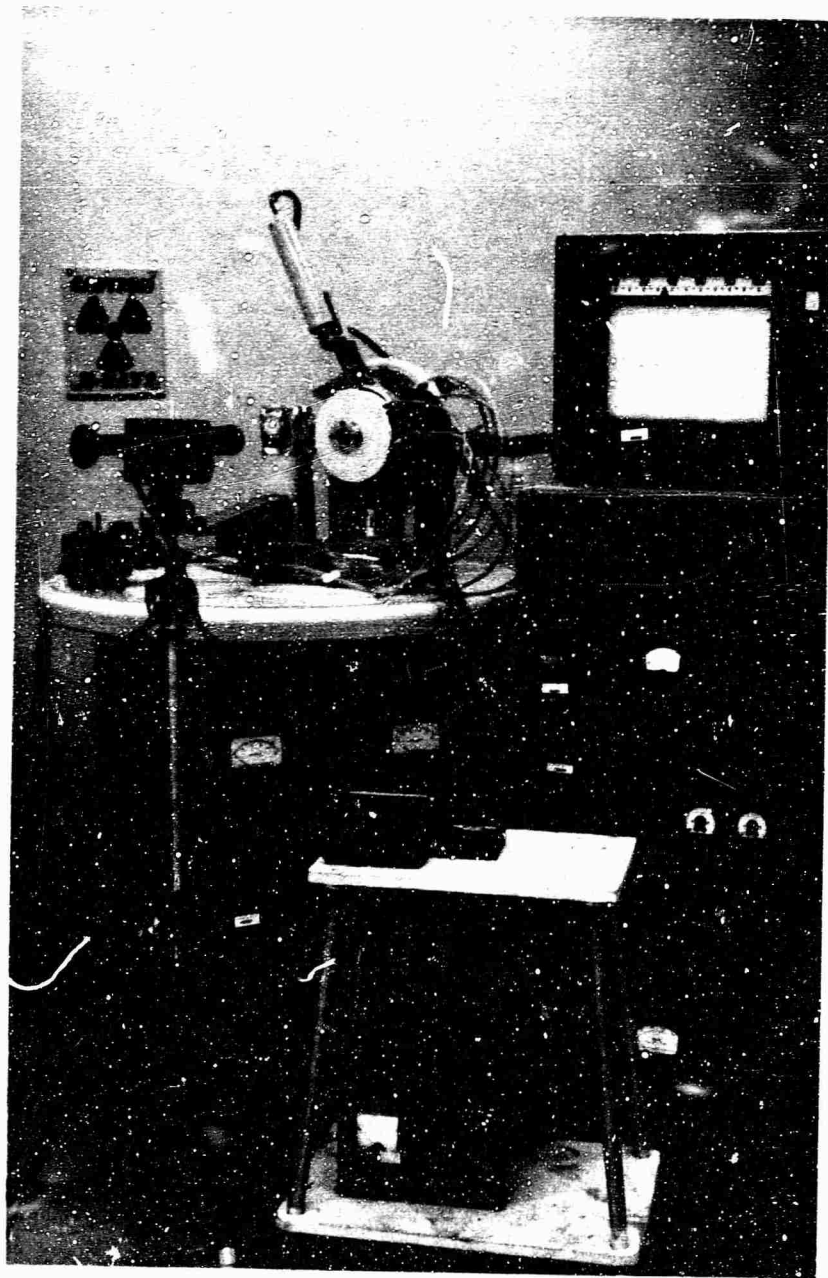


Figure 25. Experimental Set-up for Performing the Thermal Expansion Measurements Using the High Temperature X-Ray Diffraction Apparatus.

of the specimen. This method was abandoned, however, when it became apparent that excessive thermal differences existed between the sample's surface and that measured in the black body hole.

In lieu of the above method, a proven and more conventional approach was used. This procedure involved the application of a very thin layer of powdered metal on the heating element's surface. The element was preformed to a cup-shape, thus permitting the temperature measurements to be made on a side which was perpendicular to the optical pyrometer. The correct temperature can be calculated from the known emissivity values of the heating element material; in these experiments tantalum was used.

Only tantalum heating elements were available for these experiments; therefore, some method had to be sought to prevent melting between the tantalum and the material to be studied. The literature<sup>(37, 38)</sup> shows that melting occurs below 1800°C in the binaries of tantalum-rhodium, and tantalum-platinum; however, such would not be the case if rhodium or platinum were in contact with tungsten<sup>(37, 38)</sup> or rhenium<sup>(10)</sup>. It was decided to apply a very thin layer of tungsten powder to the surfaces of the heater with which the alloy materials would come into contact. The tungsten powder was then sintered onto the element in the high vacuum furnace at a temperature of 2000°C. It was found that this method was not in any way detrimental to the experimental results, and it did, indeed, allow the investigation of rhodium and platinum containing systems to be carried out at 1800°C.

The thermal expansion runs were carried out at 200°C intervals between 1000° and 1400°C and at 100°C intervals between 1400°C and 1800°C. The 420 and 331  $\text{CuK}_{\alpha_1}$  and  $\text{K}_{\alpha_2}$  peaks were scanned both from higher to lower and lower to higher angles in order to help alleviate any systematic errors which might be present in the set-up. Subsequent to each run, a room temperature scan was also performed to insure that the lattice parameter of the material remained constant, i.e. no solutioning of the tungsten in .ce occurred, and the system remained properly aligned.

The precision of measuring the angles at 1800°C was observed to be  $\pm 0.005^\circ(2\theta)$  under optimum conditions, and  $\pm 0.02^\circ(2\theta)$  under the most adverse conditions. The latter value would yield an error in the lattice parameter of the alloys measured in these studies of approximately  $\pm 0.001 \text{ \AA}$ .

For a very complete description of experimental procedures and techniques for high-temperature X-ray diffraction studies, reference should be made to an article by D.K. Smith<sup>(39)</sup>.

## (2) Temperature Calibration

The most recently published value for the emissivity of tantalum has been reported by Allen, Glaiser, and Jordan<sup>(40)</sup> for the temperature range above 2300°K. Their data was expressed in equation form given below by Thorn and Winslow<sup>(41)</sup>:

$$\epsilon_{0.65} = (0.391 \pm 0.001) - (1.26 \pm 0.04) 10^{-5} T \quad (1)$$

where  $\epsilon_{0.65}$  is the emissivity of tantalum at  $0.65 \mu$  and  $T$  is the absolute temperature (°K). Since, for all practical purposes, the pyrometric temperature measurements are carried out at a single effective wavelength of  $0.65 \mu$ , a temperature correction curve using the above  $\epsilon$  value can be calculated by inserting these values, as a function of temperature, into the well known relationship:

$$\ln \epsilon_2 = C_{2/\lambda} \{1/T - 1/T'\}, \quad (2)$$

where  $C_2$  is the second constant in Plank's law,  $\lambda$  is the wavelength (in this case  $\lambda = 0.65 \mu$ ),  $T$  is the true temperature, and  $T'$  is the apparent temperature of the tantalum surface. The temperature correction to be applied to each experimental reading is simply the difference between the true temperature and the apparent temperature of the surface. Figure 26 shows the calculated correction curve used in these investigations, along with the correction curve resulting from the absorption of the quartz window.

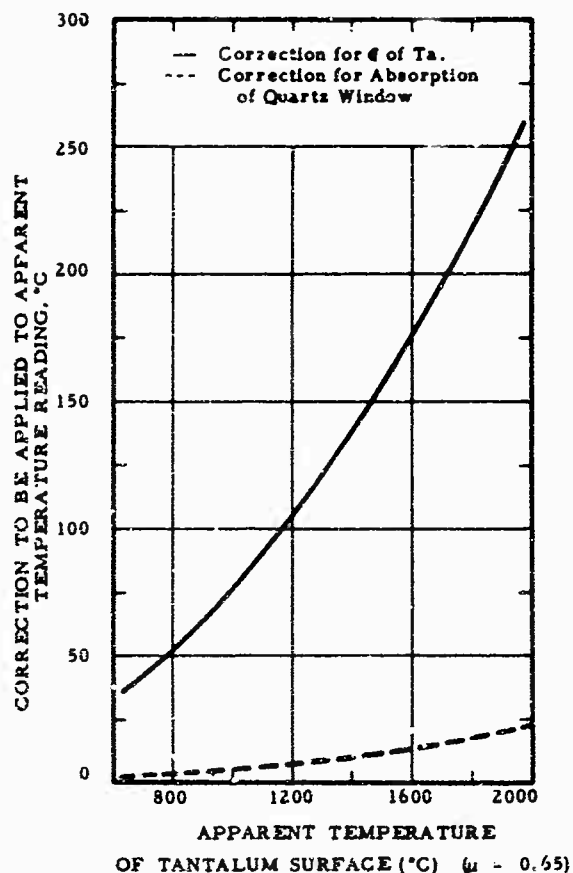


Figure 26. Temperature Correction Curve for the Pyrometric Readings on the Surface of the Tantalum Heating Elements Used in the High Temperature X-Ray Studies.

In order to check the above temperature correction curve, a calibration run was made using pure platinum as the standard. Campbell<sup>(42)</sup> has published a circular for the calibration of high-temperature X-ray diffraction cameras, using platinum as the standard, in which past literature is evaluated and best-fitted to a curve of thermal linear expansion versus temperature. The points obtained in the calibration run, in which the temperature measurements were made on the tantalum heating element, are compared in Figure 27 to the literature values as well

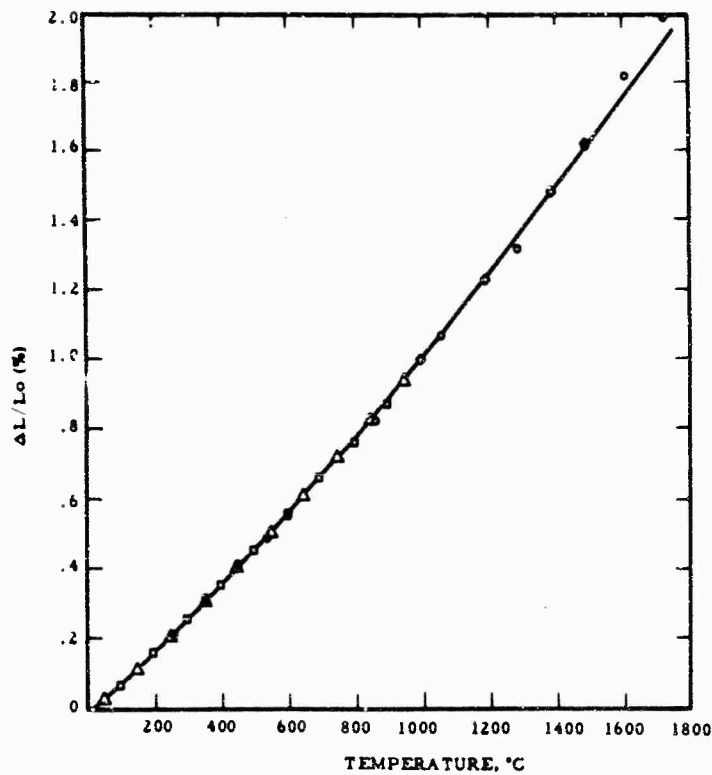


Figure 27. Literature Values and Calculated Expansion Curve for Platinum.

Calculated Curve to "Best-Fit" the Data

- ○ X-Ray Camera
- △ Dilatometer
- Interferometer
- ◇ Present Investigation

as to the curve which best fits these data. From the results of this calibration run, it is believed that corrected temperature values are accurate within  $\pm 10^{\circ}\text{C}$  up to  $1600^{\circ}\text{C}$ .

b. Dilatometric Studies

(1) Equipment

The apparatus used to perform the dilatometric investigation was a commercially available unit, Brinkmann Model TD IX, which is specified to operate to temperatures of 1600°C (Figure 28). This model operates in vacuum, and the measuring system is made of sintered alumina. However, because of certain procurement difficulties, only a low temperature measuring attachment (quartz) was available through the vendor; therefore, the thermal expansion measurements were restricted to temperatures below 1200°C; with the particular unit on hand, expansion measurements were limited to 800°C.

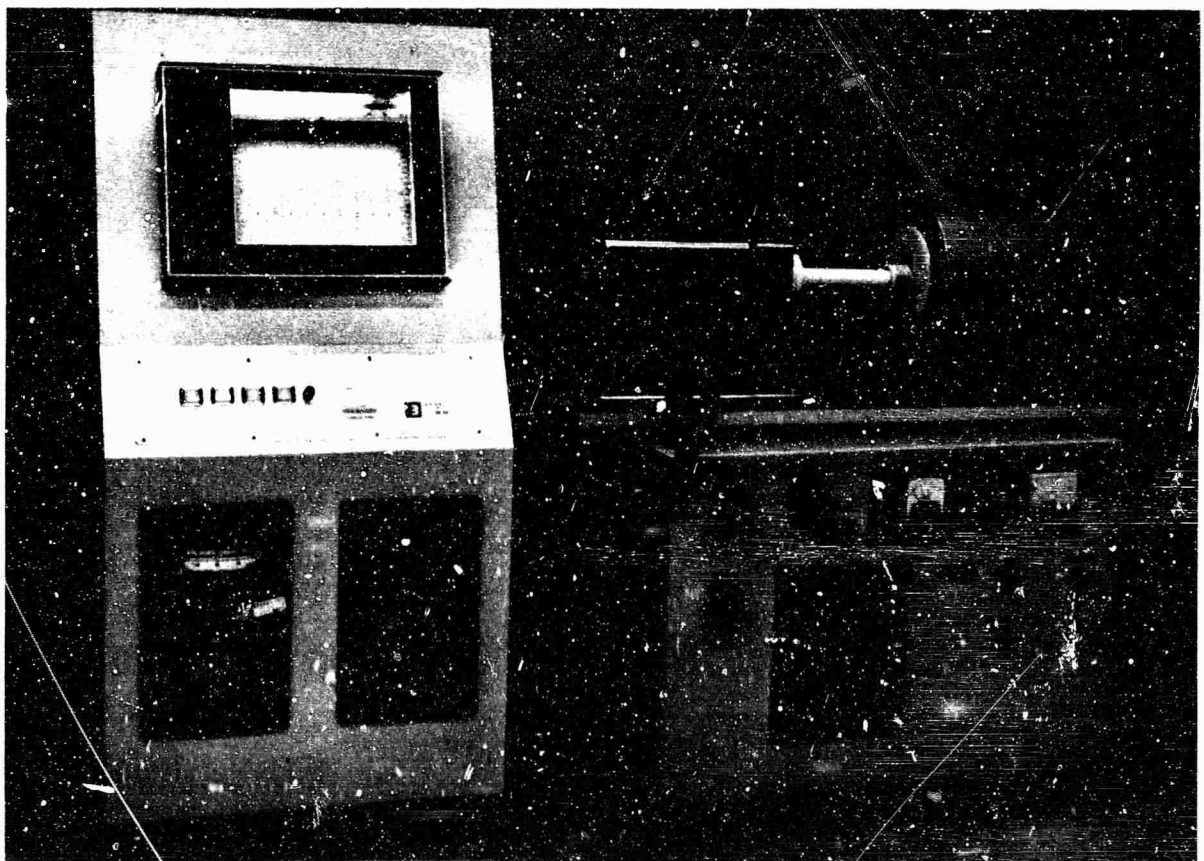


Figure 28. Brinkmann High Temperature Dilatometer, Model TD IX (Shown with the Alumina Measuring System).

The measuring system consists of a quartz vacuum tube, a sample support tube, and a push-rod as well as a transducer system. The transducer unit is composed of a dual coil which can be displaced horizontally along the outside of a quartz tube by a micrometer screw. A movable core inside the quartz vacuum sealing tube provides the inductance changes necessary. The core has a force exerted on its one side by a spring which causes it to change position in direct proportion to the expansion of the sample which presses the quartz push rod against the other side of the core. The primary side of the coil is excited with a 3000 cycle signal, and the signal in the secondary coil is proportional to the position of the core. The latter signal is demodulated, amplified, and recorded. The transducer system is enclosed in a constant temperature jacket (40°C) to restrict the influence of room temperature variation. Figure 29 gives the schematic drawing of the dilatometer set-up.

The heating elements in the furnace are silicon carbide. The heating and cooling rate of the furnace is controlled by a "West" program controller in which a photo-electric measuring device detects the proportional difference between a pointer of a galvanometer and of the cam-driven program indicator. The signal from the photo-electric circuit is amplified and used for the control of the silicon controlled rectifier which in turn supplies the power to the furnace through a step-down transformer.

The temperature of the sample is measured by a thermocouple which is in direct contact with the specimen; this signal drives one of the pens on the strip chart recorder. A representative error in the measurements was estimated to be + 2°C at 1500°C. The thermal gradient along the length of the sample is quoted by the vendor as being less than 2°C for a 2" specimen at approximately 1400°C (Figure 30).

The most sensitive recorder scale for determining the relative thermal expansion of the sample allows  $\Delta L$  values to be read to  $\pm 0.000005$ ". However, the precision assigned to each measurement

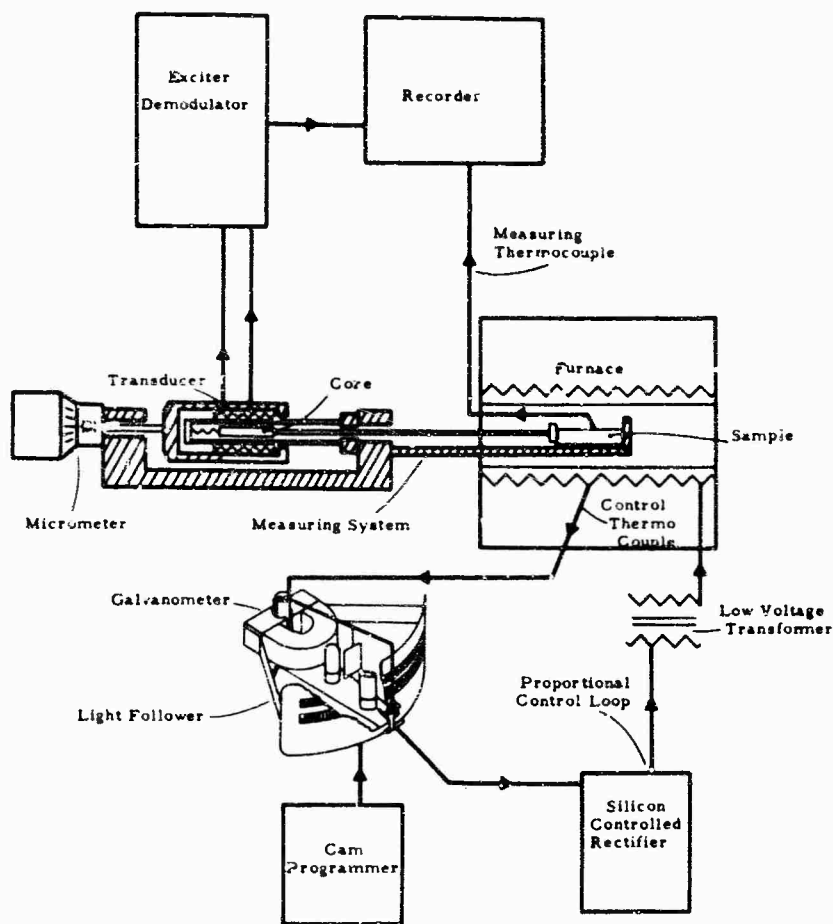


Figure 29. Schematic Drawing of the Dilatometer Set-Up.

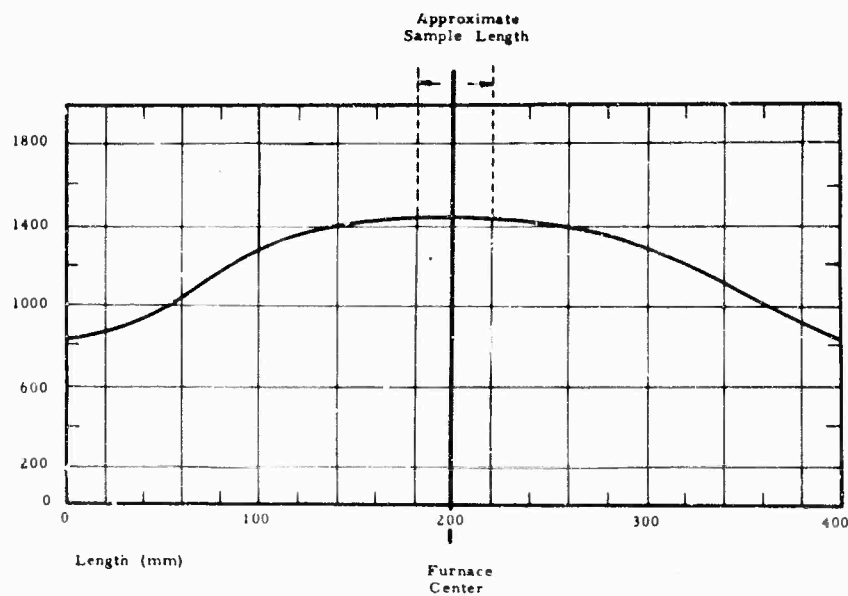


Figure 30. Thermal Distribution Curve for the Silicon Carbide Furnace of the Dilatometer (Data Supplied by Brinkmann)

is a factor of ten less precise than this value, since during the experiment, very slight changes in the system will introduce larger uncertainties in the readings.

## 6. X-Ray, Metallographic, and Chemical Analysis

All of the alloy material was examined subsequent to its particular experimental test by X-ray powder diffraction techniques. The X-ray exposures were made on a Siemens Crystalloflex II unit in either a two radian or one radian Debye-Scherrer Powder Diffraction Camera; all exposures were made in using copper  $K_{\alpha}$  radiation. The X-ray films were evaluated for phase equilibria as well as for the lattice parameters. The lattice parameters were measured using a Siemens-Kirem coincidence scale which is capable of determining  $\theta$  values to  $\pm .01^{\circ}$ . The majority of the alloys had to be stress relieved subsequent to pulverizing in order to clearly resolve the  $K_{\alpha_1}$ - $K_{\alpha_2}$  lines of the highest angle reflections.

Metallographic studies were performed primarily on carbon containing material in order to locate the eutectic compositions of the systems. The alloys were mounted in a non-conducting diallyl-phthalate base with a conductive lucite-coated copper top which provides an electrical path to the polished surface of the sample. The specimens were rough ground on silicon carbide papers with grit sizes varying between 120 and 600. Polishing was accomplished on a nylon cloth using a slurry of  $0.05\mu$  alumina and chromic acid solution. The majority of the carbon containing alloys could be examined in the as-polished condition. Metal alloys were electro-etched in the standard solutions recommended for these metals<sup>(43)</sup>.

Carbon analysis of the alloy material was performed with a 'Leco' carbon analyzer by combusting the material in a pure oxygen atmosphere and conductometrically determining the amount of  $CO_2$  in the combustion product. As would be expected with osmium containing alloys, a large amount of the tetroxide was formed during this procedure; this in turn gave readings which were erroneously high. It was found, however,

that this method could be used with some success if a certain procedure was followed. This procedure involved combusting the osmium containing alloy, recording the read-out, and then immediately recycling the same alloy and recording this value. This latter value was observed to be representative of the amount of  $\text{OsO}_4$  formed during the cycle; by subtracting the latter reading from the first, the weight percent carbon could be determined. A number of calibrations by this technique yielded fair results, i. e.  $\pm 2$  atomic percent carbon. A similar procedure was also found to be necessary for rhenium containing alloys.

### C. RESULTS

#### 1. Melting Temperatures and Phase Equilibria of the Iridium Base Metal Alloys

##### a. Melting Points of the Pure Metals

The melting points were determined for the rhenium, osmium, rhodium, iridium, and platinum starting materials used in these investigations. These temperatures were determined using the Pirani technique, and the results are presented in Table 1. The measurements were performed on cold-pressed and sintered material; runs were made both in a high purity helium atmosphere and in vacuum. Slightly higher results were consistently recorded with the specimens which were run in vacuum. It was concluded from these results that the melting points of these metals are fairly sensitive to atmospheric gases which were most likely entrapped during cold pressing and were insufficiently driven off during the vacuum sintering operation. Other evidence pointing to this conclusion is the results of an earlier series of melting point measurements of these elements. After these experiments it was found that one of the high vacuum valves had developed a leak. The results of these measurements were consistently  $15^\circ$  to  $60^\circ\text{C}$  lower than those observed later under high purity conditions.

The melting point of rhenium was observed to be inconsistently low with the reported literature value <sup>(11, 12, 13, 14)</sup> of

approximately 3180°C (Table 4). The melting temperature of  $3067^{\circ} \pm 13^{\circ}\text{C}$  was observed with two samples of material which had been electron beam molten four times. The EBM-samples were prepared only after similar low temperatures were observed with cold-pressed and sintered alloys. These results are substantiated by earlier results in this laboratory<sup>(44)</sup> in which a value of  $3075^{\circ} \pm 7^{\circ}\text{C}$  was observed from rhenium of three different batches. A comparison of the impurities of the present material with those reported by the different investigators did not yield any significant differences in purity levels; furthermore it was decided that no one impurity (in the concentrations present) would contribute significantly to melting point depression.

The other results, on the other hand, are in good agreement with the currently accepted melting points<sup>(17)</sup>; the melting point observed for osmium is slightly higher than the value  $3045^{\circ} \pm 30^{\circ}\text{C}$  chosen by Knapton, et al.<sup>(13)</sup>; however, the value presented by them is lower than the mean value of their three determinations, i.e. 3040°, 3080°, and 3065°C<sup>(13)</sup>, which yields a mean value of  $3062^{\circ} \pm 21^{\circ}\text{C}$ . However, certain experimental evidence not presented by the above authors might not warrant this mean temperature to be assumed. It should be noted that the melting point recorded for osmium was the most reproducible of the five elements; a standard deviation of  $\pm 1^{\circ}\text{C}$  was observed for five different melting point measurements.

#### b. Iridium-Rich Portion of the Metal Binary Systems

The solidus temperatures in the systems iridium-rhenium<sup>(10)</sup> and iridium-osmium<sup>(19)</sup> as well as the liquidus temperatures of the iridium-platinum<sup>(45)</sup> system have been previously investigated and published in the literature. Melting temperature investigations were carried out in the iridium-rich portion of these systems in order to confirm these data. In most instances agreement was very good between our results and those of the previous investigations (Figures 31-33); however, slightly lower melting temperatures were obtained for the face-centered cubic solid solution in the iridium-rhenium system (Figure 31).

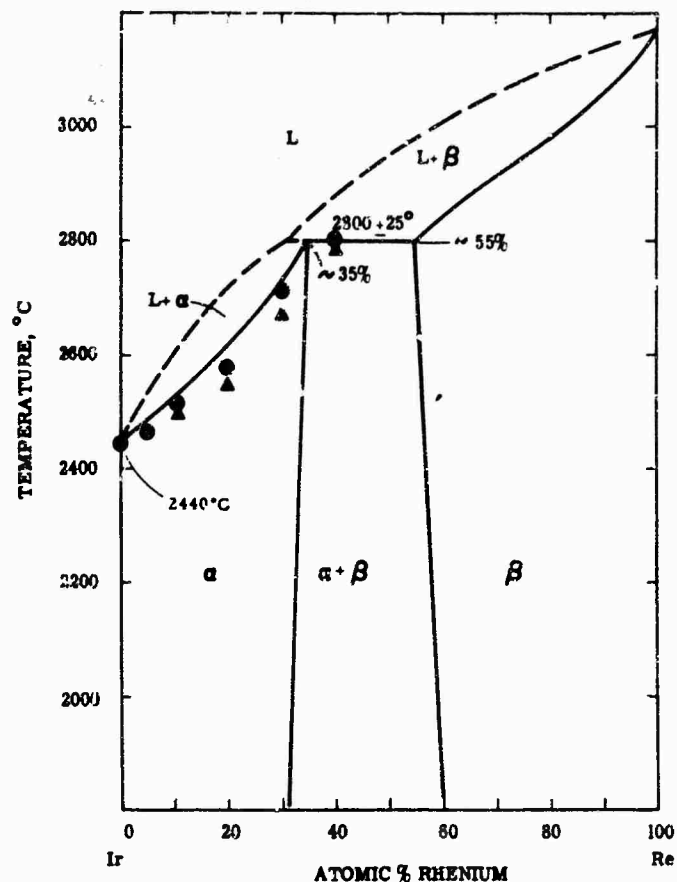


Figure 31. Iridium-Rhenium Phase Diagram, Showing Melting Data Points Obtained in this Investigation.

- ▲ Incipient Melting
- Sample Collapsed

The solidus temperatures of the iridium-rhodium system were investigated up to a rhodium concentration of 40 atomic percent. The solidus curve decreased smoothly with increasing rhodium concentrations (Figure 34).

The limits of the face-centered cubic solid solutions in the iridium-rhenium and iridium-osmium systems were not specifically investigated; however, they were indicated to be located as reported in the literature<sup>(10, 19)</sup>. The alloys in the iridium-rhenium system cored during solidification, and the second phase (hcp) was not completely annealed out

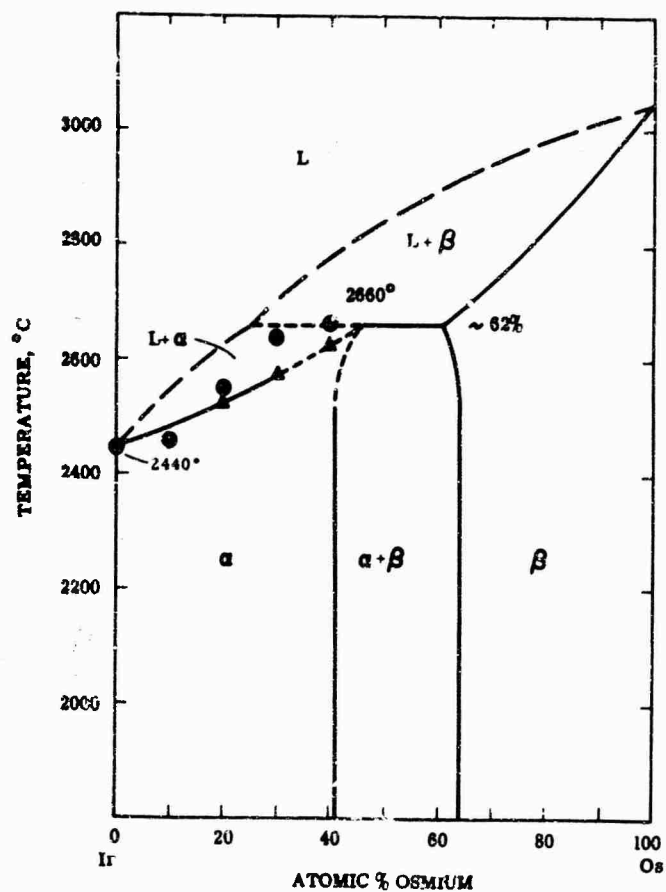


Figure 32. Iridium-Osmium Phase Diagram Showing Melting Data Points Obtained in this Investigation.

- ▲ Incipient Melting
- Sample Collapsed

during the following heat treatment; however, the lattice parameters were observed to change continuously linearly for alloys up to 30 atomic percent rhenium. The alloy with 40 atomic percent rhenium did not have a sufficient amount of the fcc-solid solution present to determine a lattice parameter at this composition. It should be noted that Tylkina et al.<sup>(10)</sup> reported the parameters of the iridium solid solution to decrease with rhenium addition; this is completely opposite to that observed in the present

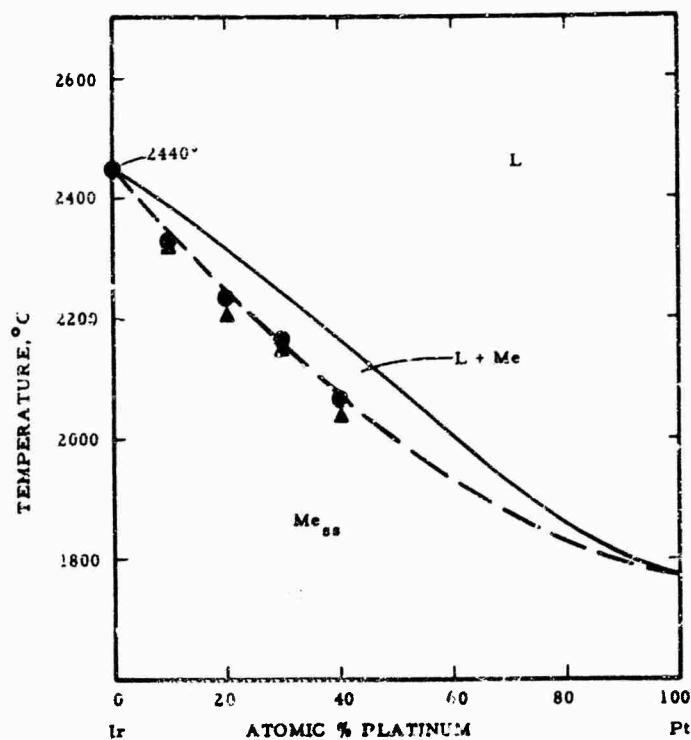


Figure 33. Iridium-Platinum Solidus-Liquidus Curves Showing Melting Data Points Obtained in this Investigation (Liquidus-Feusener and Müller, Solidus - Estimated by Darling).

- ▲ Incipient Melting
- Sample Collapsed

measurements, (compare Figures 12 and 35). Moreover, since the effective atomic radius of rhenium is larger than that of iridium<sup>(46)</sup>, one would expect the size of the iridium unit cell to increase with rhenium substitution.

The lattice parameters were observed to vary linearly with composition in the iridium-rhodium and iridium-platinum systems, and these values compare very favorably with parameters cited in the literature (Figure 33).

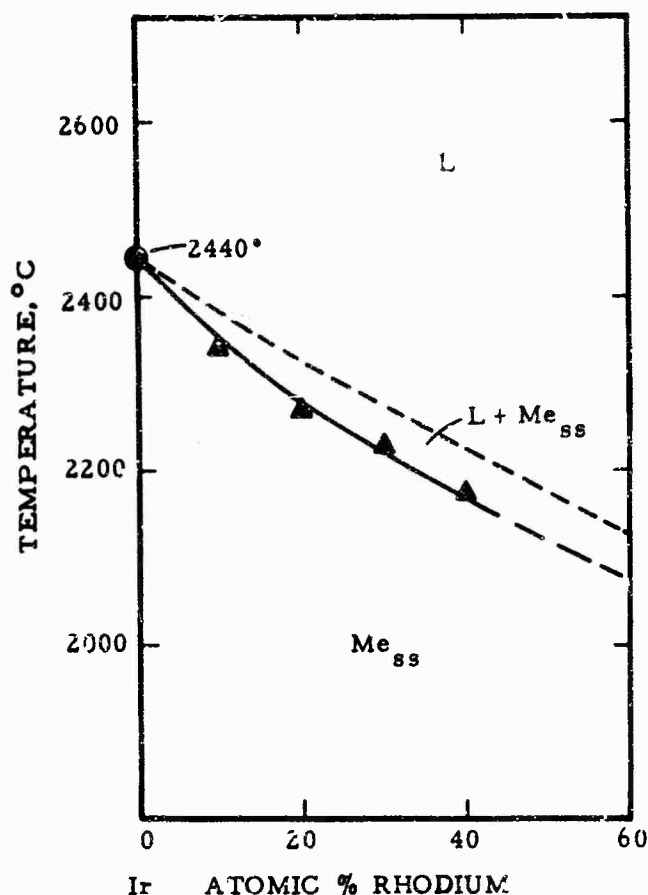


Figure 34. Iridium-Rich Portion of the Iridium-Rhodium Phase Diagram.

▲ Incipient Melting

c. Ternary Iridium-Base Metal Alloys

(1) Iridium-Osmium-Rhodium Alloys

The incipient melting temperatures of twenty-eight alloy compositions were determined using the Pirani technique. Of the alloys investigated, all solidus temperatures were found to be higher than 2150°C; the lowest melting temperature was in the iridium-rhodium binary at a rhodium concentration of 40 atomic percent. The results of these investigations are presented in Table 6 and Figure 1. Also, the

effect of various elemental substitutions on the alloys' melting temperatures are depicted graphically in Figure 36.

The highest recorded melting temperature was  $\sim 2650^{\circ}\text{C}$  corresponding to the peritectic temperature in the iridium-osmium binary system. In general, the heterogeneity of melting increased with higher osmium concentrations, and therefore, the incipient melting temperatures of these alloys are not as precise as the incipient melting temperatures of alloys with small osmium additions.

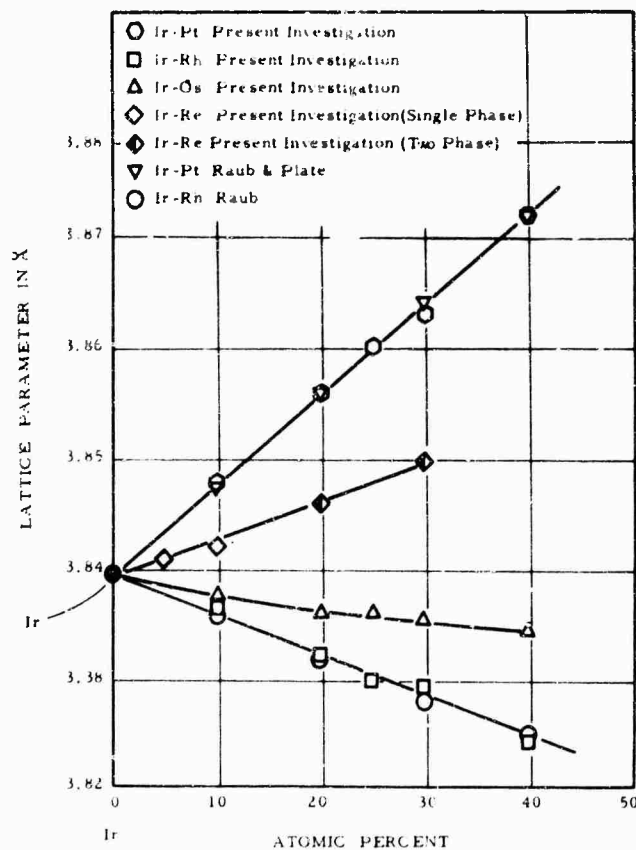


Figure 35. Lattice Parameters of the Face-Centered Cubic Solid Solutions of the Iridium-Base Binary Alloys.

Table 6. Melting Temperatures of Iridium-Osmium-Rhodium Alloys

Sample No	Composition At. %			Observed Incipient Melting Temperature, °C		Melting Characteristics
	Ir	Os	Rh	Incipient	Collapse	
1	90	10	0	2434	~2434	Fairly Sharp
2	90	5	5	2370	~2370	Fairly Sharp
3	90	0	10	2342	~2342	Sharp
4	85	10	5	2375	2406	Fairly Sharp
5	85	5	10	2339	~2339	Fairly Sharp
6	80	20	0	2532	~2532	Fairly Sharp
7	80	15	5	2396	2447	Fairly Heterogeneous
8	80	10	10	2339	2372	Fairly Heterogeneous
9	80	5	15	2308	~2308	Fairly Sharp
10	80	0	20	2283	~2285	Fairly Heterogeneous
11	75	20	5	2406	2498	Fairly Heterogeneous
12	75	15	10	2355	2406	Fairly Heterogeneous
13	75	10	15	-	2370	Fairly Heterogeneous
14	75	5	20	-	2308	Fairly Heterogeneous
15	70	30	0	2590	2632	Heterogeneous
16	70	25	5	2460	2574	Heterogeneous
17	70	20	10	2437	2508	Fairly Heterogeneous
18	70	15	15	2362	2421	Heterogeneous
19	70	10	20	2324	2398	Heterogeneous
20	70	5	25	2283	2308	Fairly Heterogeneous
21	70	0	30	2228	2228	Fairly Sharp
22	65	30	5	2519	2601	Heterogeneous
23	65	20	15	2374	2463	Heterogeneous
24	65	10	25	2308	2362	Heterogeneous
25	60	40	0	2649	2687	Heterogeneous
26	60	25	15	2393	2498	Very Heterogeneous
27	60	15	25	2324	2457	Very Heterogeneous
28	60	0	40	2171	2217	Fairly Heterogeneous

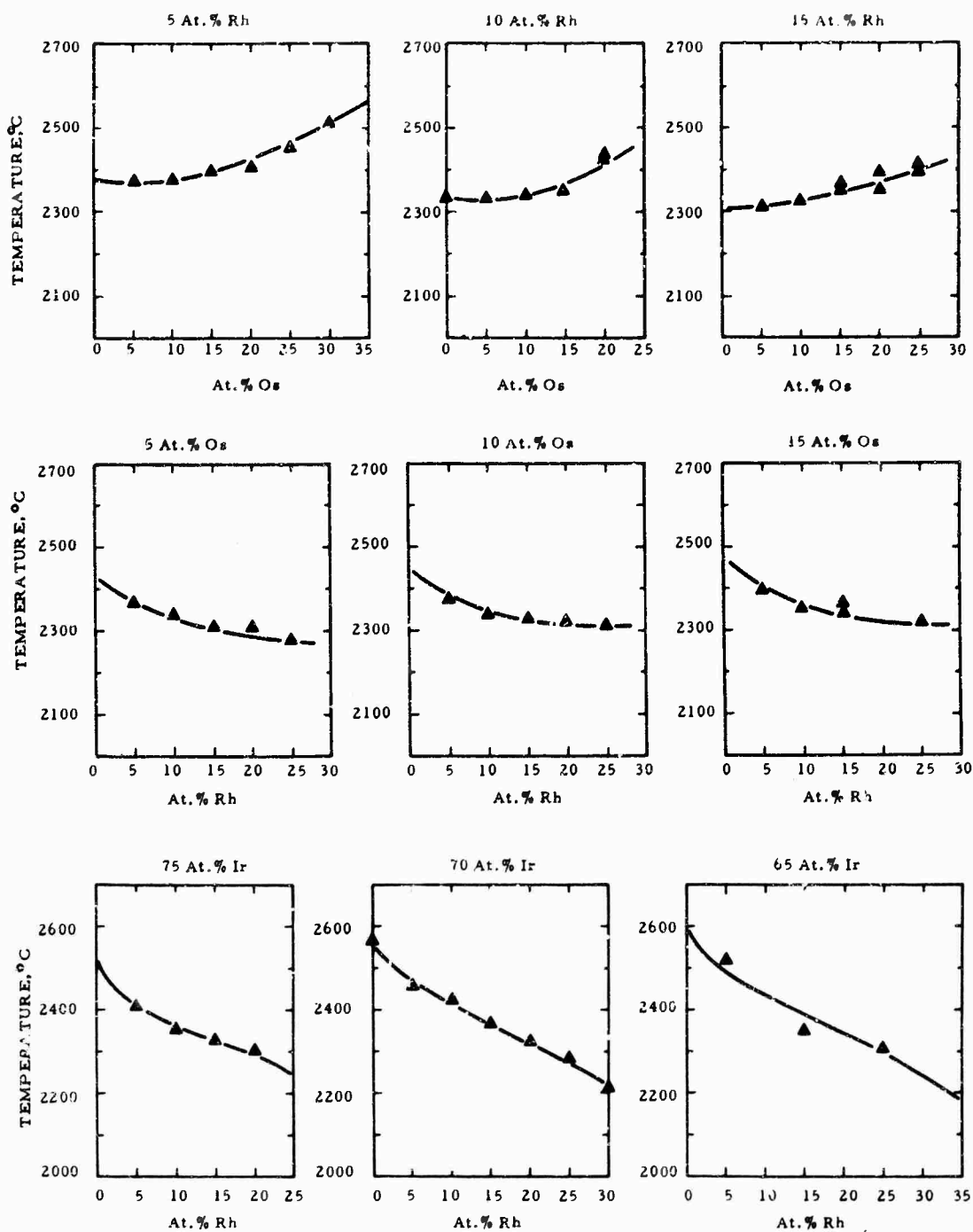


Figure 36. Incipient Melting Temperatures of Iridium-Osmium-Rhodium Alloys as a Function of Composition. (a) Constant Rhodium Concentration, (b) Constant Osmium Concentration, (c) Constant Iridium Concentrations.

X-ray diffraction patterns were made of alloys subsequent to melting; the majority of the alloys were in the single phase, face-centered cubic solid solution region. Only two alloys in the iridium osmium binary showed patterns of the hexagonal, osmium-rich, solid solution. The binary peritectic point was therefore indicated to be at a osmium concentration between 20 and 30 atomic percent; from the ternary data, the peritectic line is not indicated to protrude too far into the ternary section investigated in this work.

Both osmium and rhodium, when alloyed with iridium, reduce their cell sizes. The lattice parameters of the ternary alloys varied between  $3.839 \text{ \AA}$  and  $3.82_4 \text{ \AA}$  with the maximum value being measured for pure iridium and the minimum value in the iridium-rhodium binary system (Ir:Rh-60:40).

## (2) Iridium-Osmium-Platinum Alloys

Experiments similar to those performed on the iridium-osmium-rhodium alloy system were performed on alloys of the iridium-osmium-platinum ternary. The compositions of the alloys were the same as those investigated in the iridium-osmium-rhodium system (Figure 16).

The data are given in Table 7, and the points are also presented in graphical form to best illustrate the variance of the melting temperatures of the alloy solution as a function of individual component additions (Figure 37).

The temperature-compositional plots of the melting temperature data illustrate the expected results that platinum metal substitution in the alloy system iridium-osmium lower the melting temperatures. In comparison to the iridium-osmium-rhodium system, it can be seen that platinum has a greater effect on depressing the melting points than does rhodium. However, a comparison of Figures 5 and 6 shows that the lowest solidus temperature of each of these two alloy systems in the presence of carbon is quite close ( $2100^\circ$  and  $2150^\circ\text{C}$ ).

Table 7. Melting Temperatures of Iridium-Osmium-Platinum Alloys

Sample No	Composition At. %			Observed Incipient Melting Temperature, °C		Melting Characteristics
	Ir	Os	Pt	Incipient	Collapse	
1	90	10	0	2434	~2434	Fairly Sharp
2	90	5	5	2339	>2339	Fairly Heterogeneous
3	90	0	10	2273	(2314)	Fairly Sharp
4	85	10	5	2370	2406	Heterogeneous
5	85	5	10	2298	2355	Heterogeneous
6	80	20	0	2532	~2532	Fairly Sharp
7	80	15	5	2427	2484	Heterogeneous
8	80	10	10	2329	2403	Heterogeneous
9	80	5	15	2268	2339	Heterogeneous
10	80	0	20	2191	2231	Fairly Heterogeneous
11	75	20	5	2489	2514	Fairly Heterogeneous
12	75	15	10	2365	2453	Heterogeneous
13	75	10	15	2273	2360	Heterogeneous
14	75	5	25	2181	2276	Heterogeneous
15	70	30	0	2590	2632	Heterogeneous
16	70	25	5	2473	2540	Heterogeneous
17	70	20	10	2398	2470	Heterogeneous
18	70	15	15	2295	2386	Heterogeneous
19	70	10	20	2201	2273	Heterogeneous
20	70	5	25	2164	2273	Heterogeneous
21	70	0	30	2131	2175	Heterogeneous
22	65	30	5	2509	2596	Heterogeneous
23	65	20	15	(2308)	2437	Very Heterogeneous
24	65	10	25	2176	2255	Very Heterogeneous
25	60	40	10	2649	2687	Heterogeneous
26	60	25	15	2308	2421	Very Heterogeneous
27	60	15	25	2161	2263	Very Heterogeneous
28	60	0	40	2035	2089	Heterogeneous

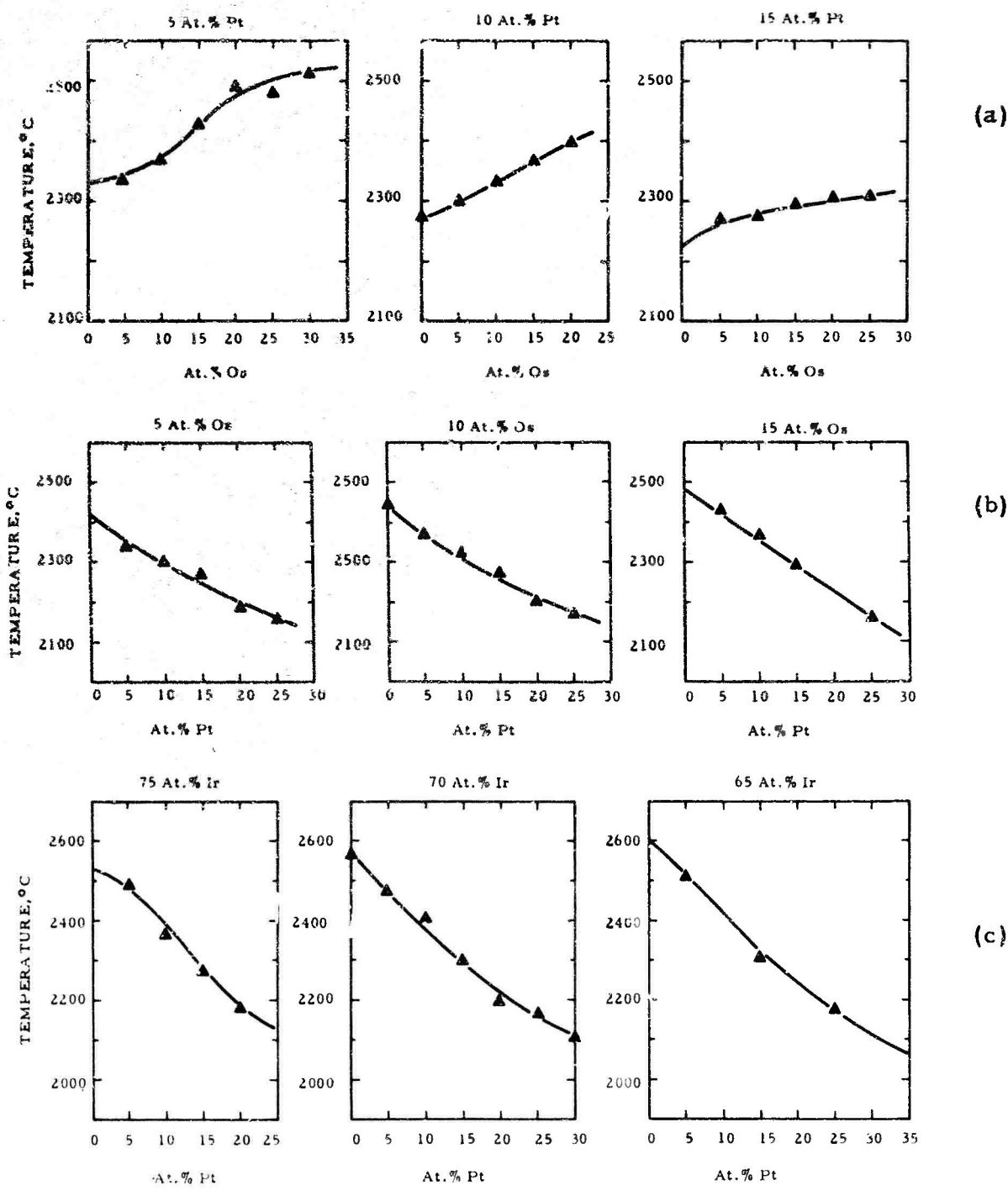


Figure 37. Incipient Melting Temperatures of Iridium-Osmium-Platinum Alloys as a Function of Composition. (a) Constant Platinum Concentrations, (b) Constant Osmium Concentration, (c) Constant Iridium Concentration.

Alloys with high osmium and platinum contents were generally found to melt very heterogeneously, thus indicating a relatively large temperature separation between the solidus and liquidus surfaces. Most of the alloys were observed to be single phase, excepting of iridium-osmium binary alloys which had approximately 30 or more mole percent osmium; however, none of the ternary alloys investigated were observed to be two phase from the X-ray diffraction patterns.

X-ray measurements showed that the ternary alloys had parameters between the limits of  $3.83_4 \text{ \AA}$  and  $3.87_2 \text{ \AA}$  which are the parameters of the limiting unit cells in the iridium-osmium and iridium-platinum binary alloys investigated in this current work.

### (3) Iridium-Rhenium-Rhodium Alloys

A total of twenty-three compositions were investigated in the iridium-rhenium-rhodium alloy system. The assumption that the rhenium containing alloys are more refractory than the osmium containing systems is borne out in the currently established experimental data. Table 8 gives a compilation of the melting points of these test specimens, and again the data are plotted as a function of various metal concentrations in order to more clearly depict the effect of particular elemental substitutions into the binary alloy system (Figure 38).

Substitution of rhodium for iridium has only a slight effect on the melting temperatures of iridium-rhenium alloys (Figure 38-b); whereas the exchange of rhenium for iridium in iridium-rhodium alloys sharply increases the incipient melting temperatures of the alloy system (Figure 38-a). It appears from these results that one can freely substitute rhodium for iridium in an iridium-rhenium alloy with only a slight drop in the original binary alloy's melting temperature.

Table 8. Melting Temperatures of Iridium-Rhodium-Rhenium Alloys.

Sample No.	Composition At. %			Observed Incipient Melting Temperature, °C		Melting Characteristics
	Ir	Ph	Re	Incipient	Collapse	
1	90	10	0	2342	~2342	Sharp
2	90	5	5	2365	2380	Fairly Sharp
3	90	0	10	2440	~2440	Fairly Sharp
4	85	10	5	2339	2360	Fairly Sharp
5	85	5	10	2447	2457	Fairly Sharp
6	80	20	0	2283	~2285	Fairly Heterogeneous
7	80	15	5	-	2324	Fairly Sharp
8	80	10	10	2427	~2453	Fairly Sharp
9	80	5	15	2488	2530	Fairly Heterogeneous
10	30	0	20	(2550)	2579	Fairly Sharp
11	75	20	5	-	2332	Fairly Sharp
12	75	15	10	2398	2411	Fairly Heterogeneous
13	75	10	15	~2487	2555	Fairly Heterogeneous
14	75	5	20	2591	2612	Fairly Heterogeneous
15	70	30	0	2228	~2228	Fairly Sharp
16	70	25	5	2314	2344	Fairly Sharp
17	70	20	10	2406	2478	Heterogeneous
18	70	15	15	2475	2501	Heterogeneous
19	70	10	20	2558	2605	Heterogeneous
20	70	5	25	-	2656	Heterogeneous
21	70	0	30	2684	2700	Very Heterogeneous
22	70	40	0	2171	2217	Fairly Heterogeneous
23	70	0	40	(2790)	2797	Heterogeneous

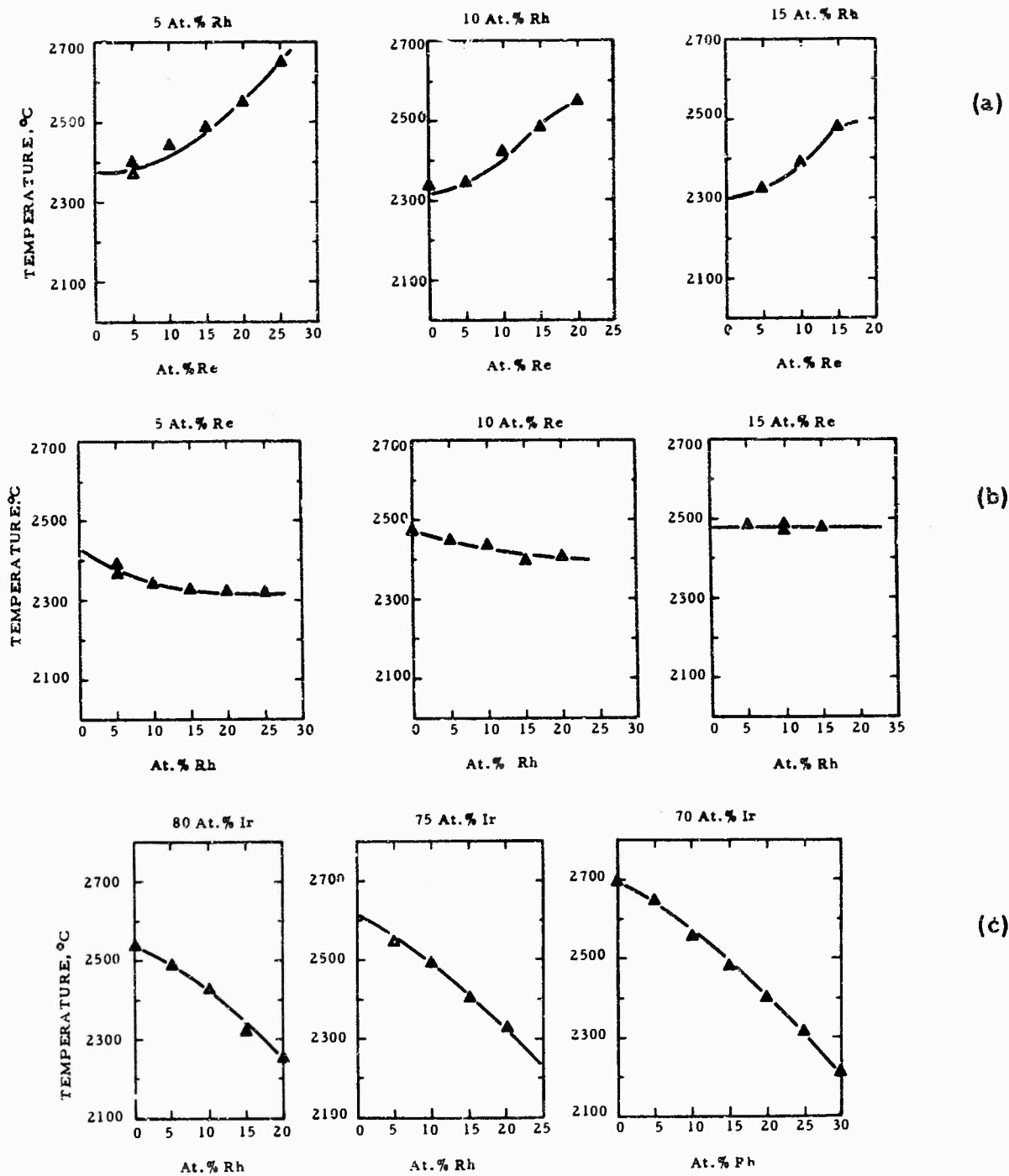


Figure 38. Incipient Melting Temperatures of Iridium-Rhenium-Rhodium Alloys as a Function of Composition. (a) Constant Rhodium Concentrations, (b) Constant Rhenium Concentrations, (c) Constant Iridium Concentrations.

In the ternary iridium-rhenium-rhodium section which was investigated, X-ray diffraction patterns of melted alloys, as well as of alloys subsequently heat treated at 1800°C, showed that the specimens, which had rhenium concentrations greater than approximately 20 atomic percent, were two-phase (fcc + hcp). However, as mentioned earlier, these alloys cored during cooling, and they apparently did not reach equilibrium during the prescribed heat treatment.

Lattice parameter values of the fcc-ternary alloys ranged between 3.85<sub>0</sub> Å and 3.82<sub>4</sub> Å; these are the limiting values measured in the respective iridium-rhenium and iridium-rhodium binaries.

## 2. Solidus Temperatures of the Alloys in the Presence of Carbon

### a. Metal-Carbon Binary Systems

Experiments were conducted in the metal-carbon systems in order to check the previously reported values of the eutectic temperatures as well as to define the composition of these eutectics. In addition, in the rhenium-carbon and osmium-carbon systems, experiments of previous investigators (29, 30, 32) were repeated in an attempt to prepare the observed carbide phases.

#### (1) Rhenium-Carbon

Melting temperature investigation by both differential thermal analytical, and the Pirani, techniques were performed in the rhenium-carbon system. The mean value for the eutectic temperature from these determinations was 2466 ± 15°C. Figure 39 shows two representative DTA curves obtained with a rhenium carbon alloy. It should be noted that curve "A" shows that the alloy super-cooled significantly before solidifying. This phenomena was observed on the majority of the runs of carbon-rich

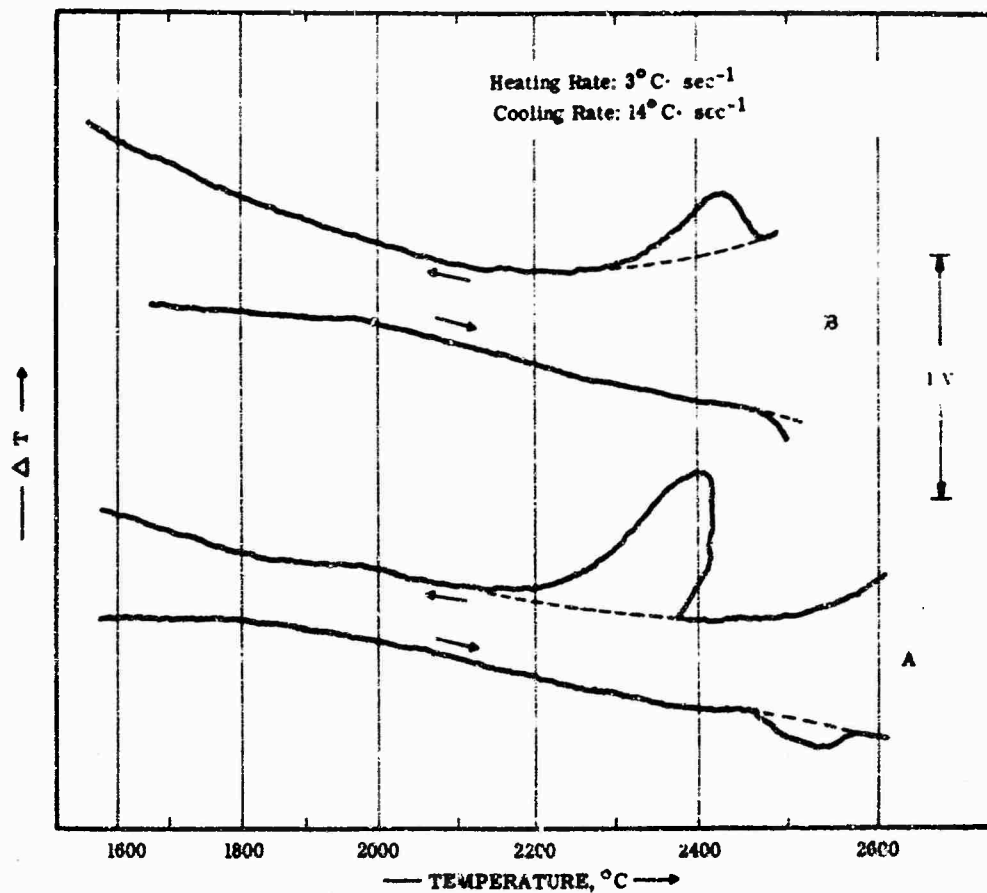


Figure 39. Differential Heating and Cooling Curves of a Rhenium-Carbon Alloy.

- A. Showing Eutectic Melting with Supercooling of the Melt.
- B. Showing Eutectic Melting and Solidification.

alloys. It was found that super-cooling could be prevented only if, as soon as melting was detected, the sample was rapidly cooled (Curve B). A plausible explanation of this observation is that above the eutectic temperature the graphite crystals grow at very rapid rate, and thus nucleation sites are not present during cooling. However, if the alloy is quenched shortly after melting, the graphite crystals do not have sufficient time to grow to large proportions, and therefore are able to provide sites for nucleation of the secondary solid phases.

Five binary specimens were prepared by arc-melting in order to locate the composition of the eutectic. These alloys were placed at 5 atomic percent intervals between 5 and 25 atomic percent carbon. From metallographic and chemical analysis of these samples, the eutectic composition was estimated to be at 20 atomic percent carbon (Figures 40-42). Although the hcp solid solution was not specifically investigated, the results showed that the  $\beta$ -phase extended to carbon concentration of at least 10 atomic percent (Figure 40). These results confirmed the finding by Hughes<sup>(27)</sup>, that an extensive rhenium solid solution is formed in the system. However, lattice parameters of single phase alloys did not yield identical results to those given by Hughes<sup>(27)</sup> who determined the lattice parameters at the terminal solid solution to be  $a = 2.792 \text{ \AA}$ ,  $c = 4.471 \text{ \AA}$ . In this work, maximum lattice parameters of  $a = 2.79_6 \text{ \AA}$  and  $c = 4.46_0 \text{ \AA}$  were calculated for an alloy near the limit of the single phase region. This result would indicate only a slight expansion of the "c" parameter and a rather larger expansion of the "a" parameter.

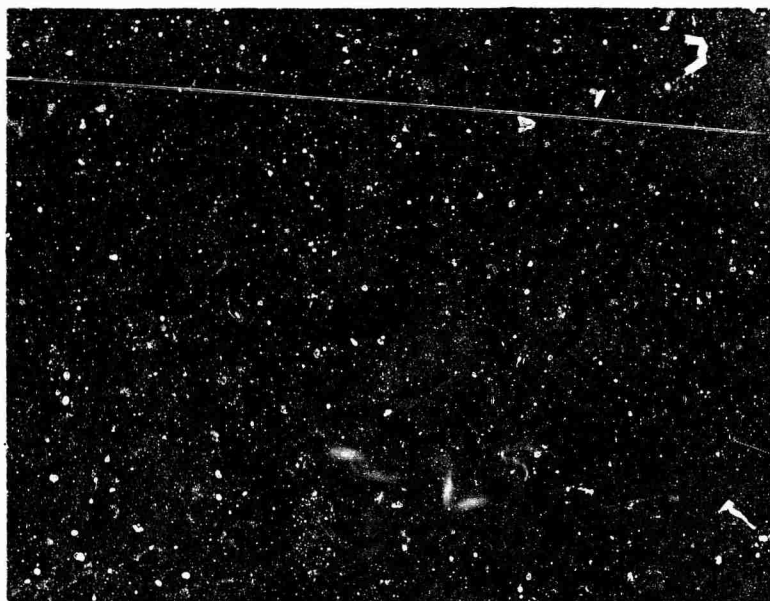


Figure 40. Re-C (90/10), Arc-Melted Alloy Showing Single Phase Rhenium Solid Solution.

X175

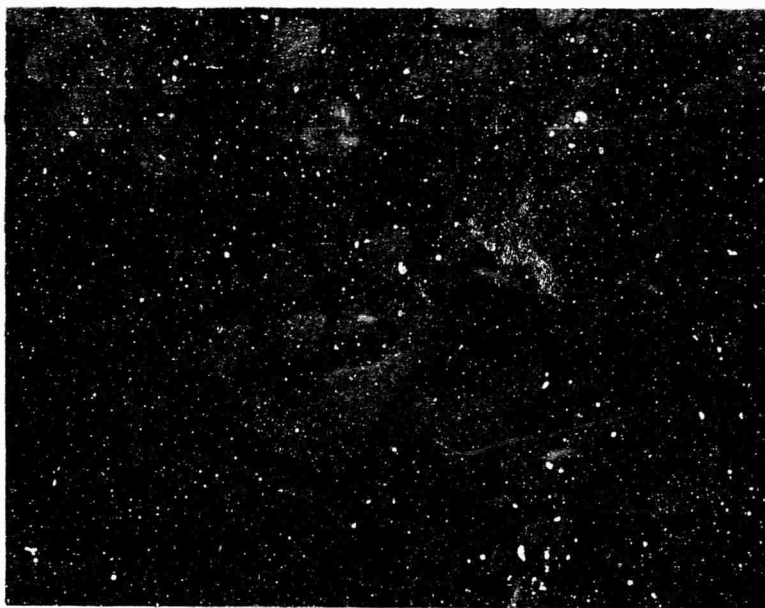


Figure 41. Re-C (82/18), Arc-Melted Alloy Showing Primary Metal in a Eutectic Matrix.

X750

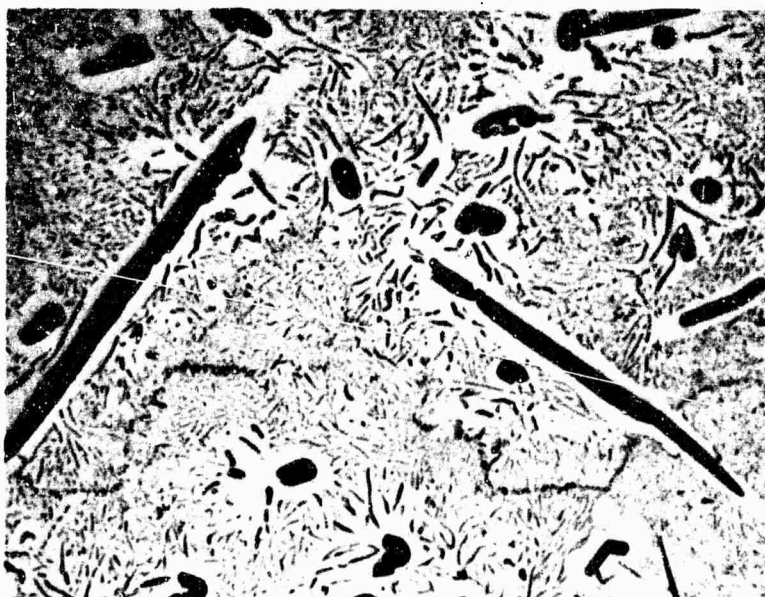


Figure 42. Re-C (76/24), Arc-Melted Alloy Showing Primary Graphite in a Eutectic Matrix.

X750

Recent work performed by Hammond<sup>(28)</sup> indicated the existence of a cubic carbide phase in the rhenium-carbon binary system. It was suggested, however, that this phase was very likely metastable. The phase was observed in diffusion couples which had received heat treatments at elevated temperatures (2 to 6 hrs at 1800 to 2000°C). In an effort to produce the carbide phase, a diffusion couple of rhenium and graphite was prepared (see sample preparation section of this report). Subsequent metallographic (Figures 43--4) and X-ray examination reveal only rhenium and carbon to be present. Also, the presence of another phase was never detected in any of the melting point, DTA, or arc-melted samples. It was thus concluded, that if the phase exists, it does not form readily under the conditions of these experiments.

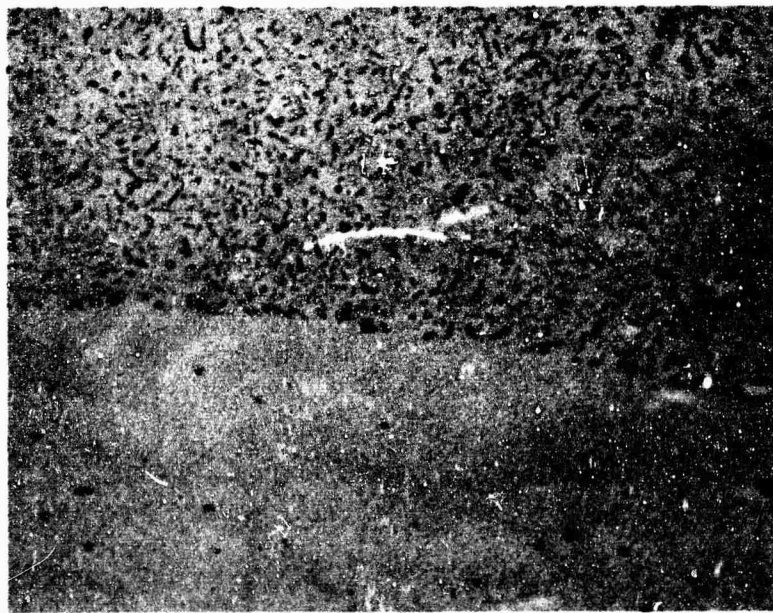


Figure 43. Rhenium-Carbon Diffusion Couple Revealing Sharp Boundaries Between Rhenium and the Re + C Eutectic.

X600

(X-Ray: hcp - Re + Graphite)

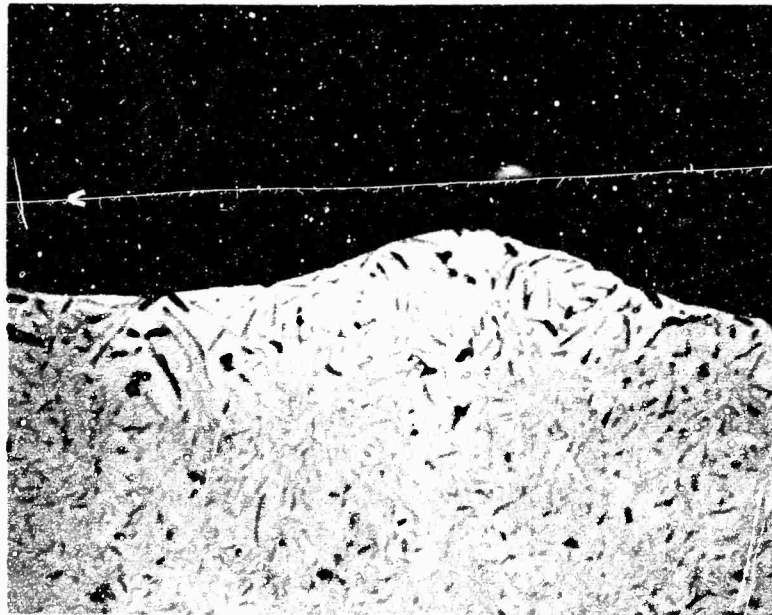


Figure 44. Rhenium-Carbon Diffusion Couple Revealing a Sharp Boundary Between Eutectic (Re + C) + Graphite.

X525

(X-Ray: hcp Re + Graphite)

From the above results it is indicated that slight modifications should be made to the rhenium-carbon phase diagram reported by Hughes<sup>(27)</sup>. The eutectic temperature should be placed at  $2466 \pm 15^\circ\text{C}$ ; the eutectic composition is indicated to be at  $20 \pm 2$  atomic percent carbon. In addition, the melting point of rhenium is observed to be  $3067 \pm 13^\circ\text{C}$ . The solubility of carbon in rhenium is the value given by Hughes<sup>(47)</sup>. Figure 45 depicts the modified rhenium-carbon phase diagram.

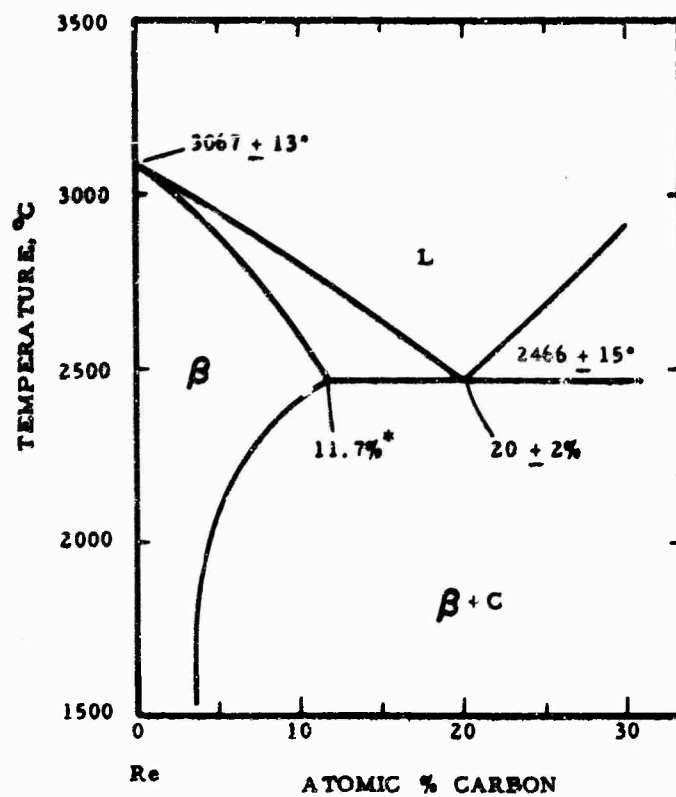


Figure 45. Modified Rhenium-Carbon Phase Diagram.

(2) Osmium-Carbon

The eutectic temperature was observed to be at  $2725 \pm 15^\circ\text{C}$  by both DTA and Pirani melting point determinations. As with the rhenium-carbon alloys, super-cooling of the melt was observed with graphite-rich osmium-carbon specimens (Figure 46). An explanation similar to that presented for the super-cooling phenomena observed in the rhenium-carbon system can also be applied for these samples. Figure 47 shows a photomicrograph of an osmium-carbon specimen which super-cooled during solidification; note the very large size of the primary graphite crystals.

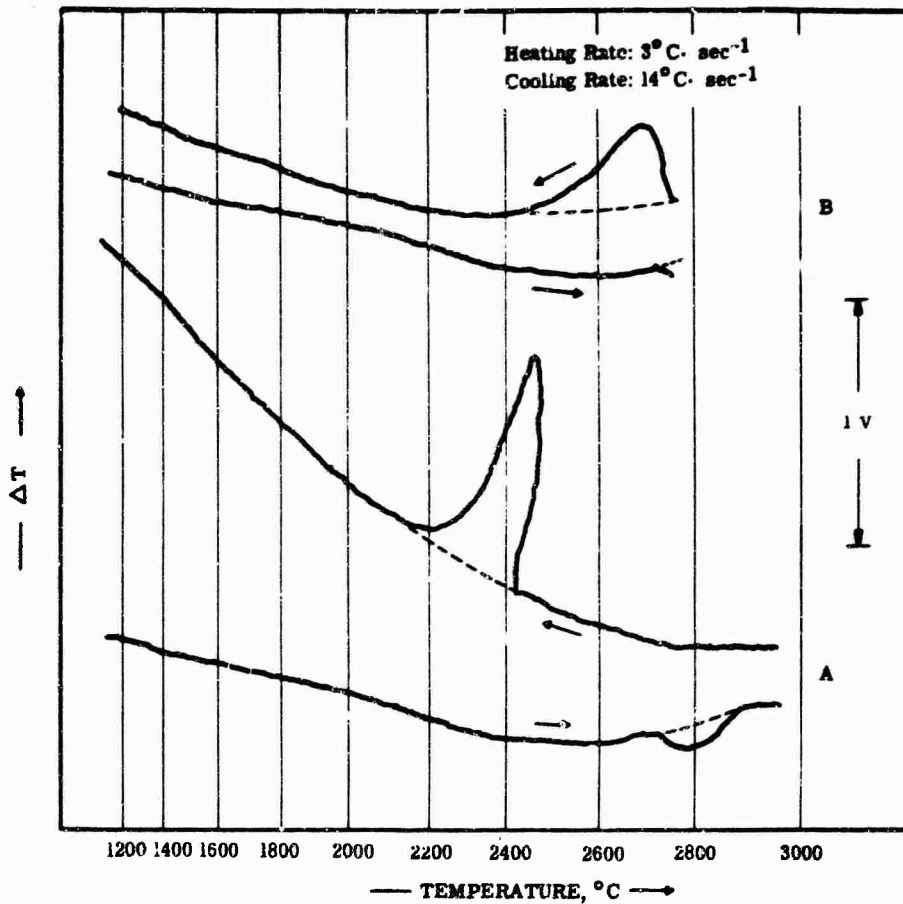


Figure 46. Differential Heating and Cooling Curves of an Osmium-Carbon Alloy .

- A. Showing Eutectic Melting with Supercooling of the Melt
- B. Showing Eutectic Melting and Solidification

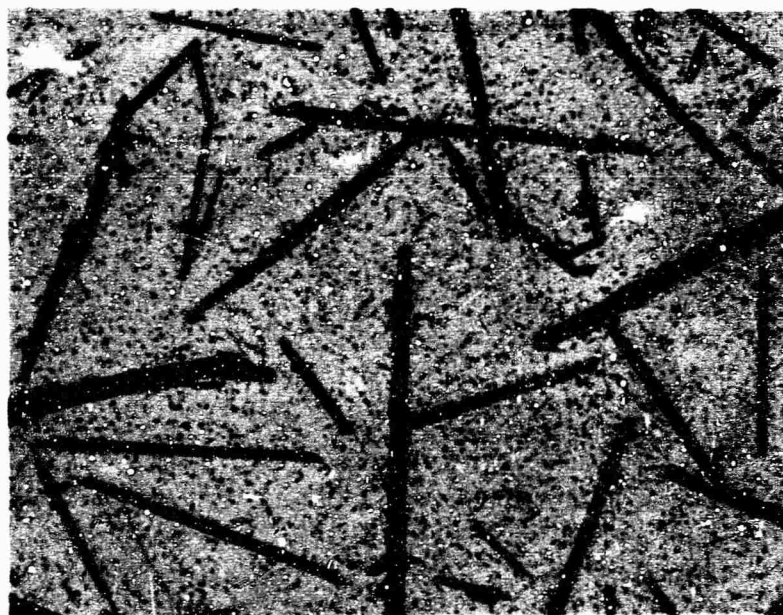


Figure 47. Os-C (73.5/26.5), DTA Alloy Cooled at 13°C per Second From 2900°C. Primary Graphite in a Eutectic Matrix. (Alloy Supercooled, Note Large Size of Primary Graphite Crystals). X175

Metallographic examination of arc-melted alloys as well as of the DTA and melting point samples indicated a eutectic composition of  $17.5 \pm 2$  atomic percent carbon (Figures 48-50). The only phases that were observed in these alloys were osmium and graphite. The solubility of carbon in osmium appears to be only nominal; lattice parameter measurements showed the 'a' parameter to be expanded slightly ( $a = 2.733$  to  $a = 2.736 \text{ \AA}$ ), whereas the 'c' parameter remained nearly constant ( $c = 4.316 \text{ \AA}$ ). However, the exact extent of the carbon solubility was not investigated. It should be noted that the lattice parameters obtained for the pure osmium melting point samples are somewhat smaller than those reported in the literature,  $a = 2.7341 \text{ \AA}$  and  $c = 4.3197 \text{ \AA}$  <sup>(4)</sup>, as compared to,  $a = 2.733 \text{ \AA}$  and  $4.316 \text{ \AA}$ , for the melted samples.

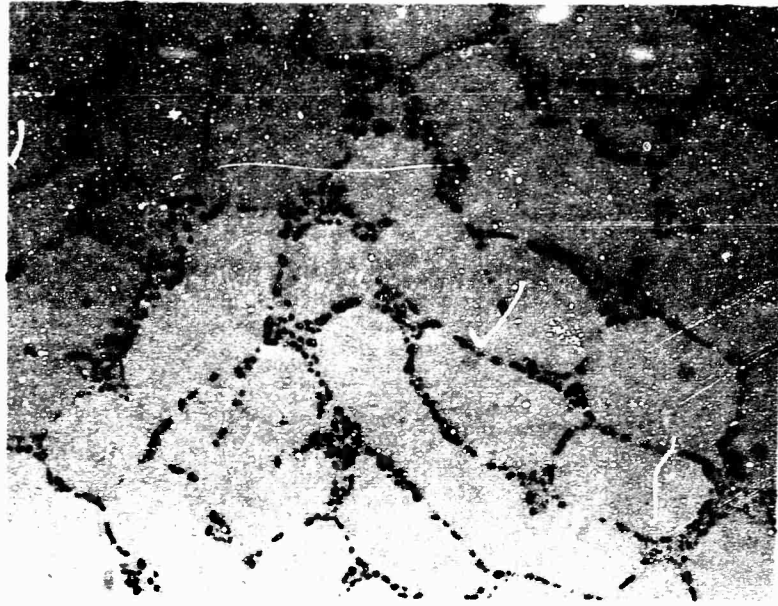


Figure 48. Os-C: (96.5/3.5): Arc-Melted Alloy Showing Primary Metal in a Osmium-Carbon Eutectic Matrix.

X600

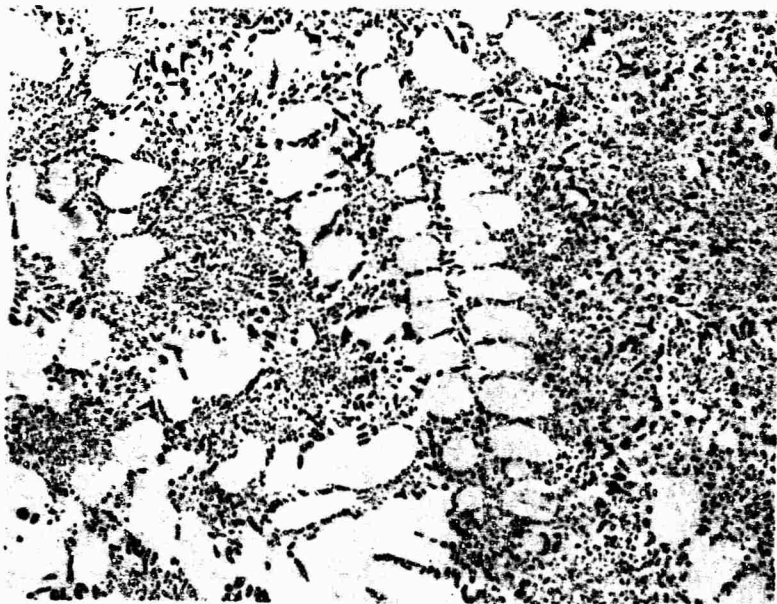


Figure 49. Os-C (91.4/8.6), Arc-Melted Alloy Showing Primary Metal in a Eutectic Matrix.

X375

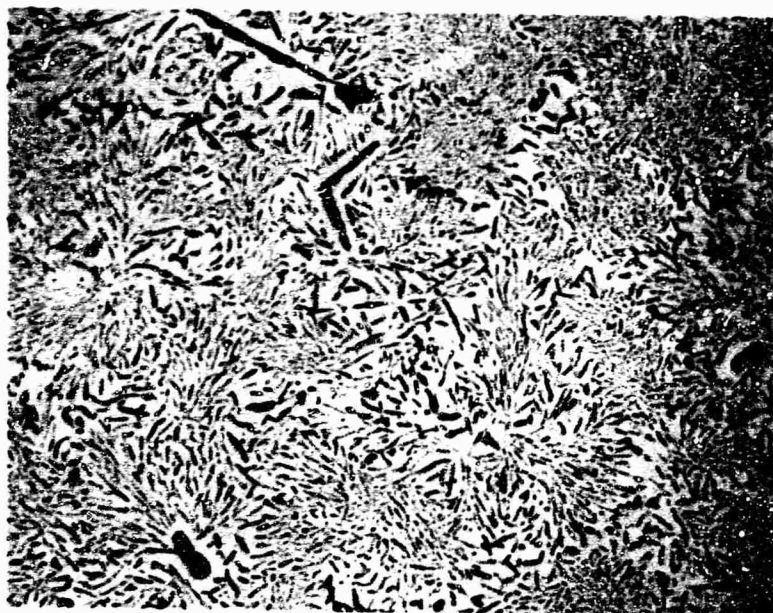


Figure 50. Os-C (81.6/18.4), Arc-Melted Alloy Showing X375  
Primary Graphite in a Eutectic Matrix.  
(Sample Very Close to the Eutectic Composition).



Figure 51. Osmium-Carbon Diffusion Couple Held at 2600°C  
for 4 hours.  
(Osmium-Graphite Interface)  
(X-Ray : hcp Os + Graphite).

In an effort to produce the carbide phase (OsC) reported by Kempter and Nadler<sup>(29, 31)</sup>, the experimental procedures described by them were repeated along with a number of other investigations (see section on special experimental studies). An over-exposed X-ray diffraction pattern of an 10:90 osmium-carbon alloy, which was equilibrated at 2600°C for 4 hours, revealed the presence of only the osmium and graphite phases. Similar results were obtained for an alloy equilibrated at 2700°C for 4 hours. X-ray and metallographic analysis of two diffusion couples, one heat treated at 2600°C for 4 hours, the other at the eutectic temperature, also did not reveal the presence of another phase (Figure 51). These results, coupled with the fact that the phase was not observed in any of the DTA, melting point, or arc-melted alloys, shed some doubt on the existence of the 'OsC' phase. However, the only conclusion that can be drawn with any certainty is, that if the phase does exist, it does not form readily under the conditions of the above described experiments.

The tentative osmium-carbon diagram resulting from these investigations is depicted in Figure 52.

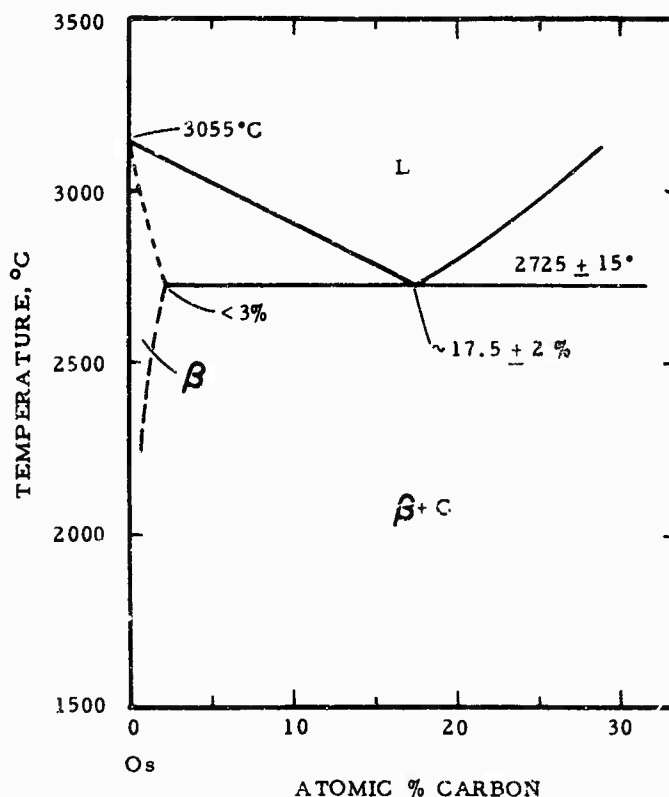


Figure 52. Tentative Osmium-Carbon Phase Diagram.

### (3) Rhodium-Carbon

The eutectic temperature for the Rh-C system was established by differential thermoanalytical techniques (Figure 53) as well as by the Pirani method; the average value from these two methods was  $1662 \pm 15^\circ\text{C}$ . From metallographic examination of chemically analyzed alloys, the composition of the eutectic was positioned at  $16 \pm 2$  atomic percent carbon. Figures 54-56 show some of the results obtained from the metallographic studies of melted alloys. The carbon solubility was indicated to be negligible since no change in the lattice parameter of rhodium could be measured. The lattice parameter of the rhodium starting material was calculated to be  $3.803 \text{ \AA}$ , which is in excellent agreement with the literature value of  $3.8031^{(17)}$ . Figure 57 gives the proposed rhodium-carbon system.

### (4) Iridium-Carbon

Initial investigations of the eutectic temperature by differential thermoanalytical techniques indicated the solidus temperature to be approximately  $2320^\circ\text{C}$  (Figure 53). Subsequent melting point determination using the Pirani-technique resulted in slightly lower melting temperatures. A weighted average for the eutectic temperature was  $2302 \pm 15^\circ\text{C}$ . This value is in very good agreement with the value of  $2296 \pm 17^\circ\text{C}$  reported by Nadler and Kempter<sup>(2)</sup>, but is considerably higher than the temperature of  $2110^\circ\text{C}$  quoted in a report by Criscione et al.<sup>(1)</sup>.

The composition of the eutectic was located by metallographic examination of DTA, melting point, and arc-melted alloys. Figures 58-60 show some of the results obtained in these investigations. Normally, when the alloys were quenched after arc-melting, extremely fine eutectic structures resulted. From these studies, the eutectic composition was positioned at  $6.5 \pm 2$  atomic percent carbon.

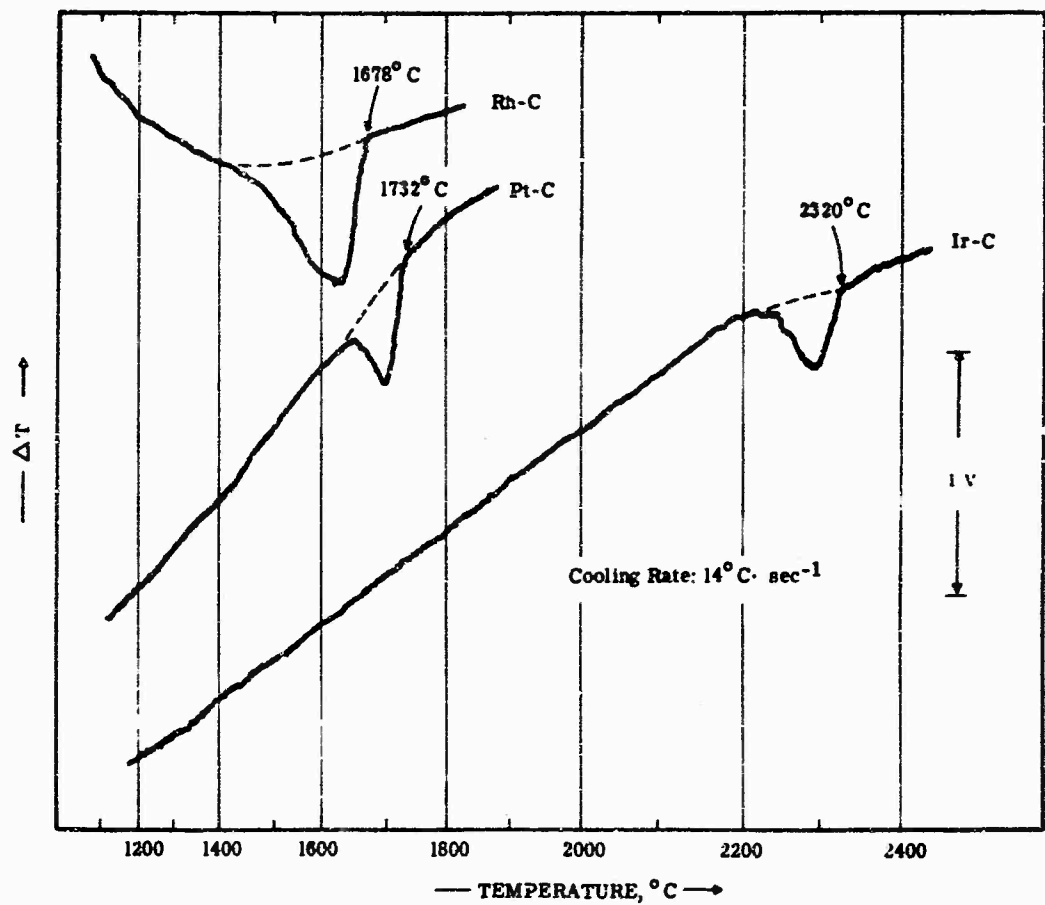


Figure 53. DTA Cooling Curves Showing Eutectic Solidification of Rh-C, Pt-C, and Ir-C Alloys.

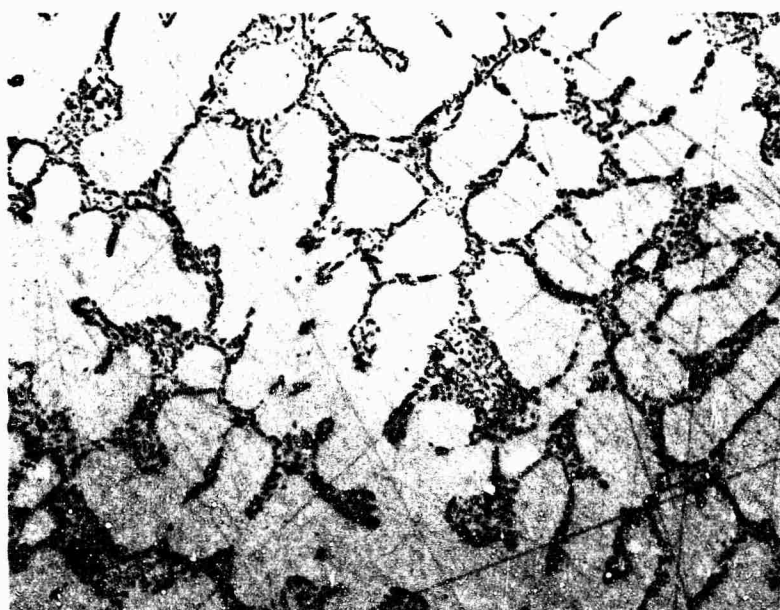


Figure 54. Rh-C (92/8), Arc-Melted Alloy Showing Primary Metal in a Eutectic Matrix.

X525



Figure 55. Rh-C (83/17), Arc-Melted Alloy Showing Primary Graphite in a Eutectic Matrix.

X475

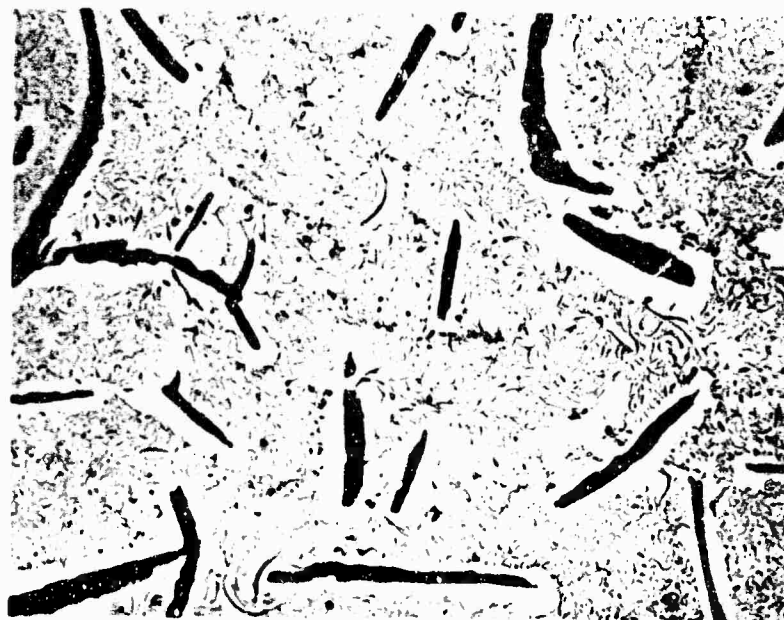


Figure 55. Rh-C (77/23), Arc-Melted Alloy Showing Primary Graphite in a Eutectic Matrix.

X600

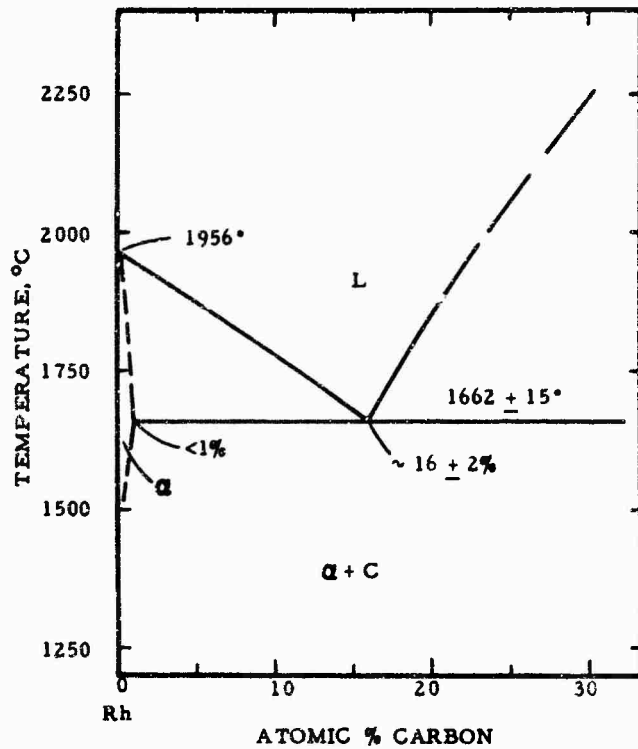


Figure 57. Tentative Rhodium-Carbon Phase Diagram.

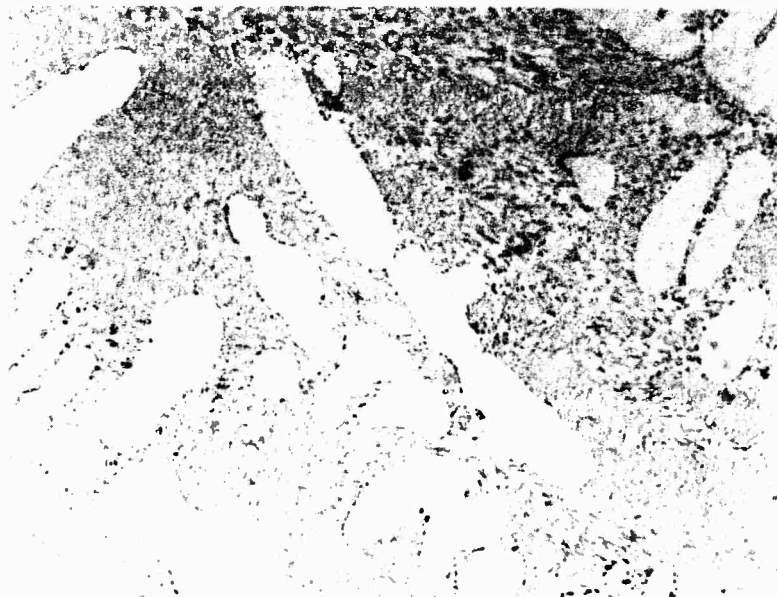


Figure 58. Ir-C: (95.5/4.5), Arc-Melted Alloy Showing X680 Primary Iridium in a Metal-Graphite Eutectic.

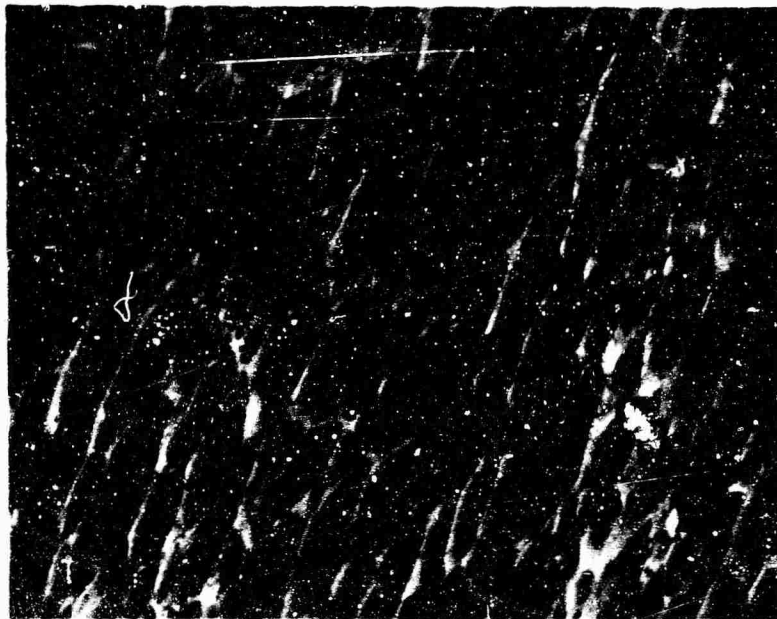


Figure 59. Ir-C: (93.5/6.5), Arc-Melted Alloy Showing X140  
Colonies of Extremely Fine Eutectic (Polarized  
Light to Reveal Structure).

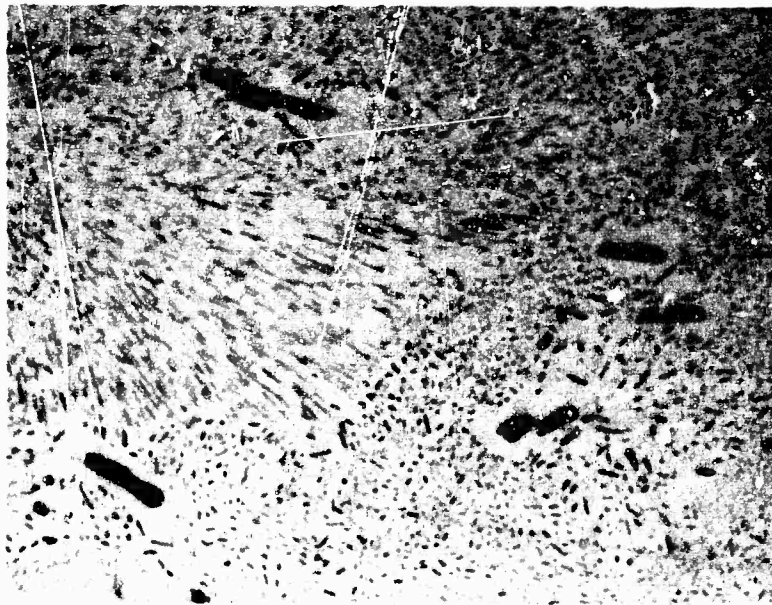


Figure 60. Ir-C: (90.8/9.2), Arc-Melted Alloy Showing X475  
Primary Graphite in a Eutectic Matrix.

Figure 61 gives the tentative iridium-carbon binary diagram. The system appears to be a simple eutectic-type since no phases other than iridium and graphite were observed. The solubility of carbon in iridium is indicated to be small since no detectable change in the lattice parameter was noted. The starting material had a lattice parameter of  $a = 3.839 \text{ \AA}$ , which agrees very favorably with the parameter presented by Taylor and Kagle<sup>(23)</sup>,  $a = 3.8394 \text{ \AA}$ .

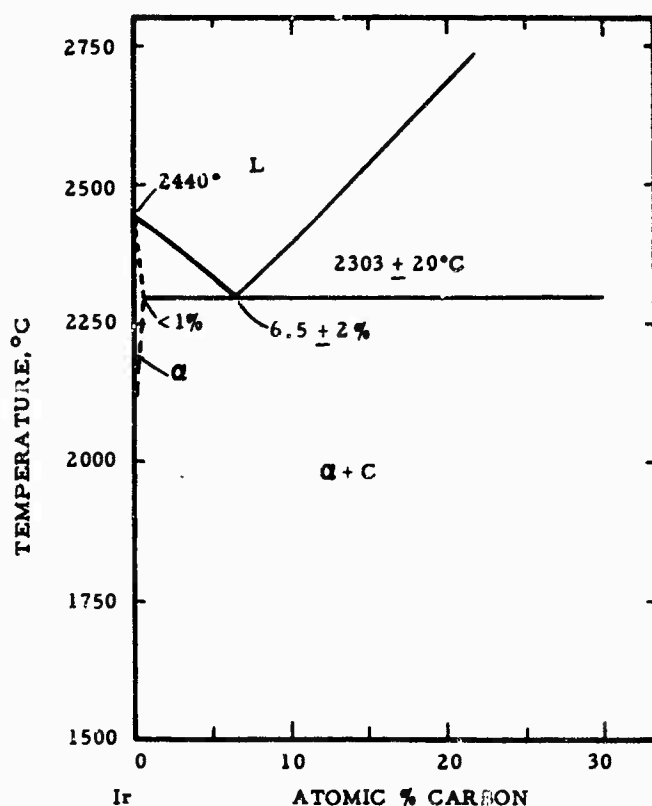


Figure 61. Tentative Iridium-Carbon Phase Diagram.

In view of the fact that it has been reported that silicon and sulfur impurities normally found in commercial grades of graphite form low melting phases with iridium<sup>(24)</sup>, an experiment was performed which would give some indication of the effects of these impurities on iridium-carbon composites. Iridium foil (approximately 0.016" thick) was heat-treated in the presence of pure lampblack, silicon doped lampblack

(approximately 1 weight percent silicon in the lampblack), and sulfur doped lampblack (approximately 1 weight percent sulfur in the lampblack). The three samples were heated to 2150°C under a helium atmosphere and were held at this temperature for three hours. Figure 62 shows the three pieces of iridium subsequent to the tests; the iridium in both the pure lampblack and sulfur doped lampblack had not melted, whereas the foil in the silicon doped lampblack definitely showed signs of melting. This would indicate that close controls of the silicon content of materials to be used for iridium-carbon composite systems must be maintained where the application temperatures are expected to exceed 2150°C. The results also conclusively show that the iridium-carbon eutectic temperature is greater than 2150°C, which is contrary to a previously reported eutectic temperature of 2110°C<sup>(1)</sup>.



Figure 62. Iridium Foils Heated to 2150°C for 3 Hours X2  
in a Helium Atmosphere.

- A. Iridium Foil + Pure Lampblack
- B. Iridium Foil + Sulfur Doped Lampblack
- C. Iridium Foil + Silicon Doped Lampblack

(5) Platinum-Carbon

Similar to the above systems, the platinum-carbon system was found to form a simple eutectic. The eutectic temperature was determined to be  $1732 \pm 15^\circ\text{C}$ ; this value is in very good agreement with that of  $1730 \pm 3^\circ\text{C}$  reported by L.J. Collier et al.<sup>(25)</sup>, and  $1736 \pm 15^\circ\text{C}$  published by Nadler and Kempter<sup>(2)</sup>. The eutectic composition was located at approximately 3 atomic percent carbon (Figures 63 and 64). In their investigation, L.J. Collier et al.<sup>(25)</sup> show that an alloy with 1.2 weight percent carbon (16.5 At. % C) contained large primary flakes of graphite, which is consistent with our results. No measurable change in the lattice parameter of the platinum starting material ( $a = 3.923 \text{ \AA}$ ) could be detected in carbon containing alloys indicating that the carbon solubility is only nominal. Figure 65 gives the resulting platinum-carbon phase diagram.

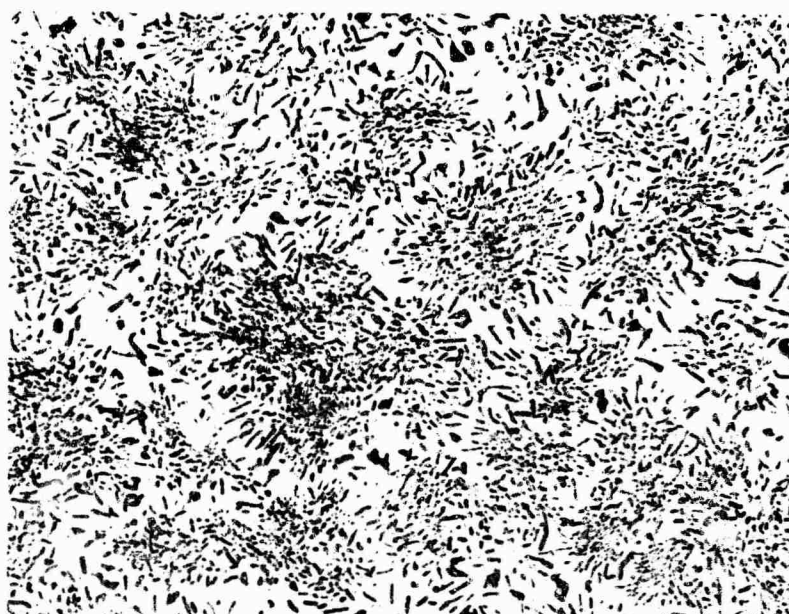


Figure 63. Pt-C (97/3) DTA Alloy Rapidly Cooled from 1800°C. Eutectic Structure.

X200



Figure 64. Pt-C (92.5/7.5), Arc-Melted Alloy Showing Primary Graphite in a Eutectic Matrix.

X550

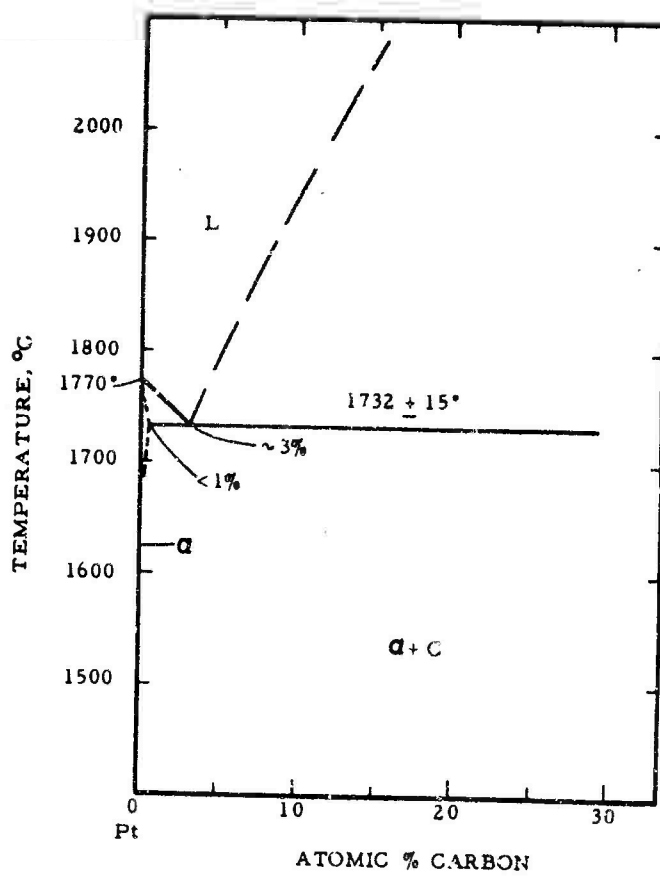


Figure 65. Tentative Platinum-Carbon Phase Diagram.

## b. Ir-Me-C Ternary Alloy Systems

The solidus (eutectic) temperatures of the iridium-rich metal ternary alloys were determined principally with the use of the DTA apparatus. These melting temperatures were checked by melting selected alloys using the Pirani technique. The results of the two methods were in very good agreement in each instance; the results of these melting investigations are given in Figure 4. Rhenium additions have a somewhat greater effect on increasing the refractoriness of the alloy systems than does osmium; platinum, on the other hand, has a slightly more pronounced effect on the melting point depression of the iridium alloy's eutectic temperature than does rhodium. Figure 66 and 67 show some representative DTA heating curves obtained in these studies.

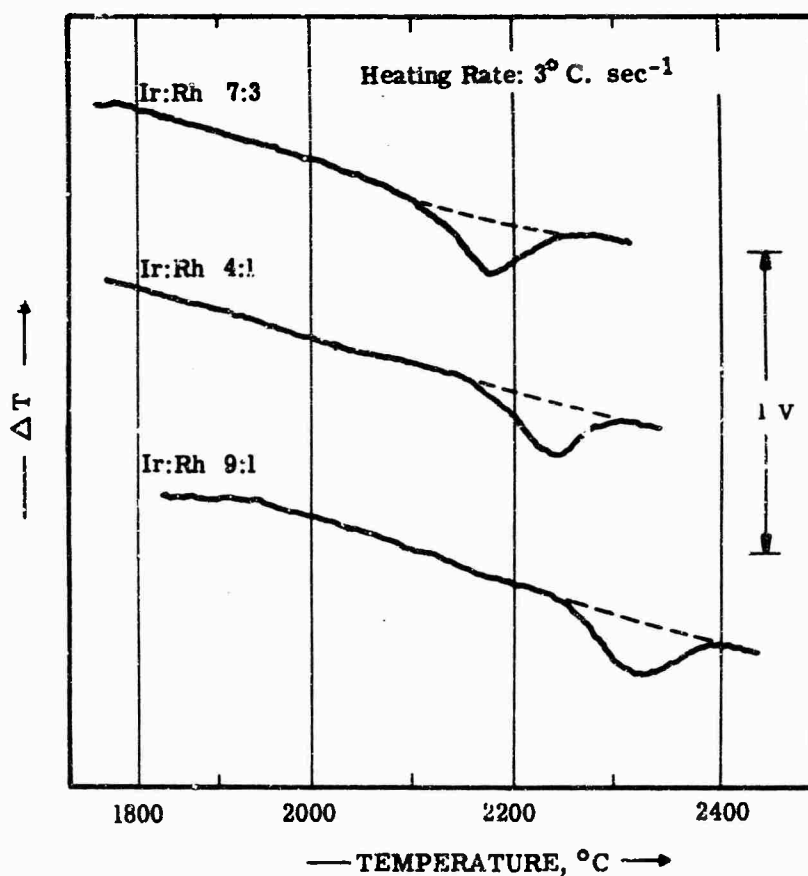


Figure 66. Differential Heating Curves of Ir-Rh-C Alloys Showing Eutectic Trough Melting.

(Ir:Rh Ratios are Given in Atomic Percent of the Starting Pure Metal Alloys).

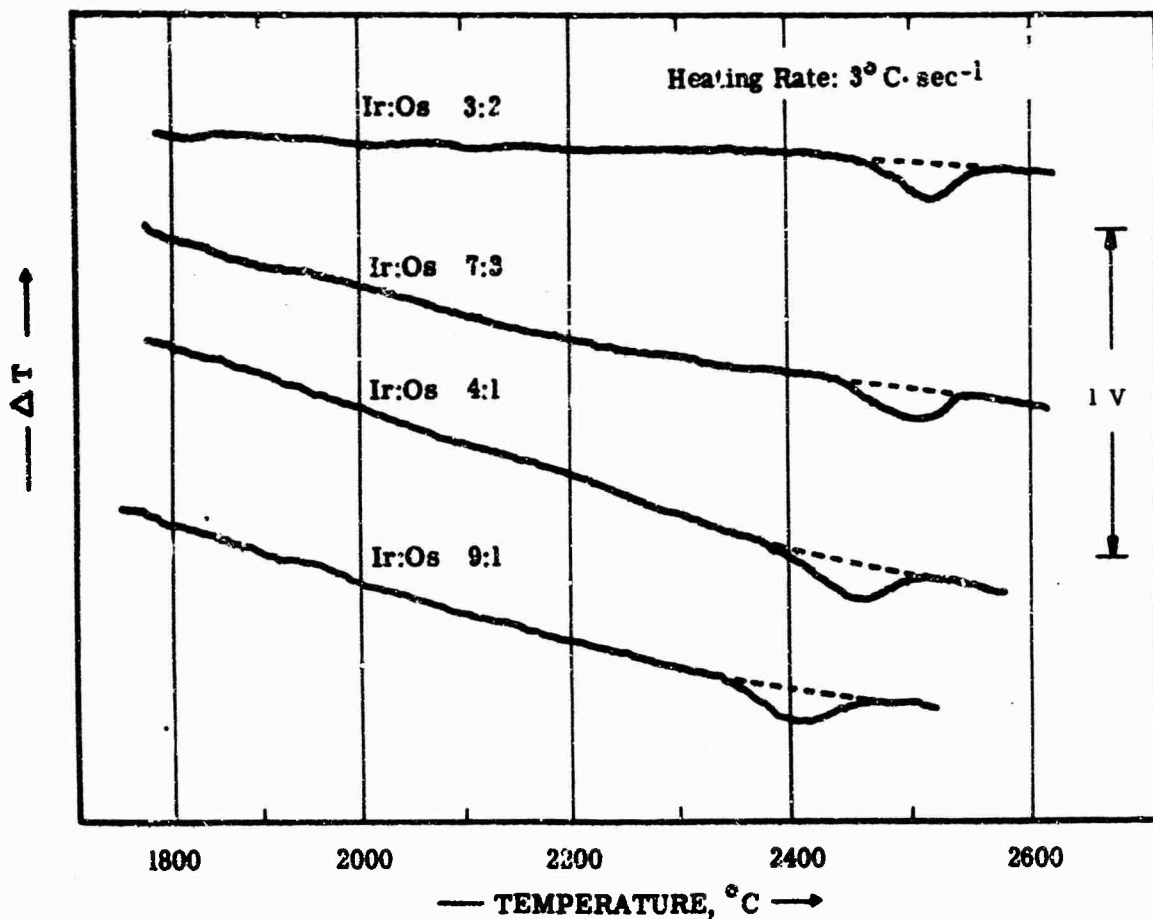


Figure 67. Differential Heating Curves of Ir-Os-C Alloys Showing Eutectic Trough Melting.

(Ir:Os Ratios Given in Atomic Percent of the Starting Pure Metal Alloys).

The compositions of the eutectic troughs were determined by metallographic examination of chemically analyzed DTA, melting point, and arc-melted alloys. The uncertainties to be associated to these values are principally due to the limited number of alloys made in each system; however, the compositions of these eutectics are believed to be correct to  $\pm 2.5$  atomic percent. Figures 68-69 show some representative photomicrographs obtained from the metallographic studies of the alloys, and Figure 70 gives the experimentally determined eutectic trough composition for the iridium-base ternary systems.

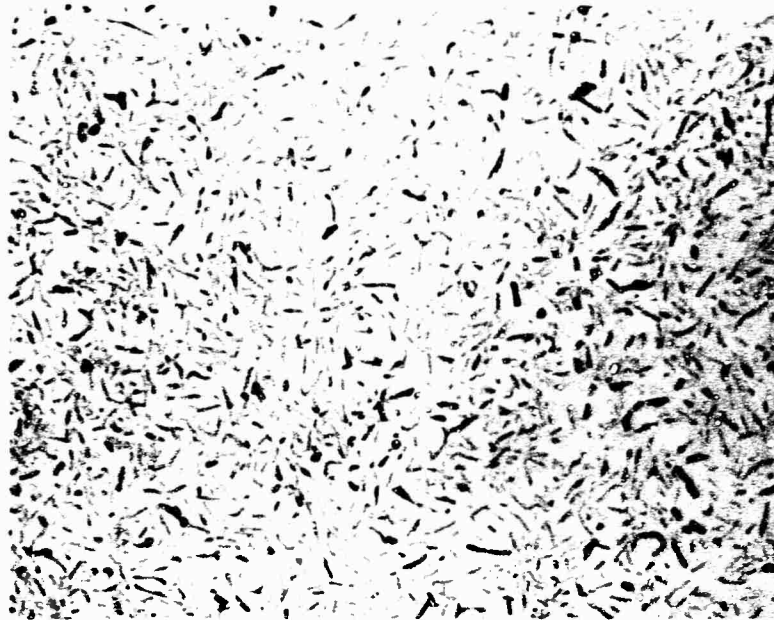


Figure 68. Ir-Os-C (81/10/9): Alloy Cooled in the DTA  
at 13°C per Second from the Melt.

X325

Approximate Eutectic Composition.



Figure 69. Ir-Pt-C (71/18/11): Alloy Cooled in the DTA  
at 13°C per second from the Melt.

X325

Primary Graphite in a Eutectic Matrix.

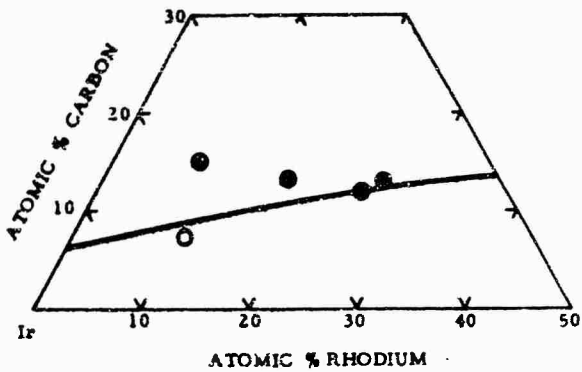
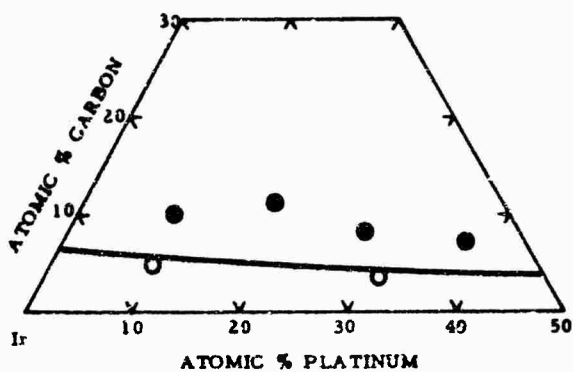
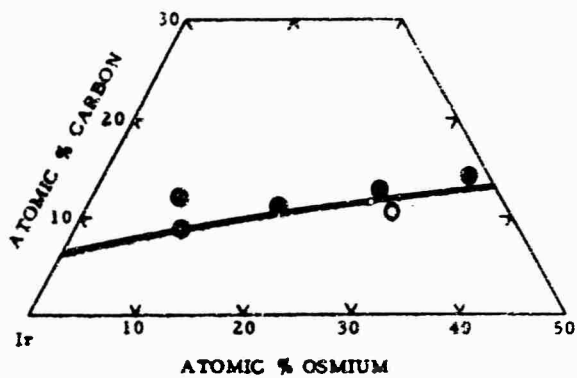
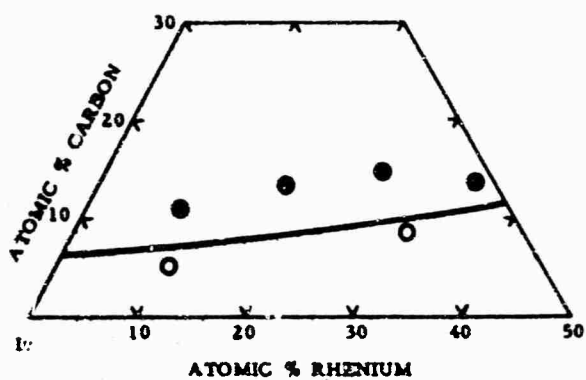


Figure 70. Compositions of the Eutectic Troughs in the Iridium-Base Ternary System.

- Primary Metal
- Eutectic
- Primary Graphite

c. Solidus Temperatures of the Ternary Iridium-Base Alloys in the Presence of Carbon

The majority of these measurements of the metal-carbon eutectic temperatures were performed with the differential thermo-analytical apparatus. The results are, in most cases, based on the data obtained from one sample that was cycled through melting at least four times. In the majority of the instances, the incipient melting temperatures were found to vary only slightly with increasing carbon pickup. The maximum analyzed carbon concentration, subsequent to melting, was approximately 26 atomic percent. However, metallographic examination of the alloys revealed that all of the samples were either entirely eutectic or had primary crystallized graphite. Selected quaternary alloy compositions were also prepared for melting temperature measurements using the Pirani technique. This data provided an independent check on the results obtained in the DTA-apparatus. In most cases the data obtained by the two different methods were in very good agreement; only when the material melted very heterogeneously, were large deviations between the two results observed. In these instances the temperatures recorded by the DTA were believed to be more accurate.

A series of quaternary alloys were also arc-melted in each of the three systems for investigations of the compositions of the eutectic surfaces in these diagrams. Metallographic and chemical analyses of these specimens, as well as of the DTA and melting point samples, provided sufficient information to estimate, with a fair degree of accuracy, the eutectic surface compositions in the quaternary systems.

(1) Iridium-Osmium-Rhodium Alloys

The solidus temperatures of the iridium-osmium-rhodium alloys in the presence of carbon were determined for the metal alloys that were discussed in Section C, 1., c. (1) of the results. These results are presented again in both tabular and graphical form (Table 9 and Figure 71) to best illustrate the compositional variance of the melting temperatures.

Table 9. Solidus Temperatures of Iridium-Osmium-Rhodium Alloys in the Presence of Carbon

Sample No.	Metal Alloy Composition			Eutectic Temperature With Carbon, °C
	Ir	Os	Rh	
1	90	10	0	2341 $\pm$ 25°
2	90	5	5	2280 $\pm$ 25°
3	90	0	10	2234 $\pm$ 25°
4	85	10	5	2276 $\pm$ 25°
5	85	5	10	2241 $\pm$ 25°
6	80	20	0	2377 $\pm$ 25°
7	80	15	5	2318 $\pm$ 25°
8	80	10	10	2278 $\pm$ 25°
9	80	5	15	~2220 $\pm$ 25°
10	80	0	20	2151 $\pm$ 25°
11	75	20	5	2333 $\pm$ 25°
12	75	15	10	2275 $\pm$ 25°
13	75	10	15	2200 $\pm$ 25°
14	75	5	20	2165 $\pm$ 25°
15	70	30	0	2445 $\pm$ 25°
16	70	25	5	~2336 $\pm$ 25°
17	70	20	10	2291 $\pm$ 25°
18	70	15	15	2233 $\pm$ 25°
19	70	10	20	2226 $\pm$ 25°
20	70	5	25	2128 $\pm$ 25°
21	70	0	30	2098 $\pm$ 25°
22	65	30	5	~2373 $\pm$ 25°
23	65	20	15	2273 $\pm$ 25°
24	65	10	25	2162 $\pm$ 25°
25	60	40	0	2456 $\pm$ 25°
26	60	25	15	~2296 $\pm$ 25°
27	60	15	25	~2178 $\pm$ 25°

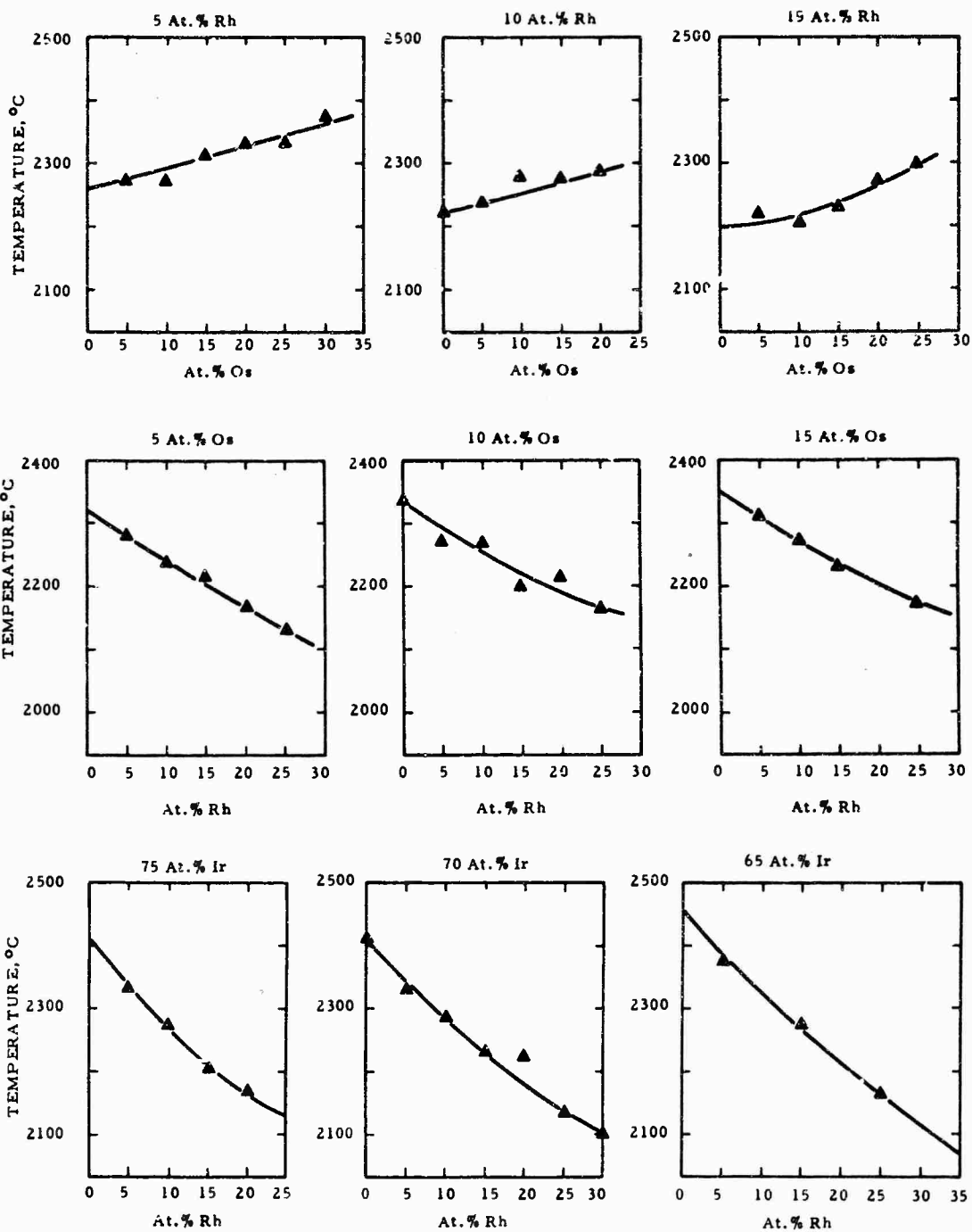


Figure 71. Solidus Temperatures of Iridium-Osmium-Rhodium Alloys in the Presence of Carbon.

- (a) Constant Rhodium Concentrations
- (b) Constant Osmium Concentrations
- (c) Constant Iridium Concentrations

A moderate depression of the melting points of iridium-osmium alloys in contact with graphite is observed by substituting rhodium for iridium ( $\sim 150^\circ\text{C}$  with 25 atomic percent rhodium substitution Figure 71); however, most of these alloys exhibited melting temperatures which were higher than  $2100^\circ\text{C}$ . Furthermore, a significant increase in the oxidation-resistant characteristics of the alloys is expected with the rhodium additions. Figure 72 shows a series of DTA heating curves obtained in these investigations.

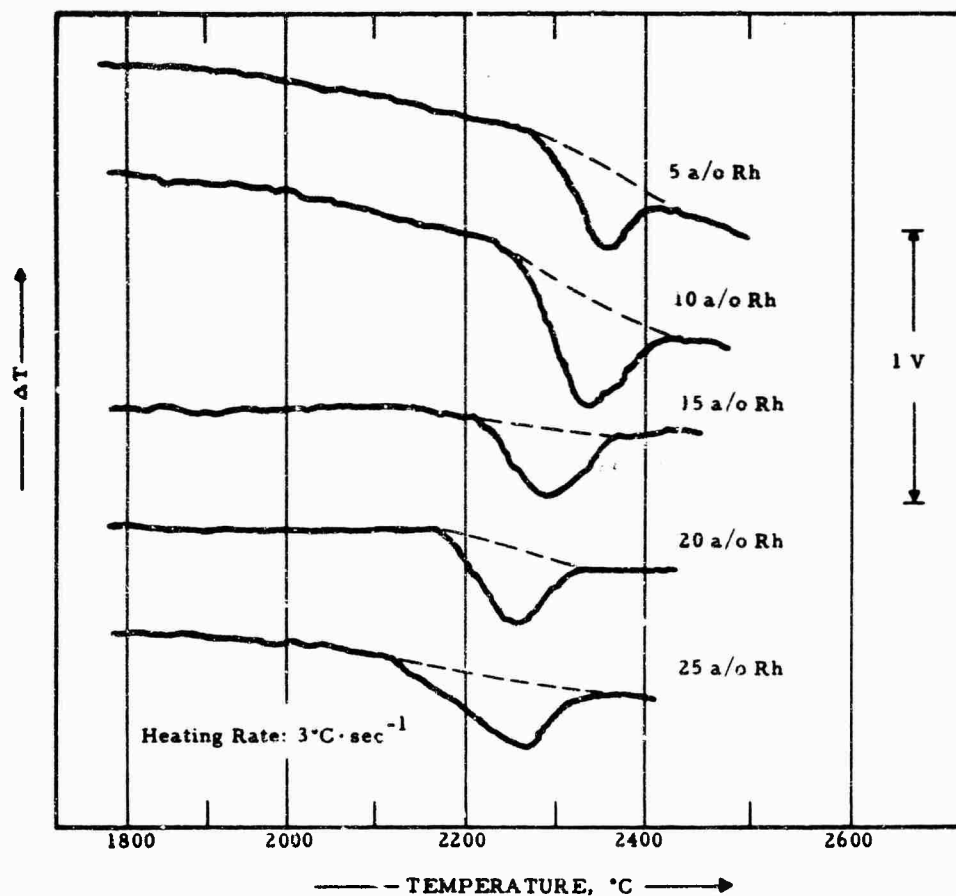


Figure 72. Representative DTA Curves Showing Eutectic Melting in the Iridium-Osmium-Rhodium-Carbon Quaternary System. The Samples Contain a Constant Osmium Concentration of 5 Atomic Percent; the Rhodium Concentrations are listed for each Curve. The Compositions are Given for the Original Metal Alloy Starting Composition.

X-ray diffraction patterns of the quaternary alloys indicated that all compositions which were investigated consisted of only two phases, the iridium face-centered cubic solid solution and graphite. Approximately one-third of the compositional region investigated had solidus temperatures which were greater than that of the binary iridium-carbon ( $\sim 2300^\circ\text{C}$ ), and approximately 95% of the alloys investigated melted at temperatures higher than  $2110^\circ\text{C}$ , which was an earlier reported iridium-carbon eutectic temperature<sup>(1)</sup>. The ternary iridium alloys that appear to be most promising for high temperature applications in a carbonaceous environment are those alloys which have solidus temperatures (with carbon) in excess of  $2200^\circ\text{C}$  and which have a secondary metal (rhodium and osmium) addition of between 2 and 25 atomic percent.

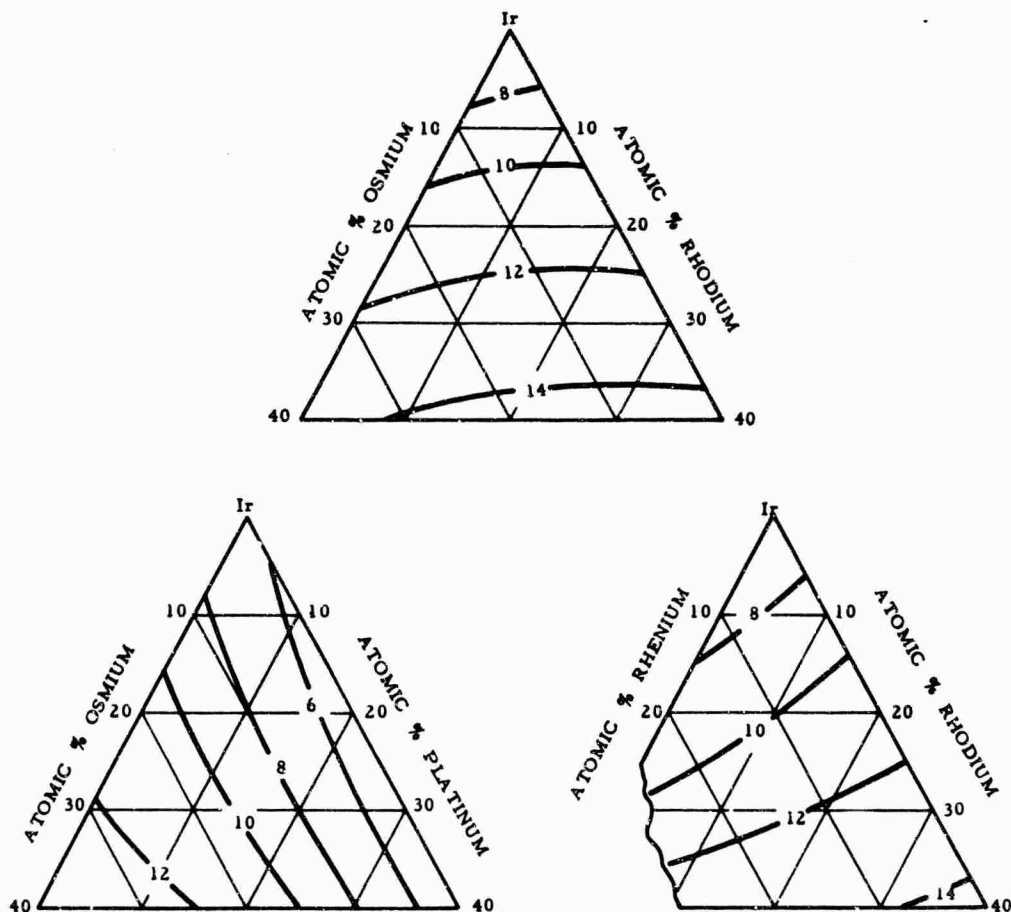


Figure 73. Approximate Eutectic Surface Carbon Concentrations for the Quaternary Systems Ir-Os-Rh-C, Ir-Os-Pt-C, and Ir-Re-Rh-C. The Isocompositional Lines Give the Carbon Concentration in Atomic Percent.

From metallographic studies of melted alloys, the composition of the eutectic surface is indicated in Figure 73. These compositions are less precisely known than the boundary binary and ternary values; however, they are believed accurate to be within  $\pm 3$  atomic percent carbon.

## (2) Iridium-Osmium-Platinum Alloys

The data pertaining to the solidus temperatures of the iridium-osmium-platinum alloys with carbon are compiled in Table 10, and are plotted in Figure 74. The metal solution-graphite eutectic temperatures were generally observed to be slightly lower than for comparable iridium-osmium-rhodium alloys; however, the majority of the eutectic temperatures are in excess of 2100°C.

The X-ray investigations of the quaternary alloy material showed all of the samples to be two-phase, metal solution (fcc) and graphite. Lattice parameter measurements found the parameters to vary nearly the same as the metal alloys without carbon additions.

The compositional field in which the promising alloys lie would be similar to that for the iridium-osmium-rhodium alloys, i.e. alloys which had solidus temperatures with carbon above 2200°C, and have secondary metal addition between approximately 2 to 25 atomic percent.

The estimated eutectic surface compositions are shown in Figure 73. The analysis of this portion of the system was similar to that described in the preceding section. Typical photomicrographs from the metallographic investigations are given in Figures 75-77.

Table 10. Solidus Temperatures of Iridium-Osmium-Platinum Alloys in the Presence of Carbon

Sample No	Metal Alloy Composition			Eutectic Temperature With Carbon, °C
	Ir	Os	Pt	
1	90	10	0	2341 $\pm$ 25°
2	90	5	5	2255 $\pm$ 25°
3	90	0	10	2210 $\pm$ 25°
4	85	10	5	2295 $\pm$ 25°
5	85	5	10	2220 $\pm$ 25°
6	80	20	0	2377 $\pm$ 25°
7	80	15	5	2295 $\pm$ 25°
8	80	10	10	2235 $\pm$ 25°
9	80	5	15	2175 $\pm$ 25°
10	80	0	20	2135 $\pm$ 25°
11	75	20	5	2290 $\pm$ 25°
12	75	15	10	2260 $\pm$ 25°
13	75	10	15	2240 $\pm$ 25°
14	75	5	20	2125 $\pm$ 25°
15	70	30	0	2445 $\pm$ 25°
16	70	25	5	2340 $\pm$ 25°
17	70	20	10	2290 $\pm$ 25°
18	70	15	15	2220 $\pm$ 25°
19	70	10	20	2128 $\pm$ 25°
20	70	5	25	(2151) $\pm$ 25°
21	70	0	30	2057 $\pm$ 25°
22	65	30	5	2366 $\pm$ 25°
23	65	20	15	2236 $\pm$ 25°
24	65	10	25	~2141 $\pm$ 25°
25	60	40	0	2456 $\pm$ 25°
26	60	25	15	2257 $\pm$ 25°
27	60	15	25	2191 $\pm$ 25°
28	60	0	40	1977 $\pm$ 25°

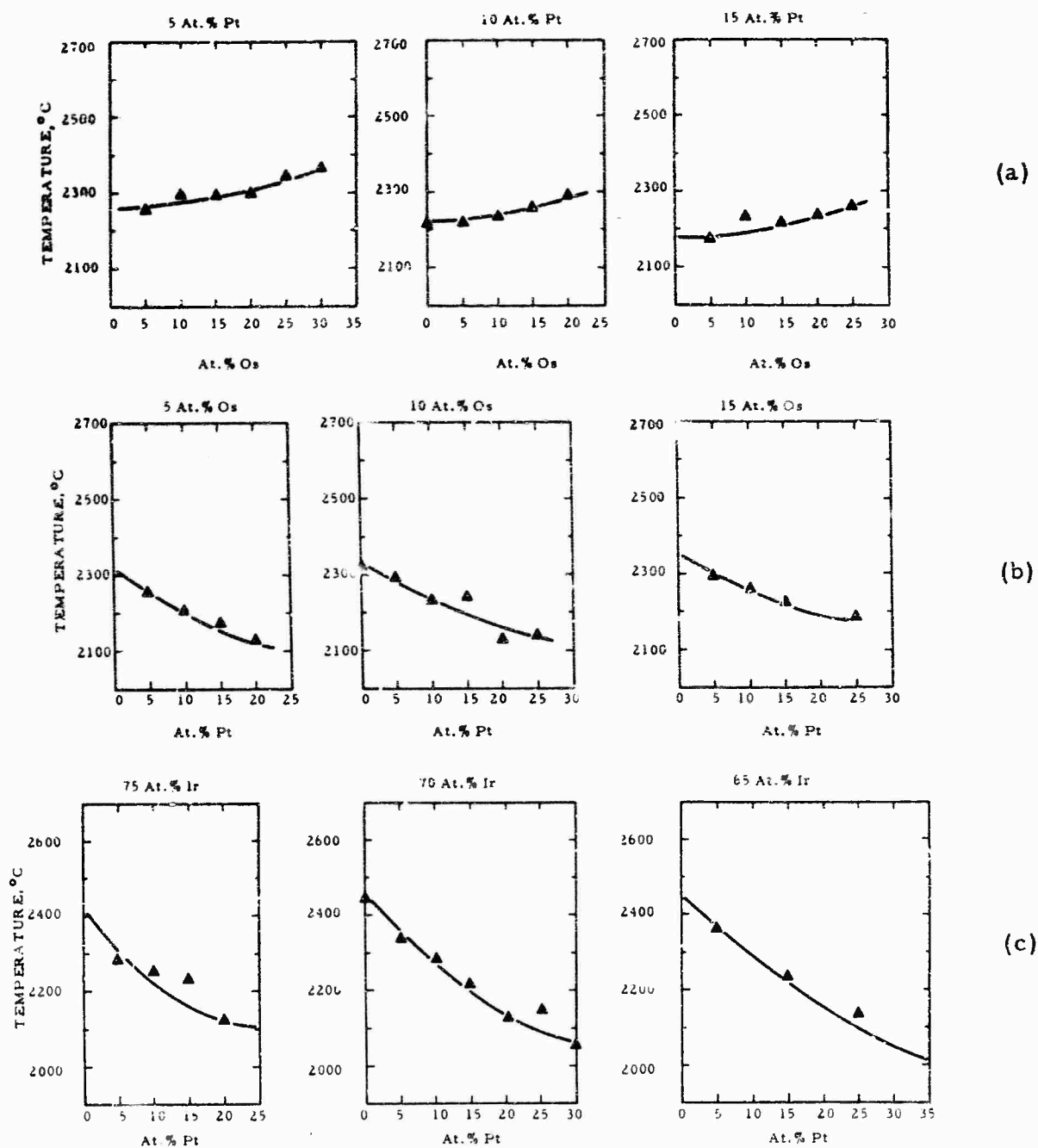


Figure 74. Solidus Temperatures of Iridium-Osmium-Platinum Alloys in the Presence of Carbon.

- (a) Constant Platinum Concentrations
- (b) Constant Osmium Concentrations
- (c) Constant Iridium Concentrations



Figure 75. Ir-Os-Pt-C (65/23/5/7): Arc-Melted Alloy X500  
Showing Primary Metal in a Eutectic Matrix.

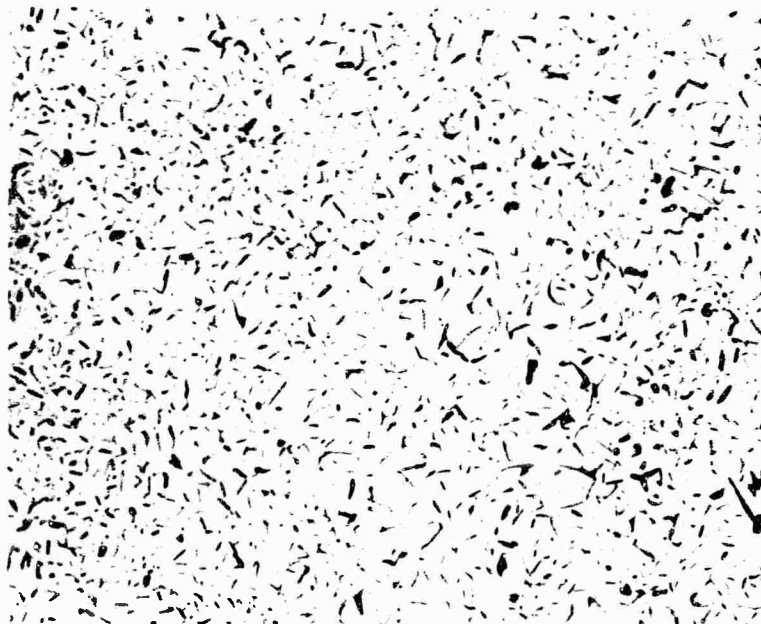


Figure 76. Ir-Os-Pt-C (76.5/9 4.5/10): Arc-Melted Alloy X500  
Showing Metal-Carbon Eutectic Structure.



Figure 77. Ir-Os-Pt-C (55/25 5/15): Arc-Melted Alloy Showing X400 Primary Graphite in a Metal Carbon Eutectic.

### (3) Iridium-Rhenium-Rhodium Alloys

As previously mentioned, the proposed application of these alloys is as an interfacial layer between the more oxidation resistant alloys from the above two systems and graphite. These refractory alloys have solidus temperatures with graphite between approximately 2150°C and 2450°C (Table 11 and Figure 78); their eutectic temperatures are, on the average, 25 to 75°C higher than alloys of similar compositions in the iridium-osmium-rhodium (platinum) systems.

From the X-ray evaluation of the melted specimens, the majority of the alloys was found to be two phase, (fcc solid solution + graphite). However, the hexagonal, rhenium-rich phase was observed at rhenium concentrations of 20 atomic percent and higher; from this result it can be assumed that the three-phase field, (fcc solid solutions + hcp solid solution + graphite), lies at concentration ranges in the quaternary

Table II. The Solidus Temperatures of Iridium-Rhenium-Rhodium Alloys in the Presence of Carbon

Sample No	Metal Alloy Composition			Eutectic Temperature With Carbon, °C
	Ir	Rh	Re	
1	90	10	0	2234 + 25°
2	90	5	5	2260 + 25°
3	90	0	10	2345 + 25°
4	85	10	5	2235 + 25°
5	85	5	10	2310 + 25°
6	80	20	0	2151 + 25°
7	80	15	5	(2170)+ 25°
8	80	10	10	2235 + 25°
9	80	5	15	2380 + 25°
10	80	0	20	(2430)+ 25°
11	75	20	5	2210 + 25°
12	75	15	10	2240 + 25°
13	75	10	15	2330 + 25°
14	75	5	20	2385 + 25°
15	70	30	0	2098 + 25°
16	70	25	5	~2205 + 25°
17	70	20	10	~2260 + 25°
18	70	15	15	2305 + 25°
19	70	10	20	2365 + 25°
20	70	5	25	2395 + 25°
21	70	0	30	2474 + 25°
22	60	0	40	2496 + 25°

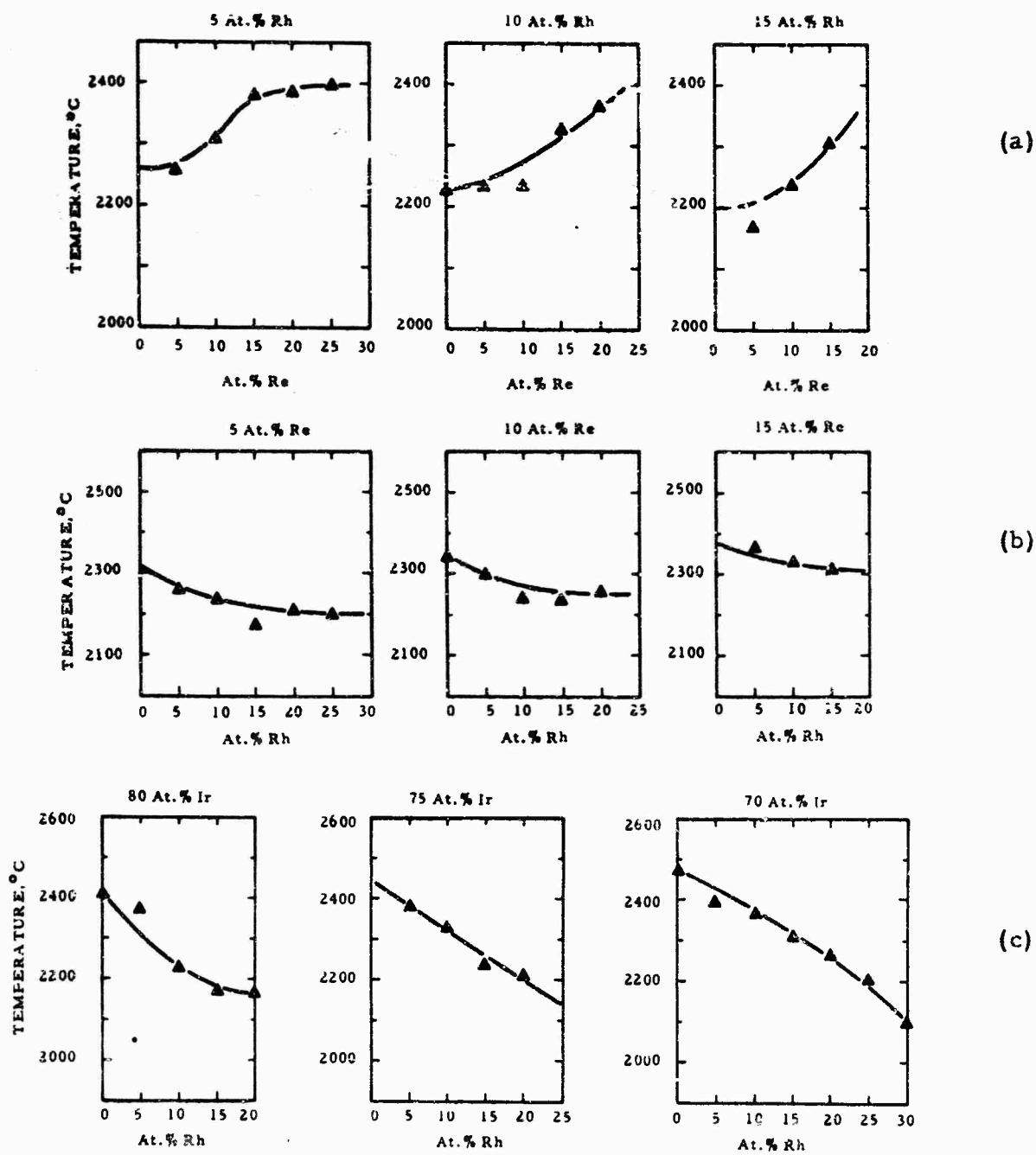


Figure 78. Solidus Temperatures of Iridium-Rhenium-Rhodium Alloys in the Presence of Carbon.

(a) Constant Rhodium Concentrations

(b) Constant Rhenium Concentrations

(c) Constant Iridium Concentrations

section which have rhenium contents greater than 20 atomic percent. Figure 73 depicts the approximate carbon concentration of the eutectic surface. The rhenium-richest portion of this figure was omitted since melting, other than the simple eutectic-type, is believed to occur in this portion of the system for a third phase (the hcp rhenium solid solution) was observed in the melted alloys. Resolution of the phase equilibria in this region was not attempted, because metal alloys which were not single phase were not of particular interest in these studies.

Similar consideration can be employed to the selection of the most promising section of the Ir-Re-Rh alloy system for coating application as were applied to the above mentioned systems.

### 3. Theoretical Analysis of the Data

A thermochemical analysis of the above data, as well as of the data from the existing platinum-metal binary system, was made with the objective of establishing numerical relations between the melting point depression and properties of the melt of the component metals. The analytical approach for the extraction of the specific parameters is given in the following sections, and the feasibility of using this data in order to predict the solidus (eutectic) temperatures between the metal components and carbon is demonstrated. In the majority of the calculations, an over simplified approach was used in lieu of a more correct and more rigorous one when the end results appeared to be reasonable. This procedure, although not strictly correct, is believed to be justifiable because its straightforwardness makes the theoretical prediction of the systems more appealing to those who might be interested in this group of alloy systems.

The highest order of system treated within this presentation is the ternary system. Higher order systems can also be predicted using this approach; however, if certain experimental data are not available (e.g. the solidus temperatures of the metal solution) the calculations can become somewhat laborous.

a. Analytical Approach

(1) Metal-Carbon Systems

For the binary metal-carbon systems two assumptions were made in order to simplify the calculations. These are as follows:

(a) The solubility of carbon in the metal phase, and the solubility of metal in the carbon (graphite) phase was assumed to be negligible.

(b) The liquid phase was defined to behave regularly.

An exception to (a) has to be made for the rhenium-carbon system, because an extensive carbon solutioning in the metal phase is observed.

The first of the above idealizations is believed to be sufficiently valid for the treatment of the platinum metals, but the latter is obviously somewhat dubious. However, previous calculations, making a similar simplification, have been performed with reasonable success<sup>(47)</sup>. Therefore, a more rigorous description of the liquid phase is not believed to be warranted here.

With the above idealizations, the partial free energy terms are greatly simplified, and the analysis of the parameters can be performed with relative ease. The partial free energy terms for the respective components then can be written as:

$$\overline{\Delta G}_c^G = \overline{\Delta G}_c^a = 0 = \overline{\Delta G}_c^L = \epsilon_L (1-x^L)^2 + RT \ln x^L + \Delta G^{G \rightarrow L} \quad (3)$$

$$\overline{\Delta G}_m^a = \overline{\Delta G}_m^G = 0 = \overline{\Delta G}_m^L = \epsilon_L (x^L)^2 + RT \ln(1-x^L) + \Delta G^{a \rightarrow L} \quad (4)$$

where  $\overline{\Delta G}_i^j$  is the relative partial free energy of the 'i' component in the 'j' phase,  $\epsilon_L$  is the interaction parameter for the liquid solution, T is the absolute temperature ( $^{\circ}\text{K}$ ),  $x^j$  is the mole fraction of carbon in the 'j' phase, and  $\overline{\Delta G}^{j \rightarrow L}$  is the relative free energy of melting of the solid phase to the liquid state. The unknown in these relationships is the interaction parameter for the liquid phase ( $\epsilon_L$ ). The evaluation of  $\epsilon_L$  is best made at the eutectic temperature, because at this temperature the equilibria concentrations of the liquid phase are best known. By equating the proper partial relative molar free energies at this temperature, the calculation of this parameter can be made.

The enthalpy of fusion for the metal elements were taken from thermodynamic values compiled by Hultgren et al. (48), and the free energy of fusion for the graphite phase was taken as

$$\Delta G_c^{G \rightarrow L} = 21,600 - 5.4T \text{ cal/gm.at.} \quad (5)$$

which is a value estimated by Kaufman (47).

Because of the fact that in the rhenium-carbon system an extensive solubility of carbon in the metal phase is observed, the assumptions that  $\overline{\Delta G}_m^\beta = 0$  and  $\overline{\Delta G}_c^\beta = 0$  cannot be used. For this case the calculations followed a previous model for evaluating the free energy of formation of an interstitial solution of carbon in a hcp-phase (49).

From a statistical analysis of the entropy of mixing, the below equation for the relative free energy of formation of the interstitial solid solution results:

$$\Delta G_f = Bx + RT \left[ x \ln \frac{x}{1-2x} + (1-x) \ln \frac{1-2x}{1-x} \right] \quad (6)$$

where the first term arises from the thermal contribution, and the second from the entropy contribution in which B is a constant to be determined. It is assumed that the thermal free energy of formation of the solid solution is proportional to the carbon concentration; the configurational free energy of formation is therefore, entirely due to the entropy of mixing of the interstitial carbon atoms among the available sites. A slight modification of this equation was made in order to obtain a better fit to the experimental rhenium-carbon diagram. Here a second constant, A, was added to the equation, and thus the thermal contribution term becomes A + Bx. The partial molar free energies for the metal and carbon components in the terminal hcp ( $\beta$ ) solid solution are then:

$$\overline{\Delta G}_m^\beta = A + RT \ln \frac{1-2x}{1-x} \quad (7)$$

and

$$\overline{\Delta G}_c^\beta = A + B + RT \ln \frac{x}{1-x} \quad (8)$$

The liquid solution for the Re-C system was also assumed to behave regularly. The evaluation of the parameters  $\epsilon_L$ , A, and B, is again performed by equating the partial molar free energies of the elemental components in the liquid to those of the solid  $\beta$ -phase at the eutectic temperature.

The values for the interaction parameters for the liquid phase resulting from the above described method of analysis are given in Table 12. The values for the parameters A and B for the rhenium solid solution were calculated to be 1,250 and 9,000, cal/gm. atom, respectively.

## (2) Metal-Metal Binary Systems

In order to calculate the ternary  $Me_1$ - $Me_2$ -C solidus temperatures, (where  $Me_1$  and  $Me_2$  stand for metals of the platinum family and also for rhenium) the behavior of the boundary metal binary have to be known. If these systems have not been experimentally determined, they must be calculated. Since an assumption is made in the

Table 12. Liquid Interaction Parameter Values Calculated from the Established Metal-Carbon Binaries. (Regular Liquid Solution Behavior)

System	$\epsilon_L$ (cal/gm.at.)
Rhenium-Carbon	3,000 $\pm$ 1,500
Osmium-Carbon	8,000 $\pm$ 1,500
Iridium-Carbon	7,000 $\pm$ 1,500
Rhodium-Carbon	-5,800 $\pm$ 1,500
Platinum-Carbon	5,950 $\pm$ 1,500

next section which makes the calculation valid only for cases which concern equilibria between the fcc-solid solution, liquid, and carbon phases; only the equilibrium between the fcc and liquid phase needs to be dealt with here.

For these metal systems, it is believed that defining the solid and liquid solutions to behave regularly is sufficiently correct. The interaction parameters for the fcc-platinum systems can, in a large number of cases, be calculated from experimentally established data. For systems which have not been determined, the interaction parameter for the solid phase can be estimated by correlating the difference in melting temperatures of the elemental constituents with the critical temperature of closure for the miscibility gap presented by Raub<sup>(9)</sup> (Figure 79). The interaction parameter for the particular liquid phases were taken as equal to, or somewhat less than, that for the solid phase.

For the isomorphous fcc-metals, the liquidus and solidus curves can be calculated by equating the relative partial molar free energies (i.e.  $\overline{\Delta G}_A^a = \overline{\Delta G}_A^L$  and  $\overline{\Delta G}_B^a = \overline{\Delta G}_B^L$ ) and simultaneously solving for the equilibrium concentration at liquid-solid boundaries.

For the binary systems involving non-isomorphous phases (fcc and hcp), an analysis of the existing equilibrium diagrams was performed in order to determine the transitional energies for the elements from one crystal modification into the other. Equating the partials at the terminal  $\alpha$ - $\beta$ -phase boundaries yields the equation below:

$$\epsilon_a^{1-x_{A(\alpha)}} - \epsilon_\beta^{1-x_{A(\beta)}} + RT \ln \frac{x_{A(\alpha)}}{x_{A(\beta)}} = \Delta G_A^{\alpha \rightarrow \beta} \quad (9)$$

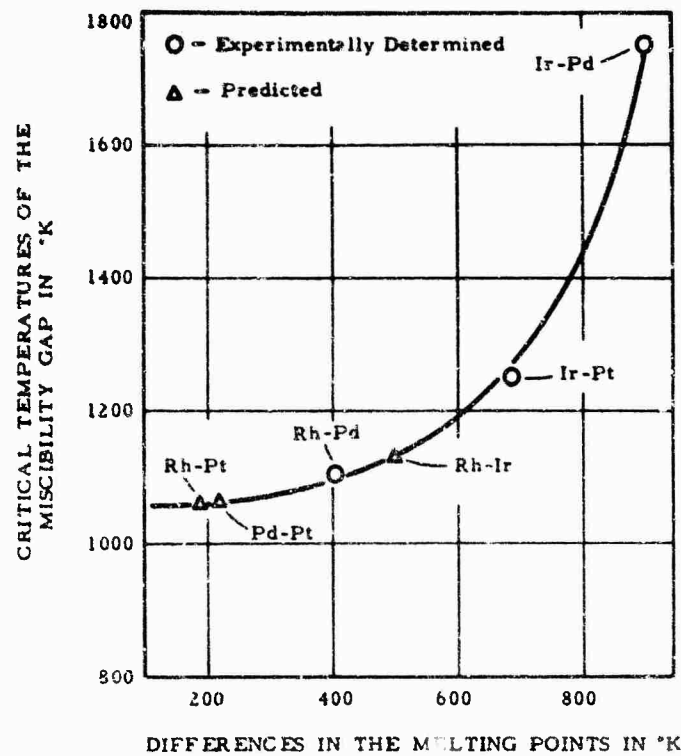


Figure 79. Correlation Between the Difference in Melting Points of the Platinum-Group Metals and the Critical Closing Temperature of the Miscibility Gap. (Raub, 1959).

where  $x_{A(j)}$  is the mole fraction of component A at the 'j' phase's boundary. A similar relation exists for the  $\Delta G_B^{\beta \rightarrow \alpha}$  value. For these systems, three separate pairs of two phase equilibria must be calculated in order to determine

solidus temperatures. However, since only the boundaries of the  $\alpha$ -fcc phase are of interest; (i.e. the  $\alpha$ -L and  $\alpha$ - $\beta$  phase boundaries), the number of calculations are greatly reduced. Again, the phase boundaries are determined by equating the proper relative partial molar free energies and solving for the equilibrium concentrations.

The available literature diagrams<sup>(10,19,50)</sup> involving the platinum metals with themselves, as well as with rhenium, were evaluated in order to obtain numbers for the transitional energies as well as for the solid solution interaction parameters arising from describing the solution as behaving regularly. For the cases at hand, it was assumed that the interaction parameters for the fcc and hcp solutions were approximately equal in value. The values for the transition energies for the fcc platinum metals were found to be in the neighborhood of a few hundred cal/gm. atom, e.g. for iridium  $\Delta G^{\alpha \rightarrow \beta} \approx 900 \pm 200$  cal/gm atom. The transitional values for the hcp-platinum metals (and rhenium) to the fcc structure were found to be approximately the same, e.g. for osmium  $\Delta G^{\beta} \approx 800 \pm 200$  cal/gm. atom (Table 13). Good agreement was not always observed between the phase diagram involving one particular hcp metal with different fcc elements (i.e. between the phase system: Re-Pt, and Re-Rh, and Re-Ir, etc). This indicates the assumption that the solutions behave regularly is not as exact a model as might be necessitated; the values calculated using this model should therefore be looked upon with some reservations. However, this approach is believed sufficiently correct to allow it to be used in evaluating the solidus temperatures in these systems. As an example, the iridium-osmium phase system was calculated using the parameters obtained in this analysis (Table 13), and a good correlation between the literature system and this system is observed (compare Figures 80 and 9).

### (3) Calculation of Metal-Carbon Solidus Temperatures

The calculation of the eutectic solidus temperatures for the binary systems, as well as for two ternary systems (Ir-Os-C and Ir-Pt-C), were carried out in order to demonstrate the feasibility of the theoretical method.

Figure 13. Relative Free Energy of Transition (fcc  $\rightleftharpoons$  hcp) for the Platinum-Group Metals and Rhenium, Along with the Approximate Solid Phase Interaction Parameter for the Metal Binary System (Regular Solution).

Metal	Structure	$\Delta G^{\alpha \rightarrow \beta}$ (or $\Delta G^{\beta \rightarrow \alpha}$ ) (cal/gm.atom)	${}^e_{\text{Re-Me}}$ (cal/gm.atom)	${}^e_{\text{Os-Me}}$ (cal/gm.atom)
Rhenium	hcp	$560 \pm 200$	-	-
Osmium	hcp	$800 \pm 200$	-	-
Rhodium	fcc	$750 \pm 200$	$10,500 \pm 2000$	-
Iridium	fcc	$900 \pm 200$	$7500 \pm 1500$	$6700 \pm 1500$
Platinum	fcc	$650 \pm 200$	$5100 \pm 1000$	-

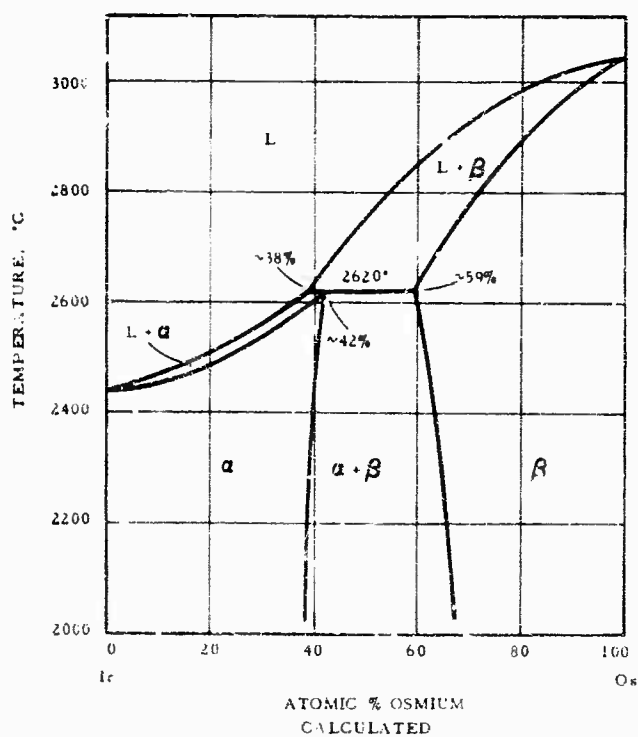


Figure 80. Calculated Iridium-Osmium Phase Diagram.

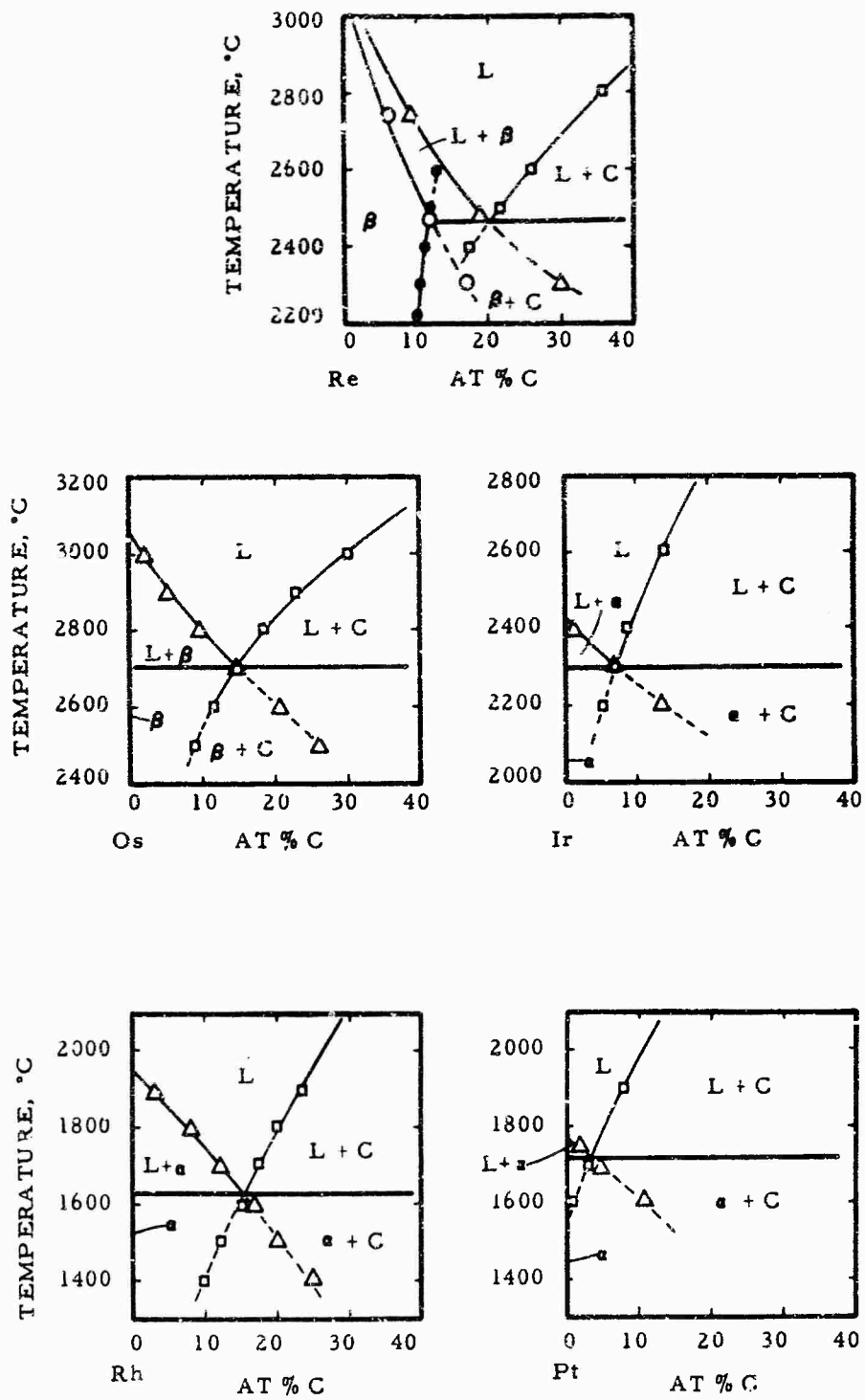


Figure 81. Calculated Metal-Carbon Binary Systems.

The estimation of the binary systems was performed using the previously mentioned assumptions and the above extracted parameters (Table 13). These diagrams are given in Figure 81, and as can be seen, the agreement with the experimentally established system is very good indeed.

For the ternary systems, the calculations relied only on the data derived from the metal-carbon and metal-metal binary systems. Additional approximations which were made in order to simplify the calculations were;

(a) the ternary interaction parameter for the liquid solution has a linear dependent value between the end binary system (e.g. for the iridium-osmium-carbon system,  $\epsilon_L$  (for a 90:10 metal alloy in equilibrium with graphite) =  $.9\epsilon_{L_{Ir-C}} + .1\epsilon_{L_{Os-C}} = 7,100$  cal.

(b) the system is to be treated as a quasi-binary system in which the alloy component is assumed to melt congruently, and that the solubility of metal in the carbon phase, and of carbon in the metal phase is negligible. The enthalpy of fusion of the alloy is approximately equal  $\Delta H_f \approx \Delta S T_f$ , where  $\Delta S$  is the entropy of fusion ( $\Delta S \approx 2.3$ ), and  $T_f$  is the melting temperature ( $^{\circ}K$ ) of the alloy.

These calculations then can be considered as treating a series of quasi-binary metal-carbon systems; the estimation of the solidus temperatures can be carried out as described for the real binary systems. One stipulation that is put on this treatment is that the metal alloys have to be single phase, since for the analysis of higher order systems, these approximations would lead to gross errors.

Figure 82 shows the calculated solidus temperatures of the two ternary systems which were considered, and a comparison is made with the experimentally obtained solidus temperatures. Agreement between the curves is very acceptable. However, no pretense is made that the theoretical treatment is a substitute for experimentally

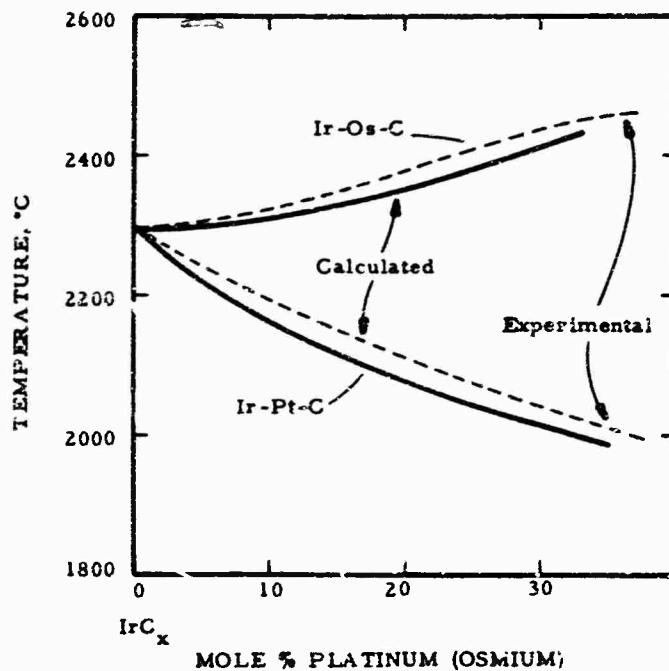


Figure 82. Calculated Solidus Temperatures for the Ternary Systems Iridium-Osmium-Carbon and Iridium-Platinum-Carbon.

obtained data. This treatment only allows a relatively quick and economical method of selecting promising systems which might be of some practical interest, thus helping to eliminate the expensive "shot-in-the-dark" type of experimentation.

#### 4. Thermal Expansion Measurements

The thermal expansion of the seven alloys were measured in order to define the thermal expansion characteristics of the metal alloy systems presently investigated. Four alloys were prepared in the respective binary systems, and one specimen was prepared in each of the three ternary alloy systems. Figures 83, 84, and 85 show the compositions of the alloys selected for thermal expansion measurements. These figures also show the compositional reg of the alloys for which the thermal expansion characteristics were estimated on the basis of the experimentally determined values.

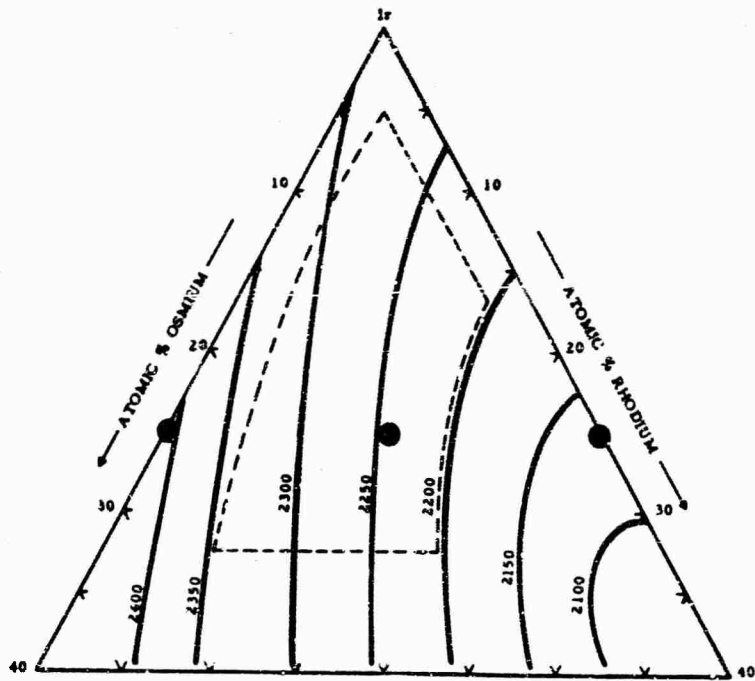


Figure 83. Compositional Field of Iridium-Osmium-Rhodium Alloys for which the Thermal Expansion Characteristics were Estimated.

● Thermal Expansion Alloys.

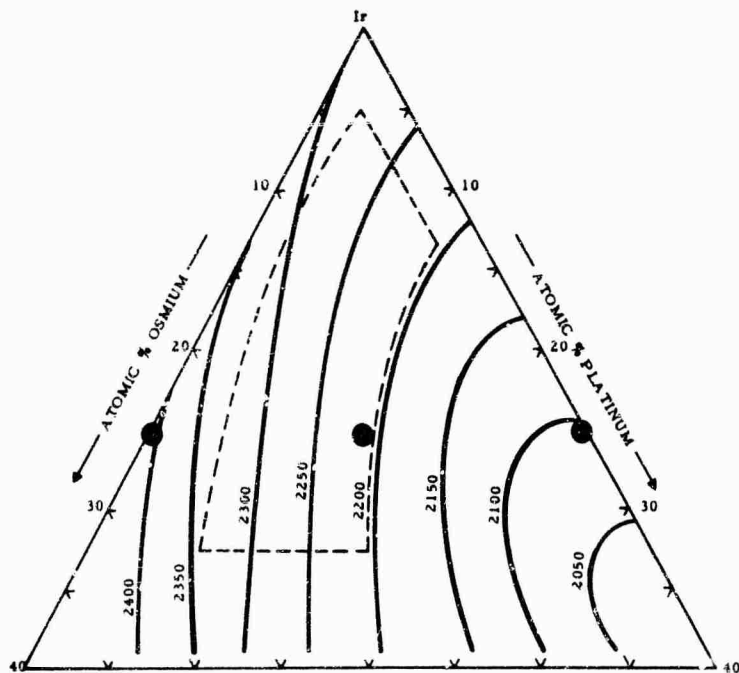


Figure 84. Compositional Field of Iridium-Osmium-Platinum Alloys for which the Thermal Expansion Characteristics were Estimated.

● Thermal Expansion Alloys.

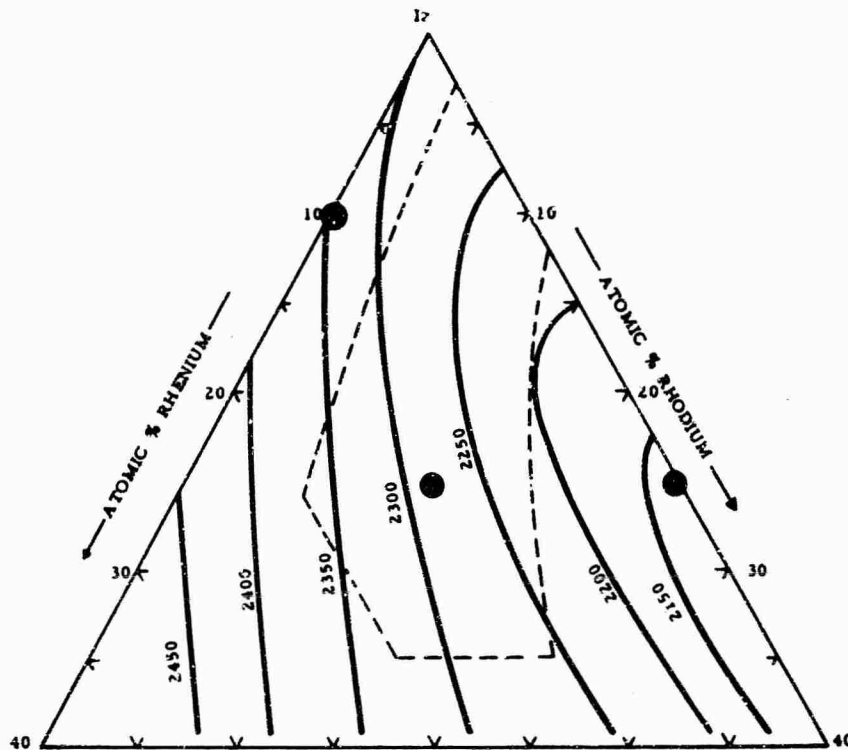


Figure 85. Compositional Field of Iridium-Rhenium-Rhodium Alloys for which the Thermal Expansion Characteristics were Estimated.

● Thermal Expansion Alloys

The measurements were determined by two separate techniques, dilatometric and X-ray diffraction. The equipment and procedures are described under the appropriate heading in an earlier section in this report.

#### a. Dilatometric Studies

These investigations were originally scheduled to be performed up to a temperature of 1400°C; however, due to certain problems experienced by the vendor, a system which would only operate to temperatures of 800°C was available for these studies. This was quite unfortunate, since the X-ray studies, which were performed earlier were carried out at a temperature above 1000°C. Therefore, a 200°C gap, rather than the expected 400°C overlap, exists in the data.

The investigations were performed on electron beam melted material which was subsequently homogenized at 1600°C for 6 hours. The samples were approximately 25mm in length and 6 mm in

diameter. The results obtained in these studies are given in the next section along with the X-ray data.

#### b. High Temperature X-Ray Diffraction Studies

The equipment and procedures for these studies are described under the appropriate heading earlier in this report. Typical X-ray diffraction peaks from the highest angle reflection measured are shown in Figure 86. The resolution of the  $K_{\alpha_1}$ - $K_{\alpha_2}$  peak was possible at all temperatures with all of the alloys. The peaks were scanned from high to low and low to high angles, and the diffraction peaks were measured to better than  $\pm 0.01^\circ(2\theta)$ . On the average, the deviation between the individual measurements of the two angles was no greater than  $\pm 0.03^\circ(2\theta)$ , which would lead to an approximate error in the lattice parameter of  $\pm 0.0005 \text{ \AA}$  or 0.01%.

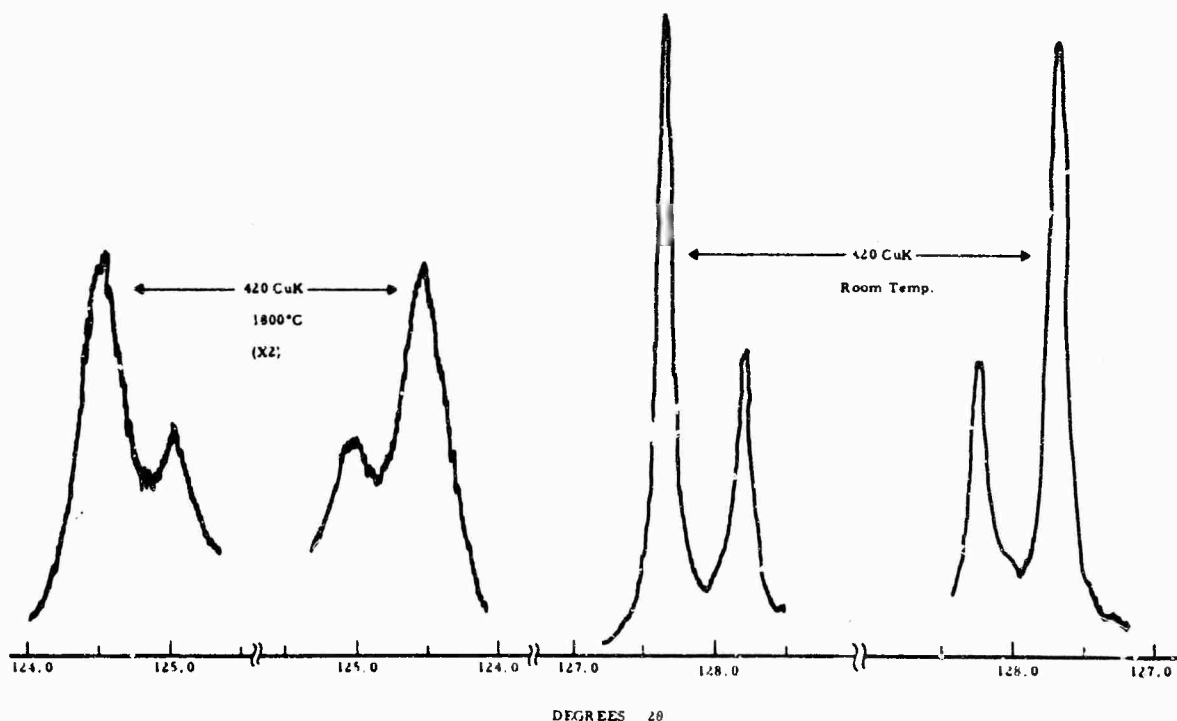


Figure 86. Representative X-Ray Diffraction Peaks Obtained During the High Temperature X-Ray Diffraction Measurement. [Iridium-Osmium (75/25) Alloy].

The data from the dilatometric and X-ray studies were evaluated by an IBM 7094 computer, and the resulting expressions for the coefficients of thermal expansion of the alloys are given in Table 3; the data is presented in Table 14. From analysis of these data, it was concluded that in each of the ternary systems, the expansion characteristics of the unmeasured alloys fall between the extreme values reported for the particular boundary binary alloys. These values are summarized in Figure 8 and are compared to the thermal expansion characteristics of present grades of commercially available graphites.

#### IV. DISCUSSION

From the results of these investigations, it can be concluded that a number of alloy combinations show promise for graphite coating applications. All of the materials investigated exhibited solidus temperatures with graphite in excess of 2000°C; the majority had eutectic temperatures of greater than 2300°C.

The thermal expansion characteristics of the alloys appear to be "border-line" in respect to their mechanical compatibility with the present commercial grades of graphite. However, recent development work has produced graphites which have thermal expansion characteristics which closely match those of pure iridium<sup>(1)</sup>, and hence, this material would also be compatible with the presently investigated iridium-base alloy materials.

The results have also indicated that factors such as the levels of specific impurities (silicon, boron, etc.) must be closely controlled, otherwise drastic melting point depression of the coating material will result. It is probable that this factor resulted in the low iridium-carbon eutectic temperature previously reported in the literature<sup>(1)</sup>.

The final evaluation of alloy material for coating applications cannot however be justifiably made with the results obtained in these investigations; this work only aids in pointing out the most desirable alloy combinations. Numerous other parameters have to be measured before the optimum coating materials are selected for these systems; i. e., adherence to graphite, strength and ductility, oxidation resistance, etc. are all vital properties which have to be taken into account.

Table 14: Thermal Expansion Data from the Dilatometric and the High Temperature X-Ray Diffraction Studies.\*

Alloy	T(°C)	$\alpha(^{\circ}\text{C}^{-1} \times 10^6)$	Alloy	T(°C)	$\alpha(^{\circ}\text{C}^{-1} \times 10^6)$
Ir-Re (90/10)	222	6.34	Ir-Os-Rh 75/12.5/12.5	207	6.65
	423	6.47		400	6.55
	600	6.83		600	6.88
	800	6.85		800	7.19
	1009	7.03		1009	7.52
	1209	7.56		1209	8.03
	1409	7.44		1409	8.08
	1509	7.80		1509	8.22
	1610	7.91		1609	8.26
	1710	8.15		1709	8.56
1810	8.12	1809	8.64		
Ir-Os (75/25)	170	6.34	Ir-Os-Pt 75/12.5/12.5	225	7.00
	350	6.12		411	6.84
	480	6.43		605	7.09
	660	6.74		810	7.50
	790	6.47		1010	7.73
	1009	7.12		1210	7.94
	1209	7.36		1410	8.46
	1409	7.54		1510	8.10
	1509	7.58		1610	8.58
	1609	7.74		1710	8.69
1709	7.88	1810	8.80		
1809	8.09				
Ir-Rh (75/25)	130	7.63	Ir-Re-Rh 75/12.5/12.5	245	6.44
	230	7.44		400	6.45
	325	7.43		600	6.78
	500	7.85		810	7.18
	595	7.54		1010	7.08
	1000	8.01		1210	7.33
	1200	8.55		1410	7.74
	1400	8.73		1510	7.66
	1510	8.86		1610	8.03
	1610	8.87		1710	8.21
1710	8.99	1810	8.25		
1810	9.44				
Ir-Pt (75/25)	105	7.38	*X-Ray data for temperatures above 1000°C		
	195	7.57			
	300	7.45			
	485	7.37			
	665	7.67			
	760	7.80			
	1200	8.29			
	1400	8.72			
	1600	9.00			
1700	9.30				
1800	9.57				

## REFERENCES

1. J.M. Criscione, R.A. Mercuri, E.P. Schram, A.W. Smith, and H.F. Volk: ML-TDR-64-173, Part II (Oct. 1964).
2. M.R. Nadler and C.P. Kempter: J. Phys. Chem., 64 (1960), 1468.
3. R.A. Orani and T.S. Jones: The Review of Sci. Inst. 25 (3) (1954), 248.
4. W.F. Roeser, F.R. Cadwell, and H.T. Wensel: J. Res. Nat'l Bur. Stds. 6 (1931), 1119.
5. H.F. Stinson: J. Res. Nat'l Bur. Stds., 65 A (1961), 139.
6. W.F. Roeser and H.T. Wensel: J. Res. Nat'l Bur. Stds., 12, (1934), 519.
7. B. Giessen: WADD-TD-60-132, Part II, Sept 1962, 147.
8. E.J. Rapport and M.F. Smith: WADD-TD-60-B2, Part II, Sept 1962, 8 .
9. E. Raub: J. Less-Common Metals, 1 (1959), 3 .
10. M.A. Tylkina, I.A. Tsyganova, and E.M. Savitskii: Russian J. of Inorg. Chem. (English Translation), 7 (1962) 990.
11. A. Taylor, B.J. Kagle, and N.J. Doyle; J. Less-Common Metals, 3 (1961), 333.
12. A. Taylor, N.J. Doyle, and B.J. Kagle: J. Less-Common Metals, 4 (1962), 436.
13. A.G. Knapton, J. Savill, and R. Siddall: J. Less-Common Metals, 2 (1960), 357.
14. F. Jaeger and E. Rosenbohm: Proc. Acad. Sci., Amsterdam, 36 (1933), 786.
15. C. Agte, H. Alterthum, K. Becker, G. Heyne, and K. Moers: Z.f. anorg. allg. Chemie, 196 (1931), 129.
16. C.T. Sims, C.M. Craighead, and R.I. Jaffee: J. of Metals, (Trans. AIME, Jan 1955), 168.
17. Anon: Platinum Metals Review, Oct. 1963, 147.
18. E. Rudy, St. Windisch, and J.R. Hoffman: AFML-TR-65-2, Part I, Vol. VI, 1966.

## REFERENCES (Cont'd)

19. R.D. Reiswig and J.M. Dickinson: *Trans. of AIME*, 230 (1964), 469.
20. G. Haase and G. Schneider: *Z. Physik*, 144, (1956), 256.
21. E. Raud and W. Plate: *Z. Metallkunde*, 47, (1956), 688.
22. A.S. Darling: *Platinum Metals Review*, Jan. 1960, 18.
23. A. Taylor and B.J. Kagle: "Crystallographic Data on Metal and Alloy Structures", Dover Publications, New York (1963).
24. E. Raub and G. Falkenburg: *Z. Metallkde.*, 55 (1964), 186.
25. L.J. Collier, T.H. Harrison, and W.G.A. Taylor: *Trans. Faraday Soc.*, 30 (1934), 581.
26. Anon: *Platinum Metals Review*, July 1964, 101.
27. J. Hughes: *Assoc. Electr. Ind., Ltd., Research Lab. Report No. A497*, Nov. 1955, Also *J. Less-Common Metals*, 1 (1959), 377.
28. M.L. Hammond: *Dissertation, Stanford University, Palo Alto, Calif.* 1965
29. C.P. Kempter and M.R. Nädler: *J. Chem. Physics.*, 33 (1960), 1580.
30. B. Jeantet and A.G. Knapton: *Planseeber. für Pulvermetall.* 12 (1964), 12.
31. C.P. Kempter: *J. Chem. Phys.*, 41 (1964), 1515.
32. P.T.B. Shaffer: "High-Temperature Materials", Plenum Press, New York (1964).
33. ASM "Metals Handbook, 2nd. Ed., Vol. I., ASM Publ, Novelty, Ohio (1961).
34. E. Rudy, St. Windisch, Y.A. Chang: *AFML-TR-65-2, Part I, Vol. I.* Jan (1965).
35. E. Rudy and G. Progulski: *FML-TR-65-2, Part III, Vol. II* (in preparation for print).
36. H.D. Heetderks, E. Rudy and T. Eckert: *Planseeber. f. Pulvermet.* 13 (1965), 105, also *AFML-TR-65-2, Part III, Vol. I* (April 1965).
37. J.J. English: *DMIC Report 152*, April (1961).
38. J.J. English: *DMIC Report 183*, February (1963), Supplement to Report 152, see Ref. 37.

#### REFERENCES (Cont'd)

39. D.K. Smith: Norelco Reporter, Vol.X., No.1 (1963), 19.
40. R.D. Allen, L.F. Glasier, and P.L. Jordon: J.Appl.Physics 31 (1960), 1382.
41. R.J. Thorn and G.H. Winslow: In "Temperature-Its Measurement and Control in Science and Industry, C.M. Herzfeld, Ed., Reinhold Pub. Corp., New York 19, Part I, Vol. 3, 421.
42. W.S. Campbell: "Platinum Expansion Values for Thermal Calibration of High-Temperature X-ray Diffraction Cameras and Diffractometer", U.S. Bureau of Mines, Information Circular 8170, 1962.
43. R.W. Douglass, C.A. Krier, and R.I. Jaffee: Report No. AD 265 624 (1961).
44. E. Rudy: Private Communication.
45. O. Feussner and L. Müller: Ann.Physik, 7 (1930), 9.
46. W. Hume-Rothery and G.V. Raynor: "The Structure of Metals and Alloys" 3rd Ed. The Inst. of Metals, London (1964).
47. L.Kaufman, H. Bernstein, A. Sarney: ASK-TR-61-445, Part III, 1963.
48. R. Hultgren, R.L. Orr, P.D. Anderson, and K.K. Kelley: "Selected Values of Thermodynamic Properties of Metals and Alloys", John Wiley & Son, Inc., New York (1963).
49. Y.A. Chang: AFML-TR-65-2, Part IV, Vol. I, June 1965.
50. Compare Literature in "Constitution of Binary Alloys", M. Hansen, 2nd Ed., with K. Anderko, McGraw-Hill Co., New York (1958).

DOCUMENT CONTROL DATA - R&D		
<i>(Security classification of title, body of abstract and indexing annotation must be entered when the overall report is classified)</i>		
1. ORIGINATING ACTIVITY (Corporate author) Materials Research Laboratory Aerojet-General Corporation Sacramento, California		2a. REPORT SECURITY CLASSIFICATION Unclassified
		2b. GROUP N.A.
3. REPORT TITLE Iridium-Base Alloys and Their Behavior in the Presence of Carbon Final Report		
4. DESCRIPTIVE NOTES (Type of report and inclusive dates) Final Report		
5. AUTHOR(S) (Last name, first name, initial) D. P. Harmon		
6. REPORT DATE October 1965	7a. TOTAL NO. OF PAGES 115	7b. NO. OF REFS 50
6a. CONTRACT OR GRANT NO.	8a. ORIGINATOR'S REPORT NUMBER(S) AFML-TR-66-290 Final Report	
b. PROJECT NO.	8b. OTHER REPORT NO(S) (Any other numbers that may be assigned this report) N.A.	
c.		
d.		
10. AVAILABILITY/LIMITATION NOTICES This document is subject to special export controls and each transmittal to foreign governments or foreign nationals may be made only with prior approval of Metals & Ceramics Div., AF Materials Laboratory, Wright-Patterson AFB, Ohio.		
11. SUPPLEMENTARY NOTES	12. SPONSORING MILITARY ACTIVITY AFML (MAMC) Wright-Patterson AFB, Ohio 45433	
13. ABSTRACT Experimental results pertaining to the melting temperatures of selected iridium-osmium-rhodium, iridium-osmium-platinum, and iridium-rhenium-rhodium alloys are described. The eutectic temperatures of these alloys with carbon were measured, and in addition, the compositions of the respective eutectics were determined by metallographic examination of chemically analyzed alloys. A brief theoretical analysis of the data was also performed with the specific objective of establishing numerical relations between the melting point depression and properties of the melt as well as the component metals.  The thermal expansion characteristics of several of the iridium-base alloys were measured up to 1800°C by high temperature, X-ray diffraction as well as by dilatometric techniques.		

14. KEY WORDS	LINK A		LINK B		LINK C	
	ROLE	WT	ROLE	WT	ROLE	WT
Iridium Alloys						
Graphite Coatings						
Melting Points						
Binary Carbide Systems						
Ternary Carbide Systems						
Quaternary Carbide Systems						
Thermal Expansion						

**INSTRUCTIONS**

1. **ORIGINATING ACTIVITY:** Enter the name and address of the contractor, subcontractor, grantee, Department of Defense activity or other organization (corporate author) issuing the report.

2a. **REPORT SECURITY CLASSIFICATION:** Enter the overall security classification of the report. Indicate whether "Restricted Data" is included. Marking is to be in accordance with appropriate security regulations.

2b. **GROUP:** Automatic downgrading is specified in DoD Directive 5200.10 and Armed Forces Industrial Manual. Enter the group number. Also, when applicable, show that optional markings have been used for Group 3 and Group 4 as authorized.

3. **REPORT TITLE:** Enter the complete report title in all capital letters. Titles in all cases should be unclassified. If a meaningful title cannot be selected without classification, show title classification in all capitals in parentheses immediately following the title.

4. **DESCRIPTIVE NOTES:** If appropriate, enter the type of report, e.g., interim, progress, summary, annual, or final. Give the inclusive dates when a specific reporting period is covered.

5. **AUTHOR(S):** Enter the name(s) of author(s) as shown on or in the report. Enter last name, first name, middle initial. If military, show rank and branch of service. The name of the principal author is an absolute minimum requirement.

6. **REPORT DATE:** Enter the date of the report as day, month, year, or month, year. If more than one date appears on the report, use date of publication.

7a. **TOTAL NUMBER OF PAGES:** The total page count should follow normal pagination procedures, i.e., enter the number of pages containing information.

7b. **NUMBER OF REFERENCES:** Enter the total number of references cited in the report.

8a. **CONTRACT OR GRANT NUMBER:** If appropriate, enter the applicable number of the contract or grant under which the report was written.

8b, 8c, & 8d. **PROJECT NUMBER:** Enter the appropriate military department identification, such as project number, subproject number, system numbers, task number, etc.

9a. **ORIGINATOR'S REPORT NUMBER(S):** Enter the official report number by which the document will be identified and controlled by the originating activity. This number must be unique to this report.

9b. **OTHER REPORT NUMBER(S):** If the report has been assigned any other report numbers (either by the originator or by the sponsor), also enter this number(s).

10. **AVAILABILITY/LIMITATION NOTICES:** Enter any limitations on further dissemination of the report, other than those

imposed by security classification, using standard statements such as:

- (1) "Qualified requesters may obtain copies of this report from DDC."
- (2) "Foreign announcement and dissemination of this report by DDC is not authorized."
- (3) "U. S. Government agencies may obtain copies of this report directly from DDC. Other qualified DDC users shall request through \_\_\_\_\_."
- (4) "U. S. military agencies may obtain copies of this report directly from DDC. Other qualified users shall request through \_\_\_\_\_."
- (5) "All distribution of this report is controlled. Qualified DDC users shall request through \_\_\_\_\_."

If the report has been furnished to the Office of Technical Services, Department of Commerce, for sale to the public, indicate this fact and enter the price, if known.

11. **SUPPLEMENTARY NOTES:** Use for additional explanatory notes.

12. **SPONSORING MILITARY ACTIVITY:** Enter the name of the departmental project office or laboratory sponsoring (paying for) the research and development. Include address.

13. **ABSTRACT:** Enter an abstract giving a brief and factual summary of the document indicative of the report, even though it may also appear elsewhere in the body of the technical report. If additional space is required, a continuation sheet shall be attached.

It is highly desirable that the abstract of classified reports be unclassified. Each paragraph of the abstract shall end with an indication of the military security classification of the information in the paragraph, represented as (TS), (S), (C), or (U).

There is no limitation on the length of the abstract. However, the suggested length is from 150 to 225 words.

14. **KEY WORDS:** Key words are technically meaningful terms or short phrases that characterize a report and may be used as index entries for cataloging the report. Key words must be selected so that no security classification is required. Identifiers, such as equipment model designation, trade name, military project code name, geographic location, may be used as key words but will be followed by an indication of technical context. The assignment of links, rules, and weights is optional.